

# Atomic-scale friction : a scanning probe study on crystalline surfaces

**Citation for published version (APA):**

Tanasa, G. (2005). *Atomic-scale friction : a scanning probe study on crystalline surfaces*. [Phd Thesis 1 (Research TU/e / Graduation TU/e), Applied Physics and Science Education]. Technische Universiteit Eindhoven. <https://doi.org/10.6100/IR596963>

**DOI:**

[10.6100/IR596963](https://doi.org/10.6100/IR596963)

**Document status and date:**

Published: 01/01/2005

**Document Version:**

Publisher's PDF, also known as Version of Record (includes final page, issue and volume numbers)

**Please check the document version of this publication:**

- A submitted manuscript is the version of the article upon submission and before peer-review. There can be important differences between the submitted version and the official published version of record. People interested in the research are advised to contact the author for the final version of the publication, or visit the DOI to the publisher's website.
- The final author version and the galley proof are versions of the publication after peer review.
- The final published version features the final layout of the paper including the volume, issue and page numbers.

[Link to publication](#)

**General rights**

Copyright and moral rights for the publications made accessible in the public portal are retained by the authors and/or other copyright owners and it is a condition of accessing publications that users recognise and abide by the legal requirements associated with these rights.

- Users may download and print one copy of any publication from the public portal for the purpose of private study or research.
- You may not further distribute the material or use it for any profit-making activity or commercial gain
- You may freely distribute the URL identifying the publication in the public portal.

If the publication is distributed under the terms of Article 25fa of the Dutch Copyright Act, indicated by the "Taverne" license above, please follow below link for the End User Agreement:

[www.tue.nl/taverne](http://www.tue.nl/taverne)

**Take down policy**

If you believe that this document breaches copyright please contact us at:

[openaccess@tue.nl](mailto:openaccess@tue.nl)

providing details and we will investigate your claim.

# **Atomic-Scale Friction: A Scanning Probe Study on Crystalline Surfaces**

PROEFSCHRIFT

ter verkrijging van de graad van doctor aan de Technische Universiteit  
Eindhoven, op gezag van de Rector Magnificus, prof.dr.ir. C.J. van Duijn,  
voor een commissie aangewezen door het College voor Promoties in het  
openbaar te verdedigen op dinsdag 8 november 2005 om 16.00 uur

door

Gheorghe Tănasă

geboren te Piatra Neamț, Roemenië

Dit proefschrift is goedgekeurd door de promotoren:

prof.dr.ir. R.A.J. Janssen

en

prof.dr. M.B. Salmeron

Copromotor:

dr.ir. C.F.J. Flipse

This research has been financially supported by Stichting voor Fundamenteel Onderzoek der Materie (FOM)

Printed at the Universiteitsdrukkerij, Eindhoven University of Technology

CIP-DATA LIBRARY TECHNISCHE UNIVERSITEIT EINDHOVEN

Tănasă, Gheorghe

Atomic-scale friction: A scanning probe study on crystalline surfaces / door Gheorghe

Tănasă. – Eindhoven: Technische Universiteit Eindhoven, 2005. - Proefschrift.

ISBN 90 – 386 – 2341 - 0

NUR 926

Trefwoorden: wrijving / atomaire krachtmicroscopie / tribologie.

Subject headings: friction / atomic force microscopy / tribology.

*"I seem to have been like a child playing on the sea shore, finding now and then a prettier shell than ordinary, whilst the great ocean of truth lay undiscovered before me."*

*Sir Isaac Newton*

*To my parents with love and gratitude*



## Table of contents

<b>Chapter 1. Introduction</b> .....	7
1.1. Friction: a general view .....	7
1.2. History of friction .....	7
1.3. Nanotribology .....	11
1.4. Aim of this work .....	16
<b>Chapter 2. Experimental</b> .....	21
2.1. Atomic Force Microscopy: unique tool for nanotribology .....	21
2.2. Experiments under well defined conditions: the Omicron UHV VT-AFM setup .....	23
2.3. The Omicron UHV VT-AFM setup .....	24
<b>Chapter 3. Chemical vapor deposition on silicon substrates: Making diamond-terminated AFM tips</b> .....	29
3.1. Introduction .....	29
3.2. Experimental procedure .....	30
3.3. Results and discussion .....	31
3.3.1. Morphology of diamond deposits on etched silicon pyramids .....	31
3.3.2. Diamond deposition on standard silicon tips .....	33
3.3.3. Diamond-terminated cantilever tests in ultra-high vacuum .....	36
3.4. Summary of results .....	37
<b>Chapter 4. Friction force measurements on diamond (100) surfaces</b> .....	41
4.1. Introduction .....	41
4.2. Experimental .....	41
4.2.1. Experimental set-up .....	41
4.2.2. Sample preparation .....	42
4.3. Results and discussion .....	42
4.3.1. Sample topography .....	42
4.3.1.1. STM measurements .....	42
4.3.1.2. FFM measurements on (100) diamond .....	43
4.4. Conclusion .....	56
<b>Chapter 5. Friction force measurements on diamond (111) surfaces</b> .....	59
5.1. Introduction .....	59
5.2. Experimental .....	60
5.2.1. AFM setup details .....	60
5.2.2. Sample/tip preparation .....	60
5.3. Results and discussion .....	61
5.3.1. Sample topography on a micrometer scale .....	61
5.3.2. Friction force measurements using standard silicon nitride tip .....	61
5.3.3. Atomic scale friction between diamond coated tips and (111) diamond surface .....	64
5.4. Conclusion .....	74

<b>Chapter 6. Effect of temperature on friction between a silicon tip and the (001) surface of NaCl observed in ultra-high vacuum .....</b>	<b>77</b>
6.1. Introduction.....	77
6.2. Experimental.....	77
6.2.1. Instrumental details.....	77
6.2.2. Sample/tip preparation.....	78
6.3. Results and discussion .....	78
6.3.1. Surface topography: micrometer scale investigation.....	78
6.3.2. Atomic-scale friction: the NaCl surface at room temperature.....	79
6.3.3. Temperature effect on friction measured within the 25 K – room temperature interval .....	80
6.3.4. Theoretical models.....	84
6.4. Conclusion .....	87
Appendix 1. Computational method.....	89
Appendix 2. Growth of (100) single crystalline diamond samples .....	91
<b>Summary.....</b>	<b>93</b>
<b>Samenvatting.....</b>	<b>95</b>
<b>Publications .....</b>	<b>97</b>
<b>Acknowledgements .....</b>	<b>99</b>
<b>Curriculum Vitae.....</b>	<b>101</b>

# Chapter 1. Introduction

## ***1.1. Friction: a general view***

It is almost impossible to imagine everyday life in the absence of friction. Friction is the force appearing when an object moves through a viscous liquid or gas or when two surfaces slide or rub against each other. It allows us to walk, to climb stairs, to sit in a chair, to stop a car, to handle tools. In technological applications friction is the evil of all motion and huge amounts of money are spent annually on energetic and mechanical losses due to friction and wear [1]. Natural catastrophes like earthquakes, landslides and avalanches are also caused by friction.

Friction forces are nonconservative, transforming the kinetic energy of the bodies in contact/motion into internal energy. A block having an initial given speed, sliding on a surface will eventually stop due to the friction that opposes its motion; the temperature of both contacting surfaces will always show an increase. An object initially at rest requires a minimum force to break the “static friction” which is followed by a jump ahead at the moment when sliding starts.

Although so commonly and widely encountered, friction remains one of the most elusive and fascinating phenomena in science.

## ***1.2. History of friction***

Along the entire history, controlling friction was one of the most challenging endeavors for mankind and all the empirical observations, experiments and emerging expertise led to a new field of research nowadays named tribology [2,3]; it studies, besides friction, the related phenomena of adhesion, lubrication and wear. Two hundred years before Isaac Newton even defined the concept of force, after numerous experiments with various items (sliding blocks, rolling weights) (Fig.1.1), Leonardo da Vinci [2] (1452-1519), the father of modern tribology, drew two important conclusions:

“Friction produces double the amount of effort if the weight be doubled.”

“The friction made by the same weight will be of equal resistance at the beginning of the movement although the contact may be of different breadths or lengths.”

So the first is stating that friction will be proportional to the normal force (applied load) and the second that (counter-intuitively) friction is independent of the contact area. Da Vinci realized how crucially friction can affect the workings of machines; he focused on all kinds of friction and made a clear distinction between rolling and sliding friction. He



also noticed that different materials do not move with the same ease and presumed that this was caused by the different roughness of the surfaces (materials). Thus well polished surfaces will show lower friction.

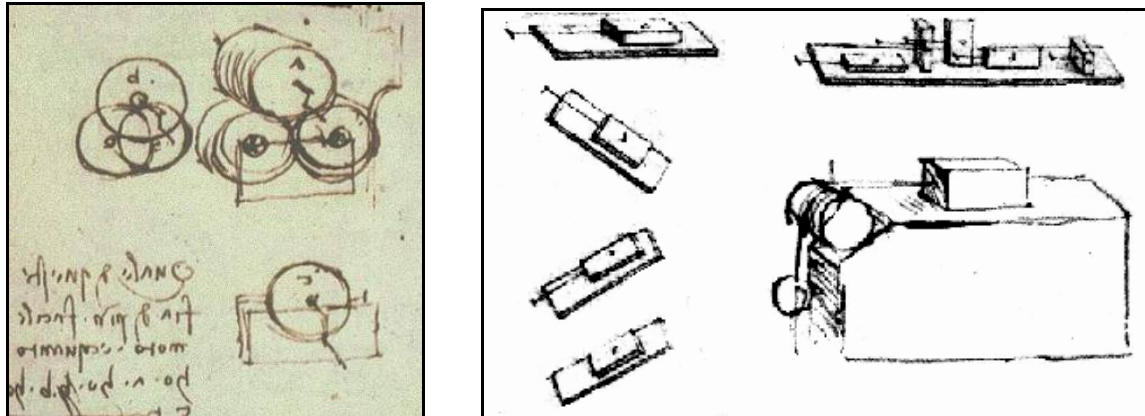


**Fig.1.1** Schematics from Leonardo da Vinci’s manuscripts on friction, showing items used in his experimental work.

Lost or hidden for centuries, Leonardo da Vinci’s manuscripts containing priceless tribological studies on friction, wear, bearing materials, plain bearings, lubrication systems, gears, rolling-element bearings and screw-jacks were finally found and read in Spain.

Other pioneers in tribology were Guillaume Amontons (1663-1705) and Charles August Coulomb (1736-1806) [2]. By studying the sliding friction between two flat surfaces in contact, Amontons rediscovered the two statements of da Vinci and came up with an original set of theories.

For the first time he speaks of an “apparent” contact area between sliding bodies. In his view friction was mostly a result of the effort required to lift one surface over the roughness of the other; the deformation or wearing of the mechanically interlocked asperities in contact were also thought to play a very important role (Fig.1.2). All of these aspects led to the classical law of friction:

$$F_f = \mu L, \tag{1.1}$$

where  $F_f$  is the friction force,  $L$  is the normal force (or applied load) and  $\mu$  is the coefficient of friction, a scalar that characterizes two materials in contact.

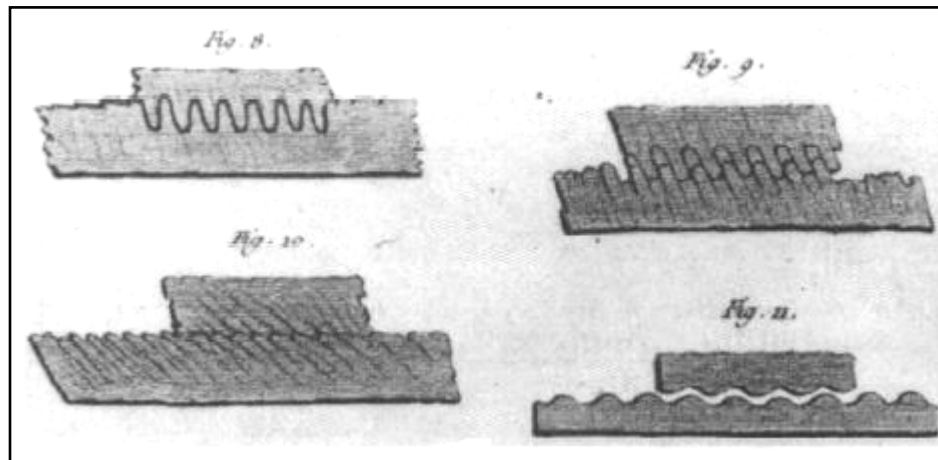


**Fig.1.2** Drawings on the interlocking theory of friction by C.A. Coulomb, *Théorie des Machines Simples* (1785) (see also Ref.2)

In 1785, the experimental work of Coulomb showed that the coefficient of sliding friction (called also kinetic friction) is generally smaller than the coefficient of static friction. Moreover, he finds that for sliding, the coefficient does not vary significantly as a function of the relative velocity of the two surfaces in contact: “The friction force is independent on velocity for ordinary sliding speeds.” Coulomb designs the first tribometer, a special device used even nowadays (in high-tech versions) to determine the frictional coefficient for certain materials.

A broad and systematic research has been performed during the last century especially in the field of engineering due to the practical importance of friction-related issues for a wide range of industrial applications. Friction, adhesion, lubrication and wear are obviously involved in the operation of car brakes, the optimization of tire quality, the lifetime and efficiency of car engines etc. All the above-mentioned research and engineering work confirm da Vinci’s, Amonton’s and Coulomb’s statements: for a very wide range of materials and under various conditions, friction between two surfaces is proportional to load, independent of the apparent contact area and weakly dependent on the relative sliding speed.

Even a surface which seems to be very flat on a millimeter scale may contain micrometer-sized asperities i.e. the surface is rough [4,5]. If two surfaces are brought in contact, only these protrusions really touch each other (as shown in Fig.1.3). Friction is due to the interaction between the asperities of the different surfaces and the resulting energy dissipation will be caused by these contacting protrusions.

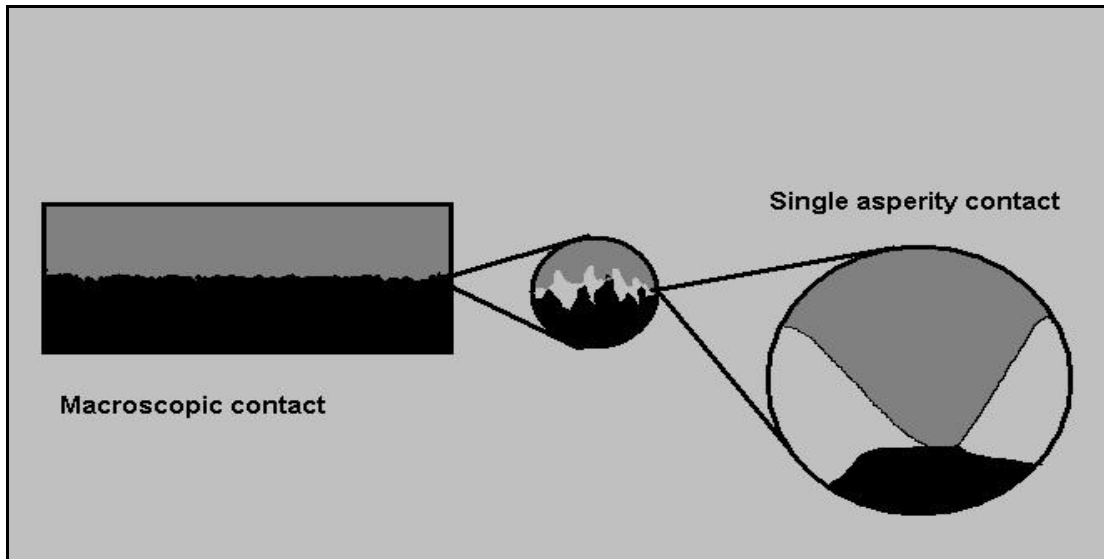


**Fig. 1.3** A macroscopic contact surface between two apparently flat and smooth objects consists in fact of multiple protrusions; a further applied load will increase the *real contact area* as more single asperities will interact with each other.

The real area of contact is a few orders of magnitude smaller than the apparent *geometric* area of contact and therefore the lack of dependence upon this area. This important fact has to be taken into account while modelling a friction process; the linear or nearly linear dependence of friction upon load results from a very complicated and nearly random geometry of the protrusions and from other complex phenomena at the interface such as adhesion-induced deformation [6] and plowing of the surface asperities by each other and by wear particles [7].

In 1950 F. P. Bowden and D. Tabor published a collection of knowledge on friction and lubrication, most of the results given in the book being their own. This book [6] and the follow-up [8] (in 1964) have become the standard references on friction and lubrication for a couple of decades. Bowden and Tabor showed a simple model for friction on a micrometer scale: the plastic junction model. The model assumes that friction is proportional to both the real area of contact and a mean lateral force per unit area, named shear strength. Since friction is proportional to the real area of contact in this model as is adhesion, the model was also called adhesion model. For dry, wearless sliding the friction force is:

$$F_f = \tau A, \quad (1.2)$$

where  $\tau$  is the shear strength of the contact.

The energy loss in the friction mechanism was explained to be due to plastic deformation of the asperities. So, the understanding of friction at the micrometer scale has been reduced to a puzzling problem consisting of two new parameters: area of contact and shear strength.

In spite of the huge efforts coming from both research and engineering fields with (it is fair to mention) remarkable practical progresses, a fundamental understanding of friction-related phenomena is still elusive and a predictive analysis of frictional properties for newly developed materials is almost impossible [9,10].

The main difficulty for most of the surface science techniques is to assess and analyze the complicated interface between the materials in sliding where all the processes involving nanometer- and atomic-scale-sized asperities take place.

### **1.3. Nanotribology**

In the last two decades a new field of research called *nanotribology* has emerged, due to considerable advances in developing new experimental techniques, computational power and theoretical methods [11-14]. This progression enabled the investigation of the friction-related processes down to unprecedented limits: nanometer-scale and even atomic scale.

The macroscopic friction is the result of a collective interaction of a very large number of small asperities and therefore the nanotribology tackles this problem by trying to create a single model asperity whose behavior could then be statistically extrapolated to bigger scales. Recent experimental techniques, using instruments such as surface force apparatus (SFA)[15], the quartz-crystal microbalance (QCM)[16], the atomic force microscope (AFM) [17,18] with its friction-dedicated version called friction force microscope (FFM) and others [19] gave the opportunity to study the friction of single asperities.

Friction force microscopy is a variation of the atomic force microscopy technique, in which a small sharp tip (radius typically 10-100 nm) attached to the end of a compliant cantilever is used. The tip, which could simulate a single asperity, is approached to the sample surface and scanned across it; as the tip moves interaction forces between the tip and sample atoms will deflect or twist the cantilever giving a measure of the topography, normal or lateral (frictional) forces. More detailed explanations will be provided in Chapter 2.

In the SFA, two molecularly smooth cleaved mica surfaces are glued to two crossed cylinders. They are mounted in a way that allows horizontal and vertical movements; the normal and frictional (lateral) forces can be directly measured by means of force-mapping springs. The contact area and the distance between the sheets are determined with a remarkable resolution (in the order of 2 Angstroms or better) using optical-beam interferometry. The typical velocities used range from 50 to 5000 nm/s. The SFA has been routinely used to study the dependence of friction on the contact area, on the relative crystalline orientation and also involved lubricant layers squeezed between the contacting surfaces [20].

The Quartz Crystal Microbalance is an instrument operating on a very short time scale and therefore capable of detecting phonons (lifetimes shorter or in the range of

nanoseconds). In the mid 80's the QCM, normally employed for micro-weighing or time standard applications, was adapted for sliding friction investigations of layers adsorbed on metallic surfaces [21,22]. By measuring at the same time the shift in the resonant frequency as well as the broadening of resonance, observed from the decrease in the QCM vibration amplitude, information upon the sliding friction between the layer and the metallic surface can be obtained. This instrument is efficient for rather low friction interfaces, since only significant sliding can result in a considerable and consequently measurable broadening of the resonance.

Semiclassical calculations using the Tomlinson and Frenkel-Kontorova models [23-24], more advanced molecular-dynamics (MD) simulations [25-27] and other types of simulations [28,29] have provided further insight in the atomic-scale processes occurring at the buried interface of the sliding bodies. In the semiclassical models, mainly the mechanics of the periodic frictional behavior is aimed; atoms at contacting surfaces in relative sliding are represented by systems of balls and variable springs and a periodic friction force will in fact reflect the periodicity of the interaction potential. The MD simulations provide local information on the vibrational motion and energy dissipation created during the discontinuous stick-slip event; excitations seem to be highly localized in the interface area. Some of these calculations suggest also considerable distortions of the tip atoms due to interfacial stresses, possibly creating a partly commensurate interface. If calculations properly allow time for structural, thermal and electronic equilibration, calculations at large velocities (MD:  $10^0$ - $10^2$  m/s) become possible to compare with experiments typically performed at much smaller speed scales (AFM:  $10^{-9}$ - $10^{-4}$  m/s) [30]. Progresses in both experimental techniques and computational power will certainly minimize this problem in the future [31].

In all the experiments involving a single asperity, the frictional force dependence of the applied load  $L$  was found to follow a general law:  $F_f \sim L^n$  where  $n < 1$ . Contact mechanics are a good tool to describe the deformations, displacements and stresses which appear when materials are brought in contact [32]. Theories trying to model the elastic deformations between bodies under load exist since the 19<sup>th</sup> century. Hertz [33] solved the contact mechanics problem for two spheres of radius  $R_1$  and  $R_2$  in the case of elastic deformations of the materials when no attractive forces (adhesive forces) are present between the two bodies. The symmetry of the problem leads to a flat circular contact area between the two materials and the dependence of load is given by a non-linear function. The relation between contact area  $A$  and externally applied load  $L$  is given by:

$$A = \pi \left( \frac{RL}{K} \right)^{2/3} \quad (1.3)$$

where  $R$  is the combined curvature radius of the two spheres of radius  $R_1$  and  $R_2$  in contact, and  $K$  is the combined elastic Young's modulus of the two materials:

$$R = \left( \frac{1}{R_1} + \frac{1}{R_2} \right)^{-1}, \quad (1.4)$$

$$K = \frac{4}{3} \left( \frac{1-\nu_1^2}{E_1} + \frac{1-\nu_2^2}{E_2} \right)^{-1}. \quad (1.5)$$

$E_1$  and  $E_2$  are the respective Young's moduli, and  $\nu_1$  and  $\nu_2$  the respective Poisson's ratios of the two spheres. The situation of a single elastic asperity (tip of radius  $R$  and a flat sample) is only a particular case in the Hertzian model, as  $R_1 \rightarrow R$ ,  $R_2 \rightarrow \infty$ ; the friction force is therefore shown to scale as  $L^{2/3}$ .

The influence of attractive (adhesive) force between soft contacting surfaces is taken into account in the Johnson-Kendall-Roberts model (JKR) [34]. The relation between applied load and contact area:

$$A = \pi \left( \frac{R}{K} \right)^{2/3} \left( L + 3\pi\gamma R + \sqrt{6\pi\gamma RL + (3\pi\gamma R)^2} \right)^{2/3}, \quad (1.6)$$

where  $\gamma$  is the work per unit area necessary to separate tip and sample from contact to infinity. A negative load is necessary to separate the surfaces, value which is often referred to as the critical load and at that moment a finite contact area still exists; obviously the friction force is non-zero even at zero applied load (i.e. a neck is formed between tip and sample).

$$L_c = -\frac{3}{2} \pi\gamma R \quad (1.7)$$

The problem of contact mechanics in the presence of adhesion is treated by a considerably different approach by Derjaguin, Muller and Toporov (DMT) theory [35] which considers that the interfacial forces do not affect the shape of the contact. The adhesion forces simply act as an extra applied load:

$$A = \pi \left( \frac{R}{K} \right)^{2/3} (L + 2\pi\gamma R)^{2/3} \quad (1.8)$$

$$L_c = -2\pi\gamma R \quad (1.9)$$

The JKR and DMT theories led to a vivid debate in the literature, trying to point out which one is the correct one. In fact both are correct, when applied to the right situation. Stiff materials with lower, longer-range adhesion forces and small radii will behave more like a DMT contact whereas softer materials with strong, short-range adhesion forces and large radii will be better described by a JKR model; situations that are in between will also be encountered.

A nondimensional empirical parameter  $\mu$ , the expression of which contains  $z_0$  as the equilibrium spacing for the interaction potential of the surfaces is normally used to determine which of the two continuum mechanics models is most appropriate:

$$\mu = \left( \frac{16R\gamma^2}{9K^2 z_0^3} \right)^{1/3} \quad (1.10)$$

The relation between contact area  $A$  and applied load  $L$  should be described by the DMT theory for  $\mu < 0.1$  while for values of  $\mu > 5$  the JKR theory should be valid. A theory that generalizes all the above-mentioned theories was created by Maugis and Dugdale (M-D) [36]. Experimentally, the SFA investigations mostly reveal a JKR-type of behavior [20], while in the FFM works nearly all types of behavior have been encountered [37].

Remarkable discoveries emerged in the field of nanotribology in the last 15 years, after the invention of the AFM. One of the most fascinating but yet elusive phenomena brought into light was the so-called atomic-scale *stick-slip* behavior of the frictional forces. The term of “stick-slip” must be used with care since it is generally associated with a discontinuous movement of large (macroscopic) contacts, involving a very big numbers of asperities (for example a bowed violin string or, on a much larger scale, the displacement of the tectonic plates during an earthquake). These phenomena seem to be extremely different but the common principle is that the friction force involved strongly depends upon the relative sliding velocity between the contacting surfaces. To be more specific, kinetic friction (during sliding) is lower than the static friction. If one of the two surfaces in contact undergoes an increasing lateral stress, the sliding will occur *only* when the static friction is exceeded by the applied stress. The sliding will continue until the lateral stress applied is no longer large enough to maintain the relative motion; the system is “stuck” again and this cycle repeats itself. Many factors, such as the roughness/topology of the surfaces in contact, the “creep”/strengthening of the interface during the “sticking” phase, and velocity-related effects in the case of viscous or visco-elastic materials, can significantly influence the stick-slip behavior.

In contrast to macroscopic stick-slip, different conditions are dealt with when investigating the frictional behavior of an AFM tip/well defined (ordered, atomically flat) sample surface; the subsequent interface is smooth and the sliding normally does not lead to wear. The atomic resolution (lattice atomic periodicity) of the lateral forces, first observed on graphite was later seen on a wide range of materials such as  $\text{MoS}_2$ , copper, mica, diamond, alkaline-halides, platinum [11, 37-39]. A two dimensional “zig-zag” stick-slip motion was experimentally observed on various materials by Fujisawa using a 2D FFM, and explained within a 2-dimensional Tomlinson model. Accordingly, on a well-defined sample surface the tip will prefer to reside in positions in registry with the sample lattice [40-41]. Therefore, simultaneously both lateral and longitudinal deformations of the cantilever will take place due to friction forces acting in the plane parallel to the sample surface.

It is essential to mention that the observation of periodic atomic-scale stick-slip features by means of contact-mode AFM does not prove that *real atomic resolution* is achieved, such as in scanning tunneling microscopy. As largely discussed in [37] almost all the of the friction images obtained on various surfaces reveal the symmetry of the lattice, exhibiting one stick-slip event per unit cell, even though in some cases the unit cell consists of two or several atomic species. The observation of more than one stick-slip event per unit cell was rare and reported only on the silicon(111)-(7x7) surface [42] and on NaF(100) [43] but only for a certain range of loads. Far from consisting of a single

atom, for typical loads and tip radii, the contact area between an AFM tip and sample is usually in the range of a few square nanometers [44] and therefore it is surprising that imaging the periodicity of the surface lattice is possible, especially when a standard AFM tip is likely to have a disordered structure which results in an incommensurate interface between tip/sample. Another interesting feature is that no observation of atomic lattice contrast was reported in the absence of the atomic-scale frictional stick-slip behavior; the measured lateral force maps, although exhibiting the same periodicities, are often clearer (sharper) than the topographic ones. These issues, partly related to the instrumental response of the cantilever and optical beam deflection setup [41, 45-47], will be further addressed in more detail in chapters 4 and 5.

The velocity dependence of friction was also investigated and modeled [38]. Another interesting phenomenon observed in AFM investigations was the friction anisotropy, showing that the friction force can strongly depend on the specific direction of motion [48-50]. The commensurability between the sliding surfaces proved to crucially influence the friction forces and a new term *superlubricity* was introduced to describe the situation when friction “vanishes” as a consequence of a mismatch between the lattices in contact [51-55]. Using a dedicated friction force sensor, called Tribolover and a special home-built FFM remarkably allowing a quantitative tracking of the forces on the scanning tip in three directions, with a particularly high resolution in the lateral forces, Dienwiebel, Frenken *et al.* have investigated the superlubricity of graphite. [56]. QCM experiments [57] showed that, surprisingly, a material can exhibit higher friction when wet and later calculations attributed this to the fact that, in the liquid phase, the rearrangements of atoms or molecules can lead to a commensurate structure with the underlying solid surface and thus to a larger friction force.

One of the most challenging tasks in the field of (nano-)tribology is to identify and understand the fundamental processes behind the excitation and energy dissipation that occurs during friction. Several mechanisms have been proposed. One of them is the excitation of surface phonon modes [58] which are, in the end, transformed into heat. The so-called electronic friction, based on sliding-induced electronic excitations, was proposed for metallic surfaces [59], still being under heavy debate. Changes in chemical bonding can also dramatically affect the frictional properties [60]. At higher loads, wear processes can appear causing rupture of atomic bonds, creation of dislocations and debris accumulation [61]. Possible creation of point defects, a way of dissipating energy when the tip-induced damage is very limited, cannot be easily proven since normally true atomic resolution is not achieved in contact mode AFM.

Other essential issues are the nature of the relative motion of the surfaces in contact (smooth sliding or stick-slip) and the influence of various parameters (contact area, applied load, scanning velocity, chemistry of possible lubricants) upon the resulting tribological behavior.



#### 1.4. Aim of this work

The main objective of this thesis is to give more fundamental insight on the atomic scale frictional behavior observed within an ideal friction experiment: diamond tip on diamond crystalline surfaces. Diamond is one of the most elegant model systems for friction study: it is the hardest natural material, single crystalline surfaces are atomically flat and the hydrogen termination of the surface leads to small adhesive forces. A diamond-diamond frictional contact is one of the most promising model systems to achieve an extremely small contact, namely a single-atom contact. As a low friction, optically transparent coating material, the growing technological importance of diamond cannot be underestimated, while doping makes it an extremely promising material for devices such as transistors in the microelectronic industry.

Investigating the temperature dependence of friction on a well-known surface in nanotribology, namely (100) NaCl, using standard silicon tips was also a challenging issue of this thesis.

All SPM measurements presented in this work have been done under ultra-high vacuum conditions in a commercially available Omicron Variable-Temperature (VT) Deflection-Beam AFM; in chapter 2 the principles of atomic force microscopy and its friction-dedicated version FFM are presented, together with an overview of the UHV experimental setup used. A method of obtaining a hard, sharp, and stable diamond termination for standard Si AFM-tips, using a hot-filament assisted chemical vapor deposition of diamond is described in chapter 3. In chapter 4, a specially prepared (100) diamond surface, exhibiting surface conductivity is further analyzed by means of STM and FFM using standard SiN and diamond coated tips. The unprecedented *atomically-resolved* topography, normal force and lateral force maps, showing periodicities corresponding to the H-atoms terminating the surface, obtained *only* when using diamond-terminated tips are analyzed and attributed to a very sharp tip describing a complicated trajectory during scanning. The nanometer-and atomic scale frictional behavior of a (111) diamond single crystal surface is investigated in chapter 5 using standard and diamond-coated tips, the latter revealing again atomic resolution. The experimental results shown in both the fourth and fifth chapters are found to be consistent with an *ab-initio* electronic structure calculation revealing that the repulsive interaction between the single-H atom at the tip end and the H-atoms of the surface, along with the subsequent complicated atomic rearrangements during scanning are of the essence in the atomic scale stick-slip behavior. Finally, the results describing the frictional behavior of a silicon tip on a (100) NaCl surface as a function of temperature within the range 25-300 K are shown in chapter 6.

## References

1. Physics of Sliding Friction, edited by B.N.J. Persson and E. Tosatti (Kluwer, Dordrecht, 1996).
2. D. Dowson, History of Tribology (Longman, London, 1998).
3. H.P. Jost, Wear 136, 1 (1990).
4. J.A. Greenwood and J.P.B Williamson, Proc. Roy. Soc. London A 295, 300 (1996).
5. J.A. Greenwood, in Fundamentals of Friction, edited by I.L.Singer and H.M. Pollock (Kluwer, Dordrecht, 1992), p. 37.
6. F. P. Bowden and D. Tabor, Friction and Lubrications of Solids: Part I (Oxford University Press, 1950).
7. D.E. Kim and N. P. Suh, Wear 149, 199 (1991).
8. F.P. Bowden and D. Tabor, Friction and Lubrications of Solids: Part II (Oxford University Press, 1964).
9. Fundamentals of friction: Macroscopic and Microscopic Processes, edited by I. L. Singer and H.M. Pollock (Kluwer, Dordrecht, 1992).
10. Workshop on Friction, Arching, Contact Dynamics, edited by D.E. Wolf and P. Grassberger (World Scientific, Singapore, 1997).
11. J. Krim, Am. J. Phys. 70, 890 (2002); and references therein.
12. J.F. Belak (Guest Editor), MRS Bull. 18, 15 (1993).
13. B. Bushan, J.N. Israelachvili, and U. Landman, Nature 374, 607 (1995).
14. Handbook of Micro/Nanotribology, edited by B.Bhushan (CRC Press, Boca Raton, 1995).
15. J.N. Israelachvili, P.M. McGuiggan, and A.M. Homola, Science 240, 189 (1988).
16. J. Krim, D.H. Solina, and R. Chiarello, Phys. Rev. Lett. 66, 181 (1991).
17. G. Binnig, C.F. Quate, and Ch. Gerber, Phys. Rev. Lett 56, 930 (1986).
18. C.M. Mate, G.M. McClelland, R. Erlandsson, and S. Chiang, Phys. Rev. Lett. 59, 1942 (1987).
19. N.Agraït G. Rubio, and S. Vieira, Phys. Rev. Lett. 74, 3995 (1994).
20. Adhesion, Friction and Lubrication of Molecularly Smooth Surfaces, by J.N. Israelachvili in [9], pp. 351-385.
21. J. Krim and A. Widim, Phys. Rev. B 38, 12184 (1988).
22. J. Krim, D.H. Solina, and R. Chiarello, Phys. Rev. Lett. 66, 181 (1991).
23. M. Weiss and F.-J. Elmer, Phys. Rev. B 53, 7539 (1996).
24. T. Gyalog and D.W. Brenner, in reference [1], p. 403.
25. J.A. Harrison and D.W. Brenner, in reference [14], p. 397.
26. U. Landman, W.D. Luedtke, and M.W. Ribarsky, J. Vac. Sci. Technol. A 7, 2829 (1989).
27. J.N. Glosli and G.M. McClelland, Phys. Rev. Lett. 70, 1960 (1993).
28. M. Cieplak, E.D. Smith, and M.O. Robbins, Science 265, 1209 (1994).
29. C. Molteni, G.P. Francis, M.C. Payne, and V. Heine, Phys. Rev. Lett. 76, 1284 (1996).

30. J.A. Harrison, S.J. Stuart, D.H. Robertson, and C.T. White, *J. Phys. Chem. B* 101, 9682 (1997).
31. J. Colchero, M. Luna, and A.M. Baro, *Appl. Phys. Lett* 68, 2896 (1996).
32. K. L. Johnson, *Contact Mechanics* (University Press, Cambridge, 1987).
33. H. Hertz, *J. Reine Angew. Math.* 92, 156 (1881).
34. K.L. Johnson, K. Kendall, and A.D. Roberts, *Proc. Roy. Soc. Lond. A* 324, 301, (1971).
35. B.V. Derjaguin, V.M. Muller, and Y.P. Toporov, *J. Colloid Interface Sci.* 53, 314 (1975).
36. D. Maugis, *J. Colloid Interface Sci.* 150, 243 (1992).
37. R.W. Carpick and M. Salmeron, *Chem. Rev.* 97, 1163 (1997), and references therein.
38. E. Gnecco, R. Bennewitz, T. Gyalog and E. Meyer, *J. Phys.: Condens. Matter* 13, R619 (2001), and references therein.
39. Enachescu, R.W. Carpick, D.F. Ogletree, M. Salmeron, *J. Appl. Phys.* 95, 7694, (2004).
40. S. Fujisawa, Y. Sugawara, S. Iti, S. Nishima, T. Okada, and S. Morita, *Nanotechnology* 4, 138 (1993).
41. S. Morita, S. Fujisawa, and Y. Sugawara, *Surf. Science Rep.* 23, 3 (1996).
42. L. Howald, R. Lüthi, E. Meyer, and H.-J. Güntherodt, *Phys. Rev. B* 51, 5484 (1995).
43. S. Fujisawa, Y. Sugawara, and S. Morita, *Philos. Mag. A* 74, 1329 (1996).
44. M. Enachescu, R.J.A. van Oetelaar, R.W. Carpick, D.F. Ogletree, C.F.J. Flipse, and M. Salmeron, *Phys. Rev. Lett.* 81, 1887 (1998).
45. D.F. Ogletree, R.W. Carpick and M. Salmeron, *Rev. Sci. Instrum.* 67, 3298 (1996).
46. U.D. Schwarz, P. Köster, and R. Wiesendanger, *Rev. Sci. Instrum.* 67, 2560 (1996).
47. R.W. Carpick, *The Study of Contact, Adhesion and Friction at the Atomic Scale by Atomic Force Microscopy*, Ph.D. Thesis (University of California, Berkeley, December 1997), chapt. 4.
48. P.E. Sheenan and C.M. Lieber, *Science* 272, 1158 (1996).
49. U.D. Schwarz, H. Bluhm, H. Hölscher, W. Allers, and R. Wiesendanger, in reference [1], p. 369.
50. M. Liley, D. Gourdon, D. Stamou, U. Meseth, T.M. Fischer, C. Lantz, H. Stahlberg, H. Vogel, N.A. Burnham, and C. Duschl, *Science* 280, 273 (1998).
51. M.R. Sørensen, K.W. Jacobsen, and P. Stolze, *Phys. Rev. B* 53, 2101 (1996).
52. M. Hirano, K. Shinjo, R. Kaneko, and Y. Murata, *Phys. Rev. Lett.* 78, 1448 (1997).
53. J.S. Ko and A.J. Gellman, *Langmuir* 16, 8343 (2000).
54. M.R. Falvo, R.M. Taylor, A. Helsen, V. Chi., F.P. Brooks, S. Washburn, and R. Superfine, *Nature* 397, 236 (1999).
55. M.R. Falvo, J. Steele, R.M. Taylor and R. Superfine, *Phys. Rev. B* 62, R10665 (2000).
56. M. Dienwiebel, G.S. Verhoeven, N. Pradeep, J.W.M. Frenken, J.A. Heimberg, and H.W. Zandbergen, *Phys. Rev. Lett.* 92, 126101 (2004).

57. J. Krim and R. Chiarello, *J. Vac. Sci. Technol. A* 9, 2566 (1991).
58. M. Cieplak, E.D. Smith, and M.O. Robbins, *Science* 265, 1209, (1994).
59. B.N.J. Persson and A.I. Volokitin, *J. Chem. Phys.* 103, 8679 (1995).
60. R.J.A. van den Oetelaar and C.F.J. Flipse, *Surf. Sci. Lett.* 384, L828 (1997).
61. A. Socoliuc, E. Gnecco, R. Bennewitz, and E. Meyer, *Phys. Rev. B* 68, 115416 (2003).



# Chapter 2. Experimental

## 2.1. Atomic Force Microscopy: unique tool for nanotribology

The invention of the atomic force microscope (AFM) just shortly after scanning tunneling microscopy (STM) was developed [1] represented a new milestone in the field of surface science techniques. The unique combination of the mechanical precision of piezoelectric materials and the optical sensitivity of lasers opened completely new horizons: instead of current, the force between a small sharp tip and a particular surface could be measured with *atomic resolution* [2]. A whole new class of technologically essential materials, namely large band gap semiconductors and insulators could now be investigated, since sample conductivity was not required anymore. The remarkable force sensitivity of such a “single asperity” method revealed information about sample topography, crystalline periodicities, adhesion, friction and wear.

In a standard contact-mode atomic force microscope measurement, a small sharp tip attached to a compliant cantilever is brought in the vicinity of the surface to be investigated. Due to adhesion forces the tip will jump into contact, leading to a initial normal bending of the cantilever. Then the tip is shifted (raster movement) across the sample surfaces. Normal forces acting on the tip will deflect the cantilever up or down while the lateral ones (i.e. friction) will tend to twist (torsion) the cantilever (as shown in Fig. 2.1)

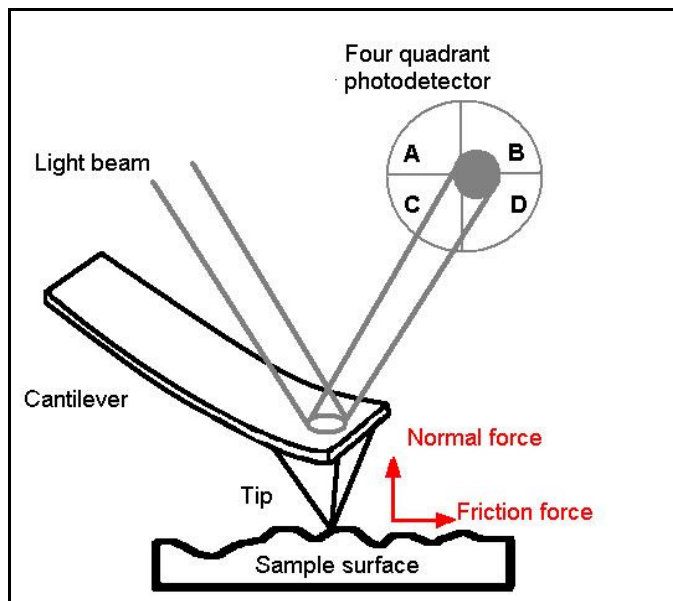


**Fig.2.1** Typical optical beam bounce AFM method.

The first AFM experiments measured the topography of a sample surface by maintaining a constant repulsive force between the contacting sample and tip while scanning [2]. The normal bending of the cantilever was monitored by placing a scanning tunneling microscope (STM) tip above the cantilever backside, which was metalized. Although STM can be very sensitive to distance variations, this way of analyzing the deflections had several disadvantages. Positioning the tunneling tip in alignment with the end of cantilever is very difficult. Also deflections of the cantilever can lead to a shift in the position of the tip on the backside of the cantilever; the roughness of the backside surface combined with the lateral movement produces a non-linear deflection signal. Moreover, the tunneling tip exerts forces on the cantilevers and therefore it is practically impossible to make a clear distinction between forces caused by cantilever-sample and cantilever-tunneling interactions.

Within the following years, new designs [3,4] proposed optical (interferometer, beam-deflection) or electrical methods (piezoelectric, piezoresistive) for measuring the cantilever deflections. One of the most notable improvements in the AFM capabilities was the detection of the lateral forces acting on the tip, first realized by Mate *et al.* [5]. Using a tungsten tip on a graphite sample under ambient conditions, a frictional (lateral) force signal varying with the graphite lattice periodicity was observed. It was the result that proved the versatility of this technique to extent the tribological study down to the atomic scale.

When topography and lateral (friction) forces are simultaneously recorded, the AFM is referred to as FFM (friction force microscope) and the optical deflection method [6-8] has proven to be preferred by all commercially available instruments and several custom designs [9-10] due to its simplicity. A light beam is focused on the reflective backside of the flexible lever and gets reflected onto a split (four-quadrant) photodetector (Fig. 2.1). The difference between the signals collected from the upper and lower halves of the detector is proportional to the normal (vertical) bending of the cantilever, while a measure of the lateral deflection is obtained from the difference between the right and left halves. The beam bounce method makes in fact use of the angle by which the cantilever is bent by the forces acting on the tip; for small angles this is linearly proportional to the tip deflections. Silicon and silicon nitride microfabricated cantilevers are the most commonly used, being commercially available. They are fabricated with a variety of force constants (0.01-100 N/m), having high resonance frequencies and small sharp integrated tips. Various coatings are also available for the cantilever tips [11-13]. Other specially designed tips, such as chemically etched tips [5], parallel leaf-spring assemblies [14] with diamond tips and tips held by double cross-hair force sensors [15] are in use, allowing further choice of tip materials.

AFM is without any doubt one of the most versatile scanning probe microscopy tools in terms of operating environment: ambient conditions, controlled atmosphere, liquids [16] or ultra-high vacuum [6, 17-19]. AFM can measure forces in two different regimes, depending on the forces experienced by the tip when approaching the sample surface: the

“attractive regime”, where interaction forces between tip/sample (electrostatic, van der Waals) are attractive, but no real mechanical contact occurs and the “contact regime” or “repulsive regime” where the outer electronic configuration of the contacting surfaces’ atoms cause electrostatic and Pauli repulsive forces (the latest used in contact-mode AFM or FFM).

Surface topography can be measured in the following way: as the tip is rastered across the sample, a feedback circuit maintains a constant normal force by varying the relative vertical displacement; the tip will follow the relief of the surface. These “constant force images” can be achieved in both attractive and repulsive regime. Several other methods (AC modulation techniques) have emerged and are designed to image in the attractive regime. The so-called dynamic operation (amplitude- and frequency- modulated) AFM techniques, in which a cantilever is deliberately vibrated, have achieved remarkable performances resolving true atomic resolution on various materials [20], but these techniques will not be discussed here, as they cannot be used for friction experiments.

## **2.2. Experiments under well defined conditions: the Omicron UHV VT-AFM setup**

The necessity of performing nanotribological measurements under reproducible and well-defined conditions is obvious. In the beginning of the AFM era, most of the experiments were performed in air, under atmospheric conditions and therefore the reproducibility of the measurements had to pay the price. For example, the relative humidity of the experimental environment can be extremely important; liquid films condensed onto the tip end from ambient vapors, or already present at the sample surface, can form a meniscus and act as a lubricant layer. Several authors [21-23] have proved how critical capillary condensation of water and changes in the relative humidity can be on the measured tribological properties. Moreover, obtaining and maintaining a really clean and well-defined sample surface for further analysis is almost impossible to imagine in air, since contamination effects will also affect friction and adhesion. Therefore UHV is a “must” for all the surface science techniques aiming at atomic-scale resolution for the properties under investigation. Along with stable and reproducible experiments, UHV-conditions could enable further *in-situ* cleaning procedures for both sample and tip and structural surface analysis (i.e. by means of low-energy-electron diffraction, LEED).

All the measurements presented in chapters 4, 5 and 6 were done with an Omicron ultra-high-vacuum (UHV) variable-temperature (VT) Beam Deflection AFM [24].

In spite of the simple name (AFM), due to a flexible design, this microscope allows contact-mode AFM, non-contact mode AFM and STM to be operated on the same machine; the testing of the home-made diamond-coated tips (chapter 3) was also performed in vacuum with the same microscope. The next paragraph will give an overview on the experimental setup, starting with a description of the AFM stage and then going through the vacuum system and experimental facilities.



### 2.3. The Omicron UHV VT-AFM setup

Omicron has developed the Variable Temperature AFM (VT Beam Deflection AFM) as a tool that combines sample cooling/heating facilities with reliable vibration isolation, straightforward tip/sample handling and high scan resolution.

A side view of the VT beam Deflection AFM is shown in Fig.2.2. Within this design of the microscope, the sample can be cooled or heated separately as the microscope stage remains at a constant temperature, very close to room temperature. Heating and cooling cycles can be much shorter compared to design solutions requiring a cryostat enclosing the whole scanning probe microscope. Considering the limited (small) thermal mass of the sample/sample plate with respect to the whole stage, the microscope will reach its thermal equilibrium conditions relatively fast. Due to a feasible combination of cooling and direct and /or resistive heating the microscope provides a large temperature range from 25 to 1500 K. Low temperatures (typically less than 25 K) are achieved using a liquid helium (LHe) continuous flow cryostat.

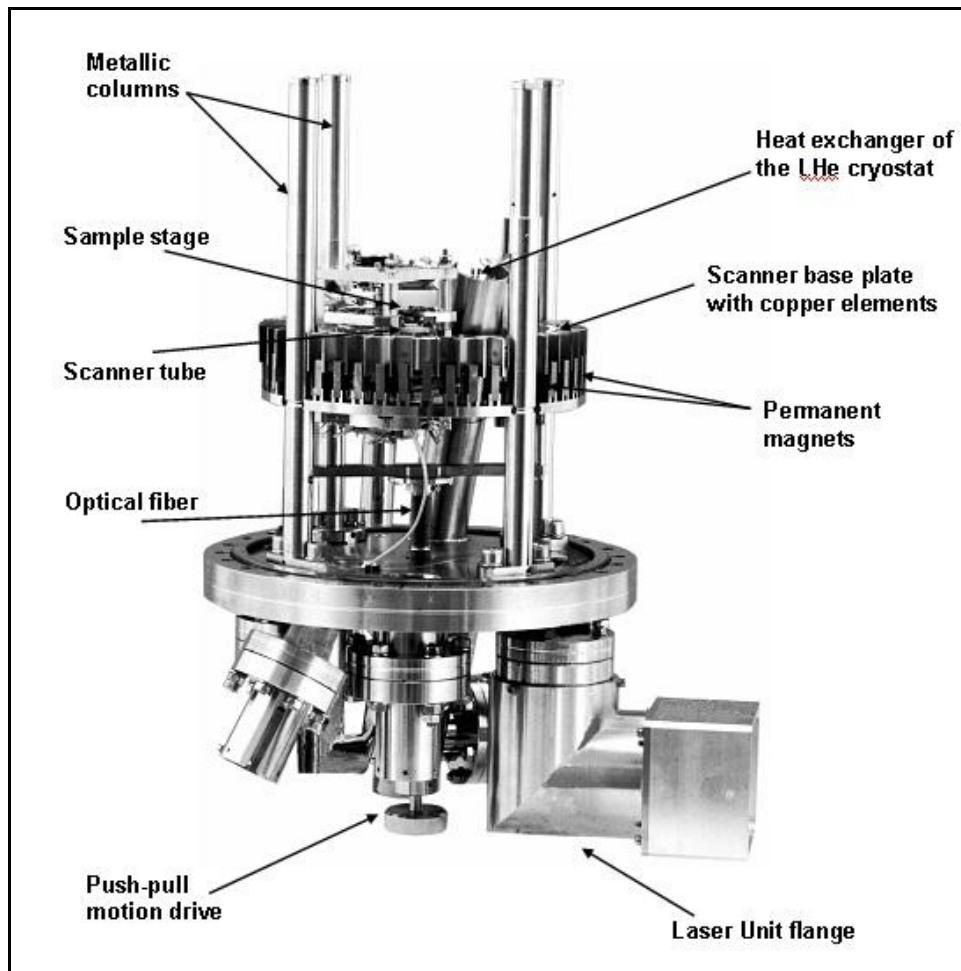


**Fig. 2.2** Side view of the 25 K VT Beam Deflection AFM

For an atomic-resolution scanning probe microscopy a high quality vibration decoupling system is essential. The AFM base plate is suspended by four soft springs which are protected by surrounding metallic columns. Such a spring suspension system has a resonant frequency of approximately 2 Hz. The vibrations of the suspension system are intercepted using a nearly non-periodic eddy current damping mechanism: a ring of copper plates is mounted at the lower end of the AFM base plate, coming down between an arrangement of permanent magnets fixed at the columns of the spring suspension. This system successfully damps excursions in all directions. The scanner base plate/spring suspension stage can be locked using a push-pull motion drive (PPM), when adjustments or sample/tip exchange (by means of a wobble stick) are required.

The cryostat is fixed to the base flange with the heat exchanger of the LHe flow cryostat projecting through the microscope base plate. Using a highly flexible copper braid the thermal connection between the cryostat and the sample is realized. The vibration input through the copper braid is minimized using a special decoupling stage. Special measures were taken to prevent that heat radiation from the hot sample slowly warms up the scanner tube, which would result in a long term drift; therefore a small but very effective shield is fitted to the top of the scanner. Both the sample plate and the sample stage are designed so that the surface of the sample is the reference plane for any thermal expansion or contraction. This allows keeping the distance between tip and sample surface practically unchanged even when in the process of cooling or heating.

In this UHV-VT AFM version the sample rests in a fixed position during operation, while the AFM/STM tip is scanned across the surface. A single tube scanner with a maximum scan range of about  $10\ \mu\text{m} \times 10\ \mu\text{m}$  and a travel of about  $1.5\ \mu\text{m}$  is used. In the Z direction a resolution better than 0.01 nm is typically achieved. (See Fig. 2.3).

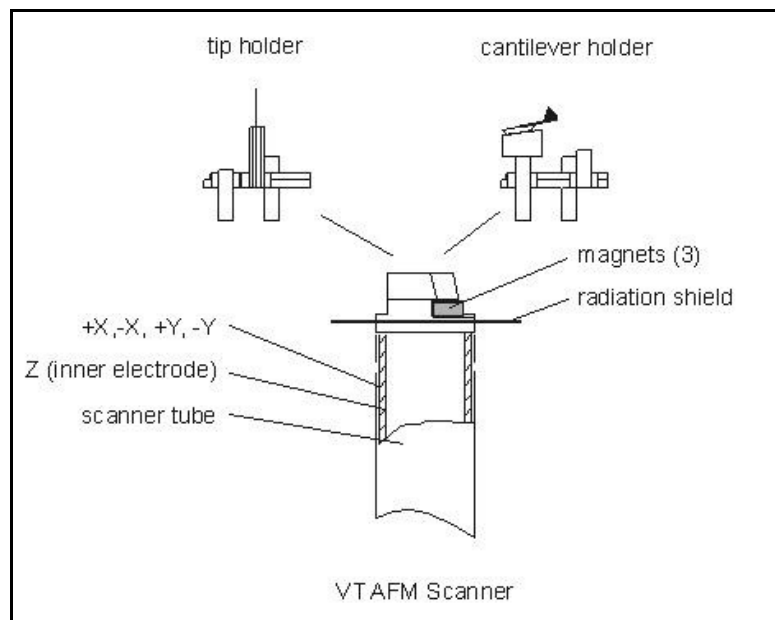


**Fig.2.3** The VT Beam Deflection AFM scanner electrical contacts.

The scanner is positioned with a 3-axes linear piezo motor, using slip/stick effects related to inertia forces when a piezo is driven in a fast/slow sequence. The sliders are magnetically coupled to three shear piezos which are driven with a sawtooth voltage input. The sliders are transported during the slow movement of the piezo and slip during the fast piezo motion due to their inertia. The optical detection system of the VT-AFM is designed to measure the bending or torsion of the cantilever by detecting the deflection of a reflected light beam onto a four-quadrant position-sensitive-detector PSD. The source of light is an infrared laser ( $\lambda = 830 \text{ nm}$ ); therefore a CCD camera is used to visualize and align the light beam. The light beam is generated in the Laser Unit connected to the Laser Unit flange. As shown in Fig. 2.4, via an optical fiber, the light is passed on through the base flange and up to the microscope stage. The beam towards the cantilever (the primary beam) can be positioned in x-direction using a small micro-slide and in y-direction using a rotatable mirror. The secondary beam (coming from the cantilever) will again encounter the y-direction rotatable mirror and an extra adjustable mirror LPSD which optimizes the position of the light onto the four-quadrant PSD. All beam positioning/adjustment elements are mounted on the coarse positioning drive and thus move along with it.

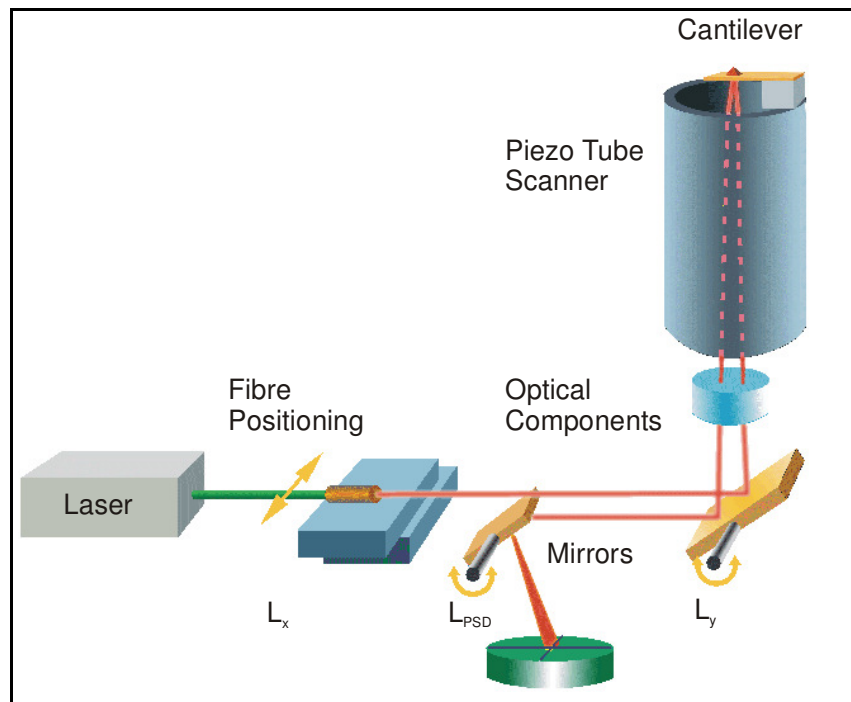


**Fig. 2.4** VT - AFM Optical detection system schematics.

The AFM/STM head is integrated in an UHV setup depicted in Fig. 2.5. The UHV system has four different chambers. The low energy electrons diffraction (LEED) chamber and the microscope (VT-AFM) chamber are connected to each other, but closed from the other two (preparation and fast entry chambers, separated in between) by means of valves.

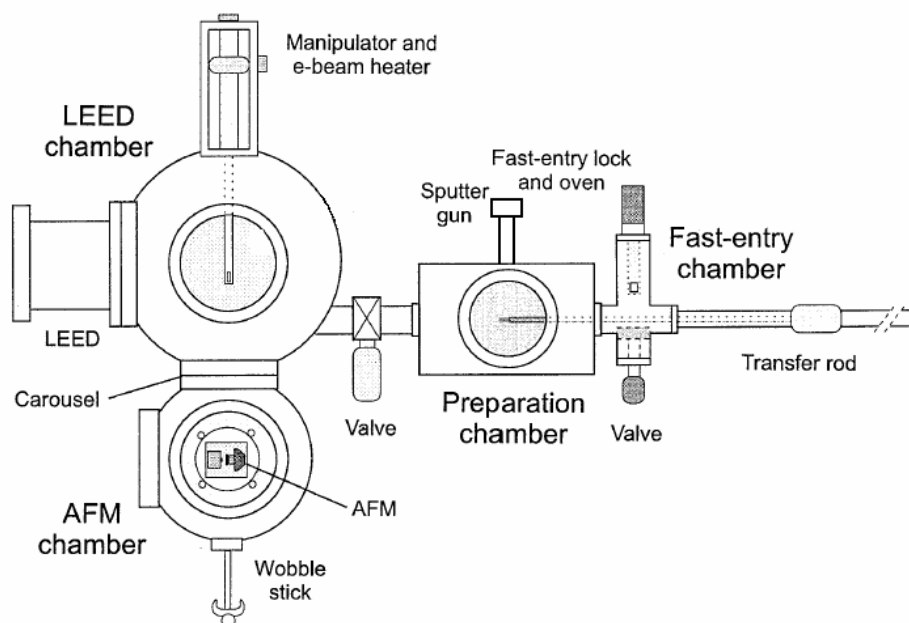


**Fig. 2.5** UHV setup general top-view

The ultra-high vacuum in the system is achieved and maintained with two ion pumps, two turbo pumps and two titanium sublimation pumps; the resulting base pressure is  $4 \times 10^{-11}$  mbar in the LEED/AFM chambers and better than  $10^{-10}$  mbar in the preparation chamber. Samples can be cleaned, annealed or sputtered in-situ; moreover, the chambers are provided with several ports/flanges which can be utilized to add to the system various facilities (for example residual gas analyzers (RGA) or mass spectrometers, deposition sources). A fast transfer of samples/tips into the system from air without breaking the vacuum is made possible via a small-volume fast-entry chamber which is quickly pumped down to high vacuum (within 30 minutes) with a rotary pump and a small turbo-molecular pump. A transfer rod collects the sample/tip and transfers it through the preparation chamber into the LEED chamber. The sample/tip can be inserted and clamped onto a manipulator; from there it can further moved with a wobble stick to the microscope or stored in a rotatable carousel, having a total capacity of twelve samples/tips.

## References:

1. G. Binnig, H. Rohrer, Ch. Gerber, and E. Weibel, Phys. Rev. Lett. 49, 57 (1982); Phys. Rev. Lett. 50, 120 (1983)
2. G. Binnig, C.F. Quate, and Ch. Gerber, Phys. Rev. Lett. 56, 930 (1986).
3. D. Sarid, Scanning Force Microscopy, 2<sup>nd</sup> ed. ( Oxford University Press, New York, 1994).
4. M. Tortonese, R.C. Barret, and C. Quate, Appl. Phys. Lett. 62, 834, 1993.
5. C.M. Mate, G.M. McClelland, R. Erlandsson, and S. Chiang, Phys. Rev. Lett. 59, 1942 (1987).
6. G. Meyer and N.M. Amer, Appl. Phys. Lett. 56, 2100 (1990).
7. S. Alexander, L. Hellemans, O. Marti, J. Schneir, V. Elings, P.K. Hansma, M. Longmire, and J. Gurley, J. Appl. Phys. 65, 164 (1989).
8. O. Marti, J. Colchero, and J. Mlynek, Nanotechnology 1, 141 (1991).
9. W.F. Kolbe, D.F. Ogletree, and M.B. Salmeron, Ultramicroscopy 42-44B, 1113 (1992).
10. Q. Dai, R. Vollmer, R.W. Carpick, D.F. Ogletree, and M. Salmeron, Rev. Sci. Instrum. 66, 5266 (1995).
11. Veeco Metrology Group, Sunnyvale, USA.
12. NT-MDT Inc., Moscow, Russia.
13. Nanosensors GmbH, Aidlingen, Germany.
14. C.-J. Lu, Z. Jiang, D.B. Bogy, and T. Miyamoto, Trans. ASME J. Tribology 117, 244 (1995).
15. M. Enachescu, S.A. Smallwood, R.J. Lad, and W.N. Unertl (in preparation).
16. O. Marti, B. Drake, and P.K. Hansma, Appl. Phys. Lett, 62, 834 (1993).
17. G.J. Germann, S.R. Cohen, G. Neubauer, G.M. Mc.Clelland, H. Seki, and D. Coulman, J. Appl. Phys. 73, 163 (1993).
18. L. Howald, E. Meyer, R. Luthi, H. Haefke, R. Overney, H. Rudin, and H.-J. Guntherodt, Appl. Phys. Lett. 63, 117 (1993).
19. M. Kageshima, H. Yamada, K. Nakayama, H. Sakama, A. Kawau, T. Fujii, and M. Suzuki, J. Vac. Sci. Technol. B 11, 1987 (1993).
20. F. J. Giessibl, Rev. Mod. Phys. 75, 949, (2003).
21. M. Binggeli and C.M. Mate, Appl. Phys. Lett. 65, 415 (1994).
22. J. Hu, X.D. Xiao, D.F. Ogletree and M. Salmeron, Surf. Sci. 327, 358 (1995).
23. L. Xu, H. Bluhm and M. Salmeron, Appl. Phys. Lett. 66, 3221 (1995).
24. Omicron NanoTechnology GmbH, Taunusstein, Germany.

# Chapter 3. Chemical vapor deposition on silicon substrates: Making diamond-terminated AFM tips

## 3.1. Introduction

AFM experiments on well-defined surfaces show that wearless friction is possible and, moreover, the classical law of friction is not valid anymore for contact areas in the range of several square nanometers [1-4]. Unfortunately, the tips of the standard silicon or silicon nitride cantilevers often get damaged either due to snapping into contact or scanning with increasing load. Therefore the results of friction experiments are affected by uncertain parameters, which cannot be accounted for by a simple model. Dealing with an “ideal” model system, single-crystalline sample and tip with known and stable characteristics should be used. The use of hard materials, such as diamond, for friction experiments on the nanometer scale could provide a stable small contact area during sliding. Diamond surfaces and diamond-coated substrates have been under intensive investigation for macroscopic tribology [5,6] but only a few reports concerning the nanometer-scale friction on this material can be found [3,4,7].

In earlier approaches, hard tips for AFM and STM were fabricated from bulk diamond by fracturing, grinding or polishing [8-10]. The developments in the field of chemical vapor deposition (CVD) techniques provided a very flexible tool for obtaining diamond layers and micro-crystals with a large range of sizes and properties [5,6]. Compared to other methods, for example the high-pressure-high-temperature method (HPHT), the crystallites can be deposited on a wide range of materials, like Si, Mo and Cr, with more or less complex shapes. For instance, individual diamond crystals or films were deposited on etched tungsten wires, silicon whiskers and tips to be used for SPM and field emission experiments [11-13]. Methods based on a moulding technique were also proposed for creating all-diamond or silicon cantilevers tips with very sharp diamond termination [14-16].

This chapter presents a method of growing individual diamond polycrystallites on the apex of a standard AFM cantilever tip. First, the optimal conditions of the CVD synthesis were investigated in order to obtain a preferential nucleation of diamond grains on the edges and tops of pyramids obtained by wet chemical etching of single-crystalline silicon substrates. Using this information diamond growth at the very apex of the silicon tips of commercially available AFM cantilevers was demonstrated. Raman spectroscopy as well as scanning electron microscopy (SEM) reveals information about the structure, quality and shape of the deposited diamond. The resulting cantilevers have been used in friction-mode AFM experiments and showed a reliable behavior of the diamond-terminated tips.

### 3.2. Experimental procedure

Prior to the CVD deposition on real AFM cantilevers, we studied the nucleation and growth of diamond crystallites on specially fabricated silicon substrates having an array of pyramidal hillocks in order to find the best conditions of deposition. The point-topped pyramids were obtained by wet chemical etching of polished (100) silicon plates in aqueous KOH solutions [17-20]. The set-up used for etching the silicon substrates consisted of thermo stated ( $\pm 1$  °C) small Teflon beakers containing the KOH etching solutions. The samples used in these experiments were p-type boron doped (100) Si wafers (14 –22 ohm\*cm). Before etching, the samples were chemically cleaned using an HF dip and subsequent rinsing in deionised water. Then, the surface of the Si substrate was scratched using a diamond scribing tool, after which the silicon surface displayed a net of parallel, equidistant scratched lines in two perpendicular directions. The distance between two neighboring lines varied from 0.2 to 0.8 mm. The aqueous KOH etchant solutions had concentrations between 20 wt% and 40 wt%. Etching was carried out for a period of 60-180 minutes at temperatures between 70-90 °C. After the chemical etching, the samples were rinsed using deionised water.

Diamond deposition was carried out in a conventional hot-filament-assisted CVD reactor as described elsewhere [21]. In all deposition runs, the substrate temperature was fixed at 750 °C for deposition times in the range of 1-6 hours. The TaC filament temperature was kept constant at  $2100 \pm 20$  °C as measured with an optical pyrometer. The CH<sub>4</sub>:H<sub>2</sub> volume ratio was fixed at 0.5%, keeping the total pressure in the range of 50-60 mbar and the total flow rate at 300 standard cm<sup>3</sup> min<sup>-1</sup>. The pre-treated/etched Si wafers (1.5×1.5 cm<sup>2</sup>) were used as substrates.

When the best conditions for CVD deposition on etched Si pyramids were found, hot-filament-assisted chemical vapor deposition (HF-CVD) runs have been performed on commercially available Si AFM tips. Silicon chips (NSC 12 series, MikroMasch) [22] with 6 rectangular cantilevers were used. All cantilevers have an Al coating on the backside for better reflectivity. The three longer cantilevers of the set are suitable for friction (lateral) force measurements. In the HF-CVD reactor, the chips containing the Si cantilevers were placed on small sapphire plates in order to provide a good heat transfer. In all runs, the above-mentioned deposition parameters were kept unchanged except for the deposition duration of 4 hours, which was found to be the most suitable. In order to enhance diamond nucleation, prior to the deposition run some of the silicon chips were immersed in a suspension consisting of ethyl alcohol and diamond powder (4-6 microns grid size) for 3 minutes. Moreover, a few of them were ultrasonically shaken in the suspension for 30-60 seconds. The results for the two types of “seeded” tips were compared to those obtained for the untreated cantilevers. Micro-Raman spectroscopy was performed using an Ar<sup>+</sup> ion laser (514.5 nm) with an output power of 50 mW and a focused laser beam diameter of about 2 μm (Renishaw System 1000). The Raman spectra were taken in the 900-2400 cm<sup>-1</sup> range, selecting the investigated deposits by optical microscopy. The shape, microstructure and distribution of the diamond grains on the Si substrate were determined by means of SEM (Philips XL 30 ESEM FEG). It is known that the electron beam used in the SEM technique can deposit thin carbon contamination

layers or even graphitise the diamond slightly; therefore Raman measurements were performed before investigating the sizes and shapes of the deposited crystals by means of SEM.

The diamond-terminated AFM tips obtained in the above-mentioned way were tested using an Omicron Variable Temperature – Ultra High Vacuum (VT-UHV) AFM-STM. As object a stepped (0001) sapphire substrate was used and topographic, normal force and lateral (friction) force maps were recorded in contact-mode AFM. The base pressure inside the chamber was  $4 \times 10^{-11}$  mbar and all the measurements were carried out at room temperature.

### **3.3. Results and discussion**

#### **3.3.1. Morphology of diamond deposits on etched silicon pyramids**

After chemical etching of the scratched Si wafers, SEM images of the samples display a uniform distribution of square-based pyramids with sharp facet edges and apexes (Fig.3.1). The size of the square base is about  $100 \times 100 \mu\text{m}^2$ , after 2 hours of etching.

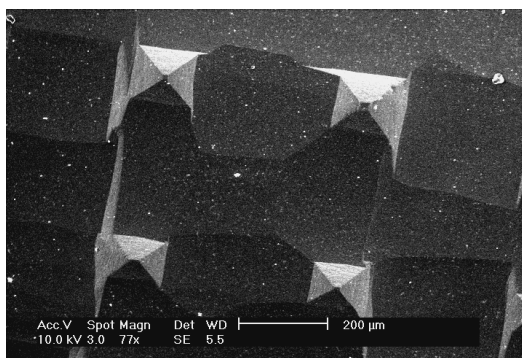


**Fig.3.1.** SEM image of the pyramids obtained after wet chemical etching in aqueous KOH solution

The average distance between the bases of two neighboring pyramids is approximately 300 micrometers and the density of pyramids is in the order of 400-450 pyramids / $\text{cm}^2$ . When increasing the period of etching, the pyramid shape becomes less sharp and the distribution of the elevations on the silicon surface is not homogeneous anymore. It was observed that the etching parameters are not necessarily uniquely defined. For instance, a specific size and shape of the pyramids could be achieved using a specific etchant concentration and duration, but the same result can be obtained by performing the etching using a higher etchant solution concentration, but for a shorter period.



On the pre-treated /etched Si wafers diamond deposition runs using hot-filament-assisted CVD have been performed. SEM images of samples corresponding to a deposition time of less than 2 hours do not show diamond grains on the silicon pyramid apexes. After 4 hours of deposition, most of the pyramids exhibit a large number (100-150) of small crystals on the apexes and edges. (Fig.3.2.a.) The size of the grains varied between 1 and 3 micrometers. Most of the grains are polycrystalline and show a spherical or blunted shape. Nevertheless single crystalline or twinned diamond particles could also be observed in about 20% of the cases. (Fig.3.2.b.)

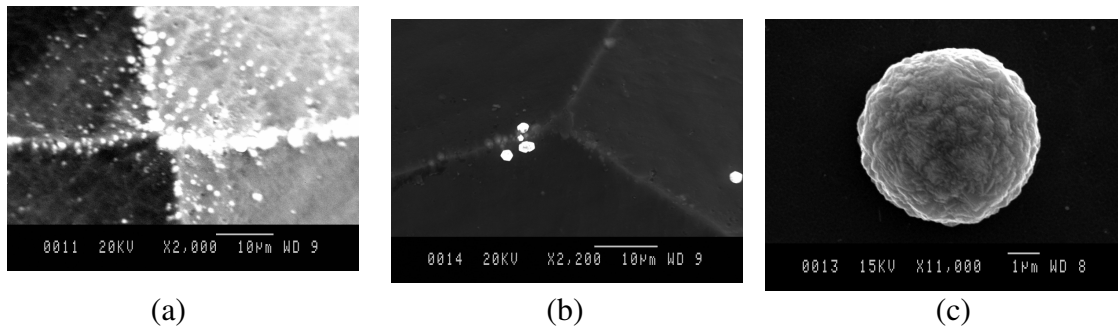


**Fig.3.2.** SEM images showing deposited grains on the top and facet edges of the Si etch pyramids. (a) Large number of diamond particles on the edges and apex of a pyramid; (b) A few isolated crystals near to pyramid tip; (c) High magnification micrograph showing the ball-shaped nature of many diamond polycrystallites

For deposition times between 4 and 6 hours, SEM and optical microscope images show the presence of crystallites on the edges and the apexes of the pyramids in 20-25% of the cases. The size of the poly-crystals was in the order of 5-6 micrometers and the spherical shape was more or less similar for all the deposits (Fig.3.2.c.). The microstructure of the grown particles is poly-crystalline, with sizes of the grains ranging from 5 to tens of nanometers. This type of ball-shaped crystallites is typical for CVD growth conditions of higher carbon supersaturation.[23]

To investigate the quality and structure of the deposited particles, further investigations using micro-Raman spectroscopy were carried out. This analysis technique is suitable, because it can distinguish clearly between diamond, graphitic and other carbon phases. Another important reason is the spatial resolution (focused laser beam diameter of about 2 µm), which is comparable to the sizes of the deposited elements on the substrate. Raman spectroscopy is very sensitive in distinguishing the different forms of crystalline and amorphous carbon. Raman spectra of stress-free, crystalline diamond show a single, sharp line at 1332  $\text{cm}^{-1}$ . Graphitic carbon gives two peaks: the so-called G peak centered at 1550  $\text{cm}^{-1}$  is the Raman line of a perfect graphite crystal, while the so-called D peak centered on at 1350  $\text{cm}^{-1}$  indicates disorder. The D mode is a common characteristic of all

disordered graphitic carbons (coals, glassy carbon, etc) which intensity relative to the  $1550\text{ cm}^{-1}$  peak, varies inversely with the size of the graphitic microstructures [6, 24-30] Finally, amorphous carbon generally gives a broad band centered on about  $1500\text{ cm}^{-1}$ .

The investigated deposits were selected by using the optical microscope fitted with the Raman spectrometer. Then, the laser light was focused on small crystals having various sizes and positions on the silicon substrate. It is known that the electron beam used in SEM technique can easily graphitise the diamond; therefore Raman measurements were performed before investigating the sizes and shapes of the deposited crystals by means of SEM. The typical Raman spectra of the deposited crystallites exhibit a sharp diamond peak positioned between  $1332.8$  and  $1336.4\text{ cm}^{-1}$  with full width at half maximum (FWHM) values between  $15$  and  $20\text{ cm}^{-1}$  (Fig. 3.3.) A broad band (approx.  $200\text{ cm}^{-1}$ ) corresponding to non-diamond forms of carbon ( $\text{sp}^2$ -bonded), centred on  $1552\text{ cm}^{-1}$  is present as well. The height ratio of the diamond peak to this band varies between  $1.1$  and  $1.9$ . Considering the large Raman scattering cross-section [27] for  $\text{sp}^2$  carbon bonds as compared to diamond, these values show good quality diamond and the presence of a small amount of other carbon phases.

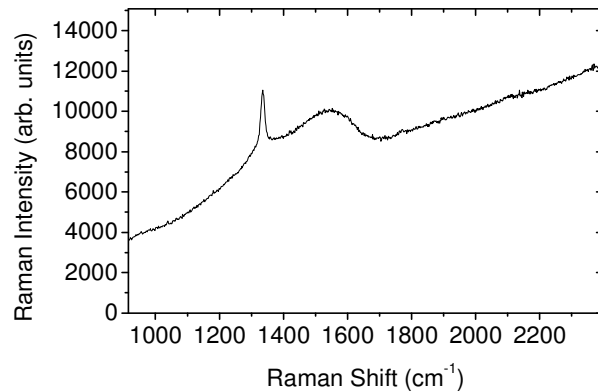
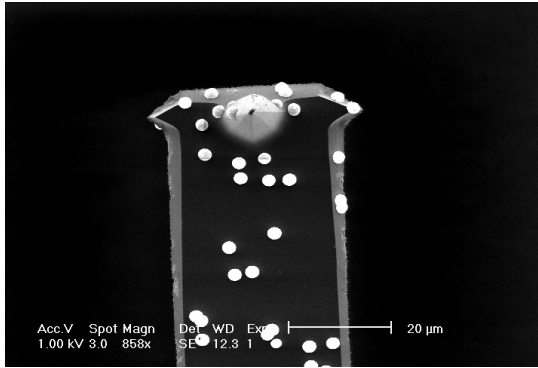


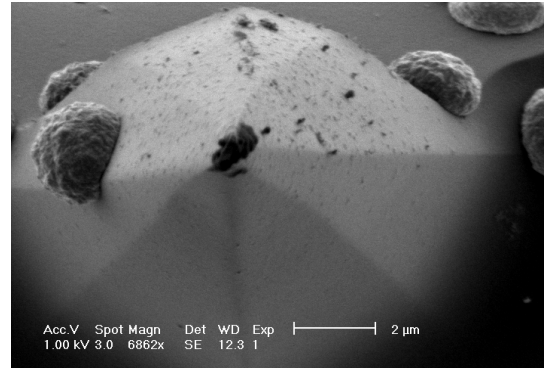
**Fig.3.3.** Typical Raman spectrum of the deposited crystallites on the etched silicon substrates

### 3.3.2. Diamond deposition on standard silicon tips

After finding the appropriate deposition parameters, diamond was grown on standard silicon tips. Deposition runs of 4 hours were carried out in all cases. As a general feature, optical microscopy and SEM pictures reveal the tendency of the crystals to grow on the apexes and edges of the pyramidal tips as well as on the edges of the rectangular cantilevers. (Fig.3.4-3.6). However, for the untreated chips and those that were seeded by immersion in a diamond powder/ethanol suspension, the results were unsatisfactory. On the other hand, for the chips that have been ultrasonically shaken in the diamond suspension, the number of the grown crystals is much larger than on the non-pretreated ones. Moreover, in this case 80-90% of the pyramidal Si tips contain a diamond crystal at the very apex. (Fig.3.6)



(a)



(b)

**Fig.3.4.** Diamond growth on standard Si tips without pre-treatment. (a) Overview showing cantilever plus tip; (b) Detail of tip; the black spot at the tip is not diamond but contamination.

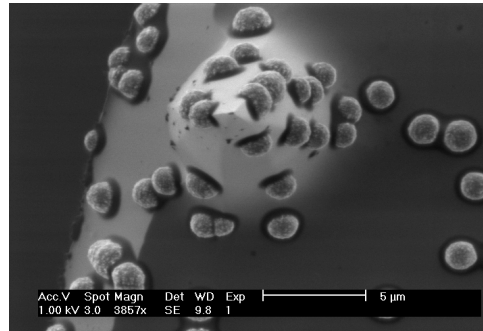


**Fig.3.5.** Deposition after seeding the standard Si tips by immersing in diamond powder/ethanol suspension, leads to an enhanced density of diamond nuclei.

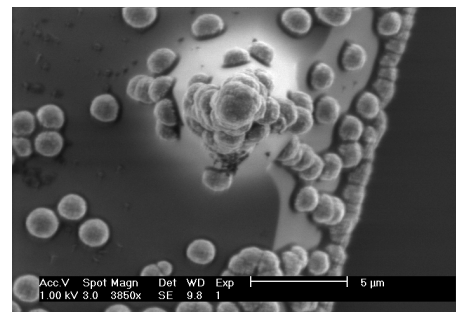
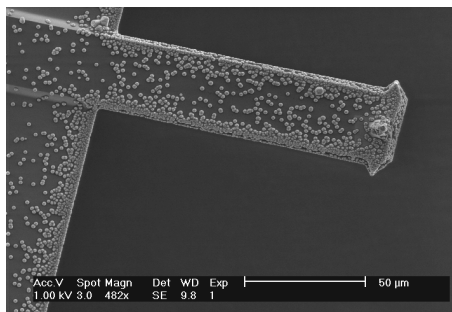


**Fig.3.6.** After ultrasonic shaking in the diamond/ethanol suspension a higher density of crystallites and crystal growth at the very apexes of the tips is obtained. In this way suitable diamond-tipped AFM probes can be produced.

The size of the deposited crystals varies from 1.5 to 2.3 microns. Sometimes, for the seeded cantilevers, even bigger deposits are observed (diameters larger than 3- 4 microns). We attribute this either to the presence of the seeding powder on the cantilevers with further diamond growth on top of these, or to coalescent crystals.

The microstructure of the deposited particles is depicted in Fig.3.7, which shows that they are spherical polycrystalline aggregates consisting of numerous crystallites of a few 10 nm in size.

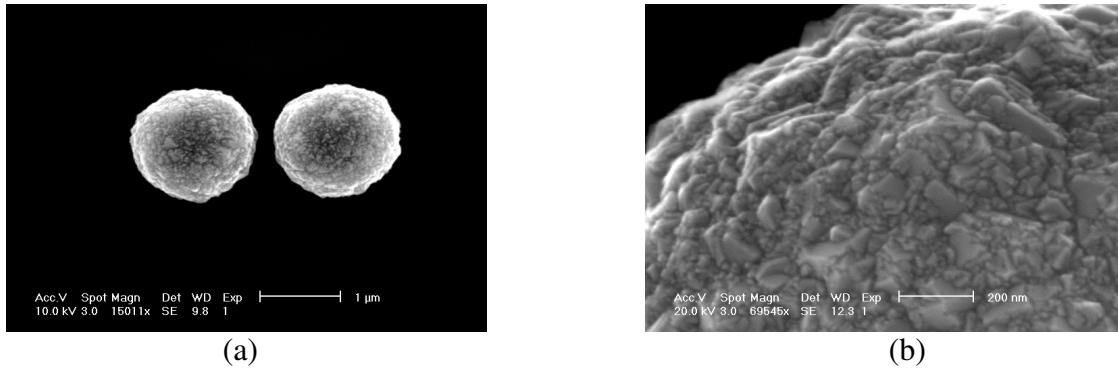


**Fig.3.7.** SEM images of the deposited diamond particles (a) showing their polycrystalline microstructure in detail (b).

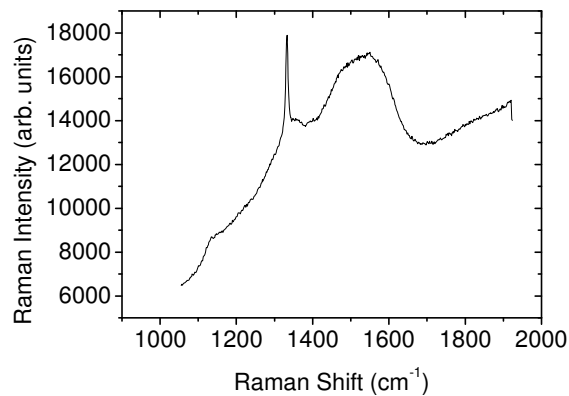


**Fig.3.8.** Typical Raman spectrum for the crystals deposited on the standard silicon tips

The best quality diamond polycrystals are grown after the ultrasonic treatment. The diamond peak is positioned in the range of 1332.8 – 1334.9  $\text{cm}^{-1}$  and the ratio diamond/non-diamond peak heights in the spectra ranged from 1.02 to 1.67 with a maximum value corresponding to the situation when the deposition was performed after ultrasonic shaking in the seeding suspension.

### 3.3.3. Diamond-terminated cantilever tests in ultra-high vacuum

The performances of the Si tips having diamond crystals at the apex were tested in UHV, using an VT-UHV-AFM / STM. After the deposition, the resonance frequencies of the cantilevers were checked and showed no major differences, still being within the range of values given by the producer. To perform nano-friction (lateral force) measurements, only the long cantilevers of the Si chips were used, because of their small spring constant values. The presence of the crystals at the very apex of the tips was verified before and after the AFM scans by means of SEM, using a lower acceleration energy for the electrons (1 kV) in order to avoid the destruction of diamond crystalline structure.

The scanning performances of the diamond-terminated tips have been investigated using a known-topography object. The sample chosen was the stepped (0001) sapphire surface. The typical way of preparing the surface and the subsequent topography are described elsewhere [31,32]. Sapphire is a very hard material and therefore its vicinal (0001) stepped surface provides a very good tool for checking the adhesion of the diamond deposits to the silicon tips while scanning in contact-mode AFM at different loads. Moreover the presence of the terraces and steps can give us precise information about the achieved lateral resolution.

It is important to mention that when focusing the laser beam on the backside of the cantilevers with diamond deposits, the resulting intensity on the four-quadrant photodiode was much lower (factor of 5-6) than that achieved in the case of regular cantilevers. This is not surprising because diamond nucleation normally occurs on both sides of the cantilevers, producing a scattering of the focused light. Moreover, the heating in the HF-CVD reactor definitely affected the reflectivity and maybe the flatness of the Al coating, as SEM investigation revealed. One should realize that the temperature of deposition (750 °C) exceeds the melting point of Al, which is 660 °C. Nevertheless, good quality images could be obtained in contact-mode regime.

The AFM micrographs shown in Fig.3.9 are recorded in contact-mode and exhibit topographic, normal force and lateral (friction) force maps of the same  $2 \times 2 \mu\text{m}^2$  area of sapphire surface. Topographic images reveal that the sample surface is covered with faceted steps with heights ranging from 2 up to 6 nm and the terraces are several 100 nm wide. The zigzagging shape of the step edges is very clearly visible on both normal and friction force windows.

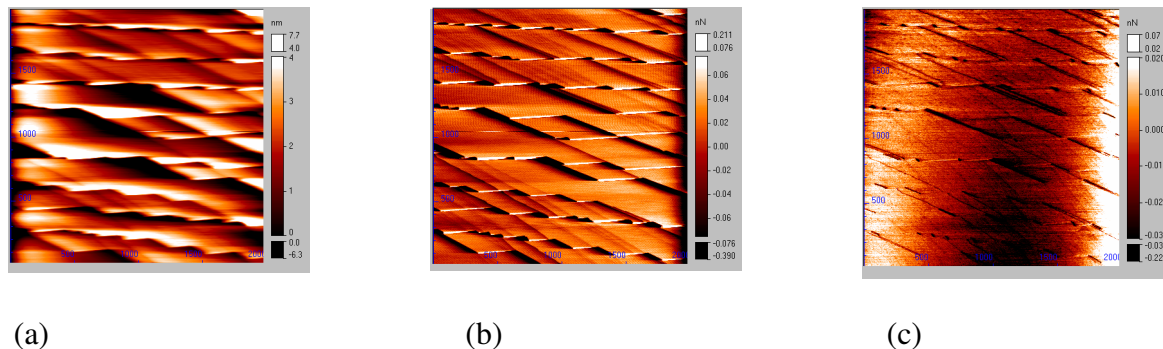


**Fig.3.9.** Topography (a), normal force (b) and friction (lateral) force (c) maps in contact mode AFM of a zigzag stepped surface of (0001)  $\text{Al}_2\text{O}_3$ . The applied load is 1nN.

Although at first sight the diamond termination of the Si tips seems rather big and blunt, the part of the diamond particle (i.e. a corner of one of the nanocrystallites in the aggregate) really in "contact" with the scanned surface is extremely small and sharp. From the resulting good quality of the scan images of the sapphire steps we can estimate the tip radius of curvature to be between 10-20 nm, which is very good by AFM standards where typical radii are in the range of tens of nanometers. After scanning with increasing values of the load (up to 4 nN), the status of the tip was checked by means of SEM and no apparent damage of the diamond termination at the tip could be observed. This proves that the bonding of the deposited diamond to the silicon substrates is strong and no wear is present.

### 3.4. Summary of results

In this chapter a method to produce diamond-terminated Si tips for contact-mode atomic force microscopy, by using HF-CVD is demonstrated. The first step was to confirm the preferential growth of diamond crystals at the apex of pyramids on a silicon substrate in order to simulate diamond deposition on standard AFM tips. This point - topped pyramids, which were homogeneously distributed on the silicon wafers, were obtained by wet chemical etching in aqueous KOH solutions. SEM and optical microscopy images proved that the apexes and the edges of the pyramids were favorable sites for the nucleation and further growth of diamond poly-crystals. After finding the optimum conditions for diamond growth, then standard Si tips were used as substrates for HF-CVD of diamond. The resulting AFM tips have been used in nano-friction measurements of a stepped surface of sapphire crystal showing the reliable behavior, good stability, sharpness and hardness of the diamond termination.

## References:

1. W. Carpick, N. Agrait, D.F. Ogletree, and M. Salmeron, *J. Vac. Sci. Technol. B* 14, (1996).
2. W. Carpick, N. Agrait, D.F. Ogletree, and M. Salmeron, *Langmuir* 12, 3334 (1996).
3. M. Enachescu, R.J.A. van den Oetelaar, R.W. Carpick, D.F. Ogletree, C.F.J. Flipse, and M. Salmeron, *Phys. Rev. Lett.* 81, 1877 (1998).
4. M. Enachescu, R.J.A. van den Oetelaar, R.W. Carpick, D.F. Ogletree, C.F.J. Flipse, and M. Salmeron, *Tribol. Lett.* 7, 73-78 (1999).
5. R.E. Clausing, L.L. Horton, J.C. Angus, and P. Koidl, *Diamond and Diamond-like Films and Coatings (NATO ASI Series, Series B: Physics Vol.266, 1991)*.
6. K.E. Spear, J.P. Dismukes, *Synthetic Diamond: Emerging CVD Science and Technology*, A Wiley- Interscience Publication, 1994.
7. G.J. Germann, S.R. Cohen, G. Neubauer, G.M. McClelland, H. Seki, and D. Coulman, *J. Appl. Phys.* 73, 163 (1993),.
8. O. Marti, B. Drake, and P. Hansma, *Appl. Phys. Lett.* 51, 484 (1987).
9. R. Kaneko, S. Oguchi, *Jpn. J. Appl. Phys.* 29, 11854 (1990).
10. E. Visser, J. Gerritsen, W. van Enckevort, and H. van Kampen, *Appl. Phys. Lett.* 60, 3232 (1992).
11. G. Germann, G. McClelland, Y. Mitsuda, M. Buck, and H. Seki, *Rev. Sci. Instrum.* 63, 4053 (1992).
12. N. Liu, Z. Ma, X. Chu, T. Hu, Z. Xue, and S. Pang, *J. Vac. Sci. Technol. B* 12, 1856 (1994).
13. E. Givargizov, V. Zhirnov, A. Stepanova, E. Rakova, A. Kiselev, and P. Plekahnov, *Appl. Surf. Sci.* 87/88, 24 (1995).
14. E. Oesterschulze, W. Scholz, C. Mihalcea, D. Albert, B. Sobisch, and W. Kulisch, *Appl. Phys. Lett.* 70, 435, (1997).
15. W. Kulisch, A. Malave, G. Lippold, W. Scholz, C. Mihalcea, and E. Oesterschulze, *Diamond. Relat. Mater.* 6, 906 (1997).
16. C. Mihalcea, W. Scholz, A. Malave, D. Albert, W. Kulisch, and E. Oesterschulze, *Appl. Phys. A* 66, S87-S90 (1998).
17. S.- S. Tan, M. Reed, H. Han, and R. Boudreau, *J. Micromech. Microeng.* 4, 147-155 (1994).
18. L.M. Landsberger, S. Naseh, M. Kahrizi, and M. Paranjape, *J. Micromech. Systems* 2, 107 (1996).
19. J.-H. Liu, T.M. Betzner and H.T. Henderson, *J. Micromech. Microeng.* 5, 18 (1995).
20. A.J. Nijdam, E. van Veenendal, H.M. Cuppen, J. van Suchtelen, M.L. Reed, J.G.E. Gardeniers, W.J.P. van Enckevort, E. Vlieg, and M. Elwenspoek, *J. Appl. Phys.* 89, 4113 (2001).
21. G. Janssen, *Homoeptaxial diamond synthesized by CVD processes*, PhD Thesis, University of Nijmegen (1994).
22. Martech Scientific Instruments, Eindhoven, The Netherlands.
23. S. Buhlmann, E. Blank, R. Haubner, and B. Lux, *Diamond. Relat. Mater.* 8, 194 (1999).

24. A.M. Bonnot, Phys. Rev. B 41, 6040 (1990).
25. L.H. Robins, E.N. Farabaugh, and A. Feldman, J. Mater. Res.11,(1990).
26. R.G. Buckley, T.D. Moustakas, L. Ye, and J. Varon, J. Appl. Phys. 66 (8), 3595, (1989).
27. R.E. Shroder and R.J. Nemanich, Phys. Rev. B 41, 3738 (1990).
28. S.C. Sharma, M. Green, R.C. Hyer, C.A. Dark, T.D. Black, A.R. Chourasia , D.R. Chopra, and K.K. Mishra, J. Mater. Res., 11, 2424 (1990).
29. C.P. Chang, D.L. Flamm, D.E. Ibbotson, and J.A. Mucha, J. Appl. Phys.63 (5), 1744 (1988).
30. F.G. Celii, P.E. Pehrsson, H.-T. Wang, and J.E. Butler, Appl. Phys. Lett.52 (24), 2043 (1988).
31. O. Kurnosikov, L. Pham Van, and J. Cousty, Surf. Sci. 459 (2000) 256.
32. L. Pham Van, O. Kurnosikov, and J. Cousty, Surf. Sci. 411 (1998) 263.





# Chapter 4. Friction force measurements on diamond (100) surfaces

## 4.1. Introduction

Recent developments in the field of chemical vapor deposition (CVD) techniques provided an extremely versatile way of obtaining diamond layers and microcrystals with a large range of sizes and properties [1,2]. In comparison to other methods (high-pressure-high-temperature, HPHT), crystallites or films can be deposited on various materials and in the beginning most of the work focused on polycrystalline coatings. Research on homoepitaxial diamond growth [3-9] made diamond a very attractive and promising material for tribological, electronic, optical and biological applications (biosensors) [10,11] and therefore having high quality diamond films with atomically flat surfaces, low defect density and low residual impurities is of the essence. Atomic force microscopy and scanning tunneling microscopy have become powerful tools in investigating mechanical, frictional and electrical properties of such surfaces on the sub-micron level.

In the present chapter, an ultra-high vacuum STM/ FFM study on a specially grown conductive (100) diamond surface is described. A very flat surface exhibiting perpendicular domains and rows of dimers, typical to a (2x1) hydrogen reconstructed surface, is revealed by tunneling scans. The complicated structure of the hydrogen terminated (100) plane is also atomically resolved in topography, normal force and friction force by FFM when making use of a diamond-coated tip. Moreover, the reproducible visualization of atomic steps between individual neighboring C-H dimers seem to indicate an atomically sharp tip. The analysis of the normal/lateral force signals demonstrate frictional contributions in two orthogonal directions leading to a complicated trajectory of the tip between the H-atoms of the surface. The results are compared to an ab-initio electronic structure calculation (See Appendix 1), describing the forces experienced by a diamond tip with a single hydrogen atom at the tip end when slid over a hydrogen-terminated diamond surface. The very good agreement leads to the conclusion that the Coulomb repulsion between the hydrogen atoms of tip/sample termination, causing a complicated tip trajectory during scans, governs the atomic stick-slip behavior observed both experimentally and theoretically.

## 4.2. Experimental

### 4.2.1. Experimental set-up

All measurements have been performed in the same Variable-Temperature Ultra High Vacuum AFM/STM (Omicron) as described in Chapter 2. Due to a special treatment during growth (See Appendix 2), surface conductivity measurements were possible on

the (100) diamond sample. Electrochemically etched tungsten tips were used in all the STM experiments. For the nanofriction measurements standard silicon nitride tips (NT-MDT) and diamond coated tips (Veeco, ULCT-DCBO) have been used.

#### **4.2.2. Sample preparation**

The sample investigated in these experiments was a homoepitaxially grown hydrogen terminated (100) diamond surface (See Appendix 2). The growth process was quite complex and resulted in a conductive surface. Prior to the STM/FFM measurements the crystal ( $2.5 \times 2.5 \times 0.4 \text{ mm}^3$ ) was installed on a tantalum holder and annealed in UHV at  $410 \text{ }^\circ\text{C}$  for 1 hour to remove residual water and other possible contaminants.

### **4.3. Results and discussion**

#### **4.3.1. Sample topography**

##### **4.3.1.1. STM measurements**

In friction force microscopy the influence of topography upon measured lateral force can be very important and therefore is of the essence to have a good indication of the surface roughness and morphology; this way experimentally seen frictional features can be more easily understood and interpreted. Therefore we made use of the surface conductivity provided by the special surface treatment during hydrogenation and performed scanning tunnelling (STM) experiments on this sample.

STM images of the sample show very flat surface over large areas (roughness RMS =  $0.549 \text{ nm}$  over  $1 \times 1 \text{ } \mu\text{m}^2$ ). The whole surface is covered with square, pyramidal features following the symmetry of the substrate (HPHT crystal, Appendix 2) used during growth. (See Fig. 4.1.) When zooming in, very high resolution could be achieved; terraces separated by monoatomic steps are visible in topography and current maps, (Fig.4.2.). The surface consists of  $(2 \times 1)$  reconstructed domains rotated by  $90$  degrees with respect to each other. The cigar-shaped features, separated by a distance of approximately  $5$  Angstroms, correspond to the C-H dimer rows of the hydrogen terminated  $(2 \times 1)$  diamond surface.[3-9, 12] The size of the antiphase terraces is limited to a few square nanometers; this is normally attributed to growth at a relatively low substrate temperature, effect seen also in Si homoepitaxy [7,13]. The temperature is not high enough so that both domains on a terrace can rearrange or coalesce to form a single domain; the surface diffusion during growth is limited and the long range correlation of the atomic motion is small. A single domain (100) surface has been reported by Tsuno et al. [14] when using an off-angle cut substrate.

After obtaining the information upon the sample roughness and morphology further contact-mode AFM measurements have been carried out.

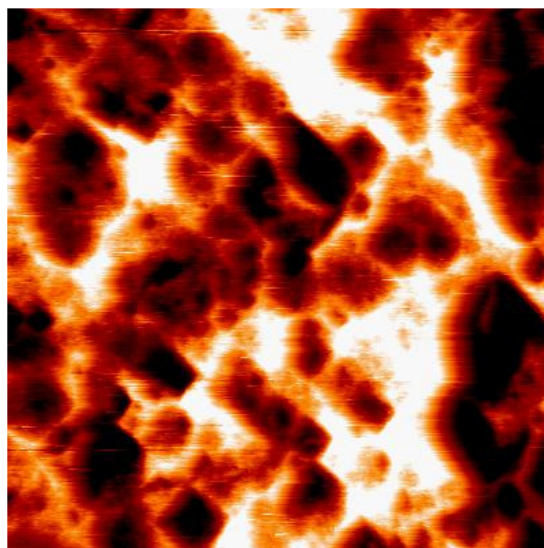
#### 4.3.1.2. FFM measurements on (100) diamond

In contact-mode AFM, when the electronic feedback is switched on, the positioning piezo will maintain a constant applied load by altering the tip-sample separation; this mode of operation is normally called *constant force* or *height mode*, enabling to obtain topographic images. When investigating atomic-scale friction, the interplay between the bending and torsion of the lever is complicated, since normally the tip end follows a zigzag motion trying to find positions of minimum energy in between the surface atoms. Therefore throughout our measurements, when focusing on the lateral forces, a rather soft feedback (small loop gain value) was used. The feedback was not switched off in order to avoid problems related to drifts. Moreover, STM measurements shown in the previous paragraph revealed a complicated structure of the (100) surface, with numerous perpendicular terraces/domains separated by steps; during the scan a small gain value was still set in order to avoid uncontrollable vertical movements of the tip or possible damage to the tip.

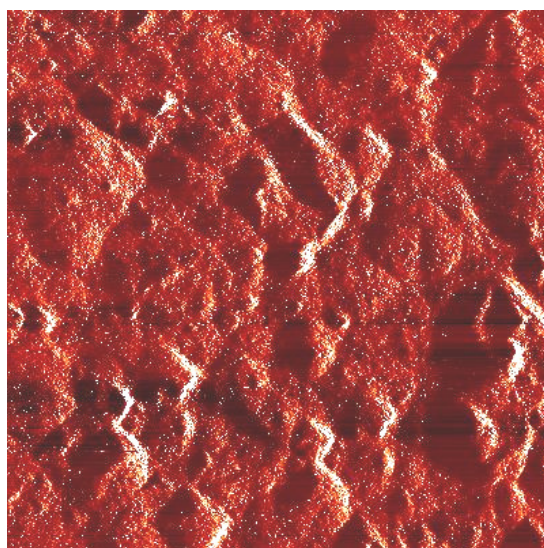
Besides the height and lateral force signal, the normal force error signal was recorded (as being the difference between the actual normal force (deflection) experienced by the tip and the pre-determined value set for the applied load).

A first set of friction measurements was done using standard SiN tips, with normal spring constant values of 0.12 and 0.58 N/m. The cantilevers were annealed in-situ at 150 °C for 1 hour, to remove water or possible contaminants. On the microscopic scale features similar to the ones seen in STM images are obtained in topography, normal force error signal and lateral force (Fig.4.3).

When scanning over smaller areas (nanometer-scale), only a in a few situations and after exchanging several tips and various scan parameters (load, velocity, loop gain) periodical features were observed (Fig.4.4 and 4.5) in topography, normal and lateral force; however the quasi-periodicity seen could not be attributed to the expected (2x1) reconstructed (100) diamond lattice. Still, by making a comparison between these images and the STM maps like the ones depicted in Fig.4.2, it was interesting to notice that most of the topography, normal force and frictional features (rows) seem to be parallel to the same direction as the “cigar-shaped” dimers, i.e. one of the main crystallographic directions of the (100) surface. While in Fig. 4.4 a certain unclear (possibly atomic) structure is visible also on a perpendicular direction, in Fig.4.5 parallel rows are observed only, probably due to an asymmetric tip shape, as previously reported [15] in lateral force signals by Germann et al.

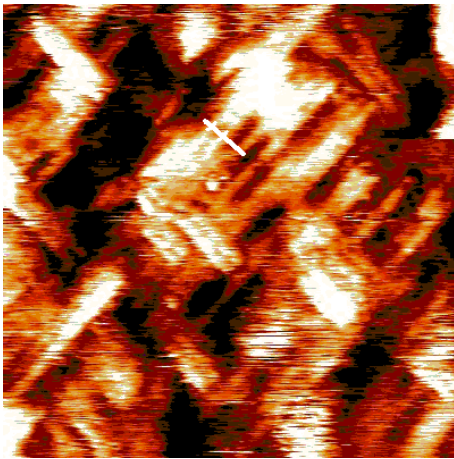


(a)

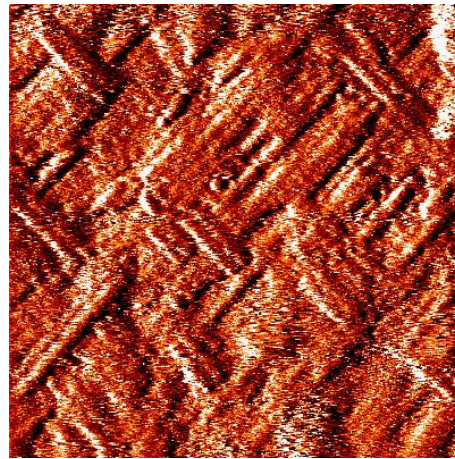


(b)

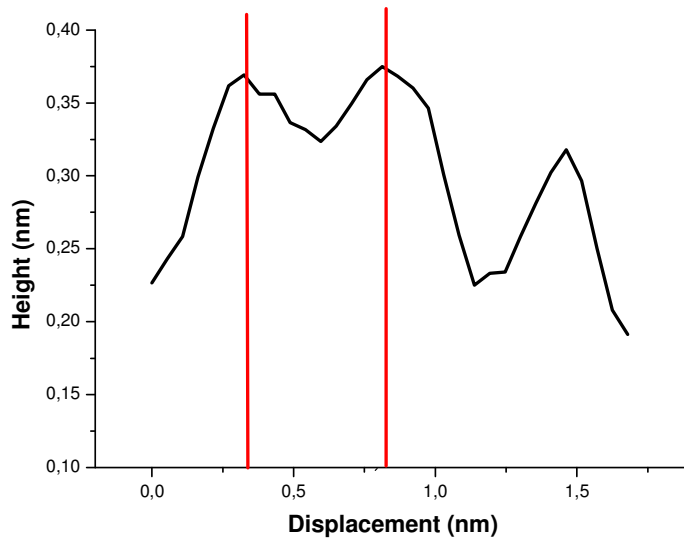
**Fig.4.1.** STM topography (a) and current (b) maps ( $1 \times 1 \mu\text{m}^2$ ) revealing an extremely flat (100) diamond surface (RMS: 0.549 nm and AM: 0.445 nm). Square-based crystallites having edges parallel to the main crystallographic directions of the substrate are visible.  $I = 0.8 \text{ nA}$ ,  $V_{\text{bias}} = 1.5 \text{ V}$ . For topography the grey scale ranges from 0 to 3.7 nm (bright areas).



(a)

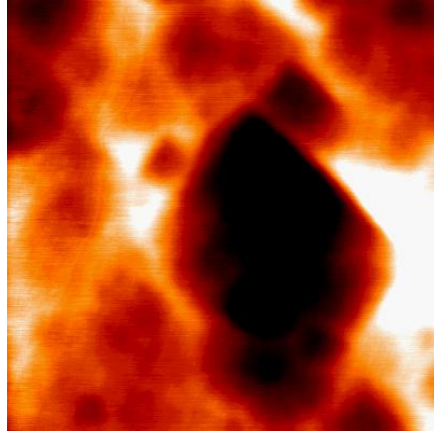


(b)

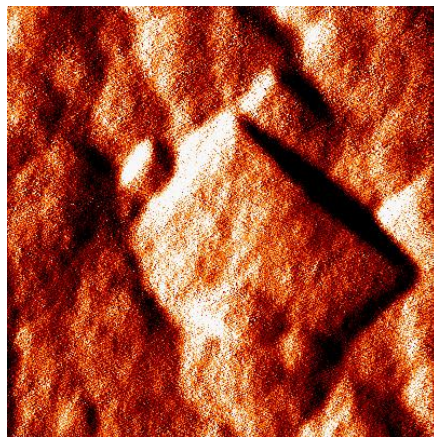


(c)

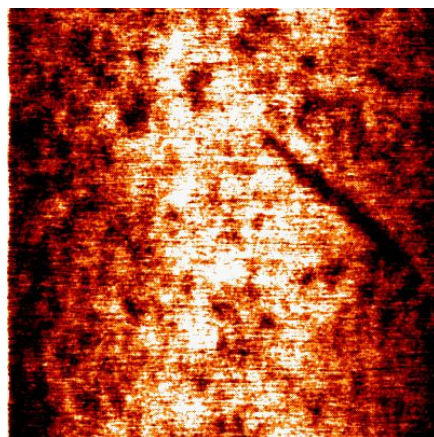
**Fig.4.2.** Atomically resolved features corresponding to carbon dimers of a (2x1) hydrogen terminated (100) diamond surface: (a) topography and (b) current map. Perpendicular reconstructed domains can be seen. (c) The spacing between the “cigar-shaped” rows is 0.5 nm (white profile line from figure (a)). Scan parameters:  $I = 0.9$  nA,  $V_{\text{bias}} = 1.5$  V. Size  $15 \times 15$  nm<sup>2</sup>.



(a)

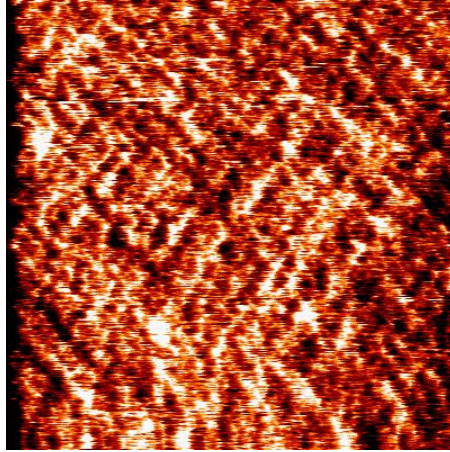


(b)

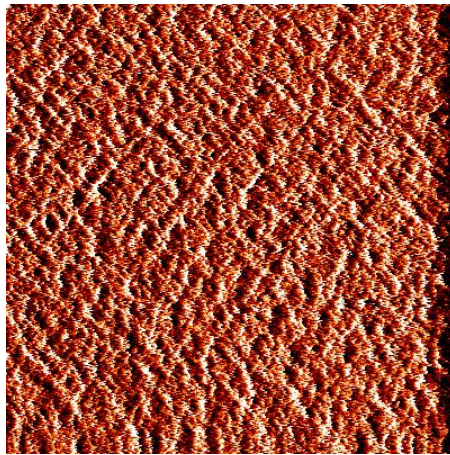


(c)

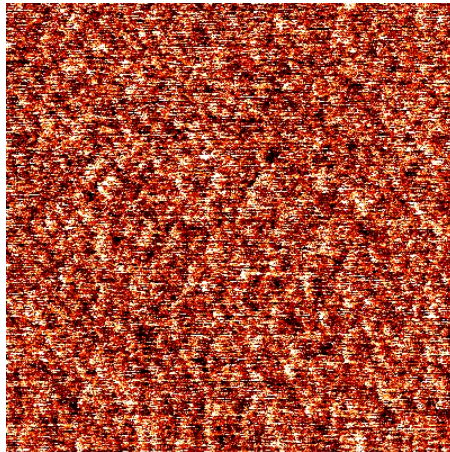
**Fig.4.3.** Contact mode AFM images of a  $500 \times 500 \text{ nm}^2$  (100) diamond surface using a SiN tip ( $C = 0.58 \text{ N/m}$ ). (a) Topography, (b) normal force error signal and (c) lateral force signals. Scan velocity:  $400 \text{ nm/s}$ . Applied load:  $2 \text{ nN}$ .



(a)



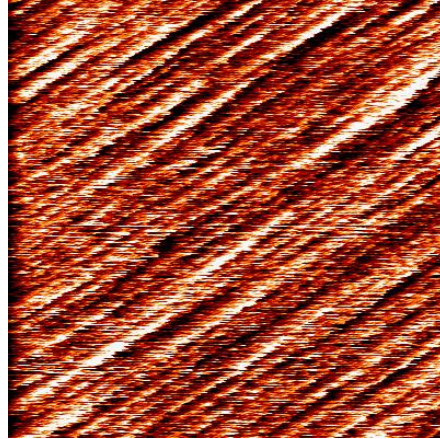
(b)



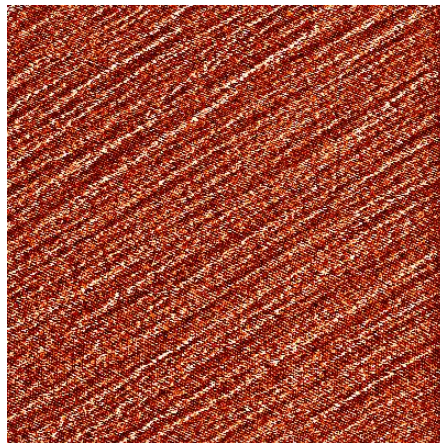
(c)

**Fig.4.4.** Good resolution achieved in contact mode. (a) Topography, (b) normal force error signal and (c) friction force. SiN tip. Scan size  $20 \times 20 \text{ nm}^2$ . Applied load 3.25 nN. Scan velocity 50 nm/s.

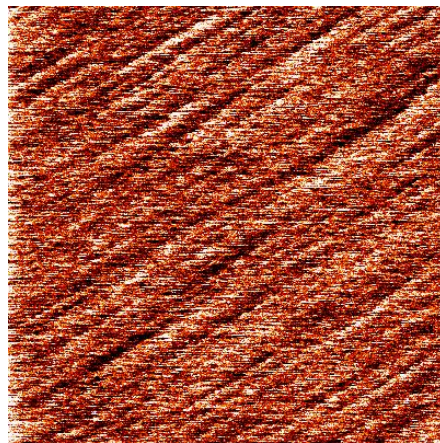




(a)

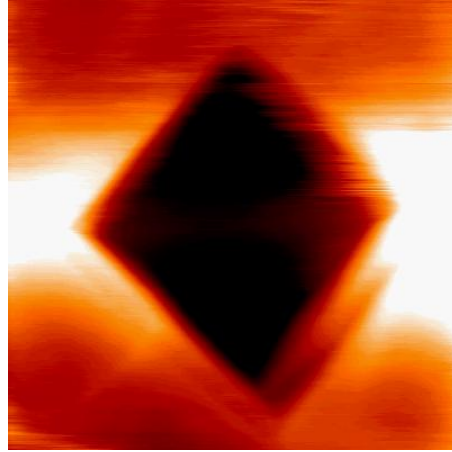


(b)

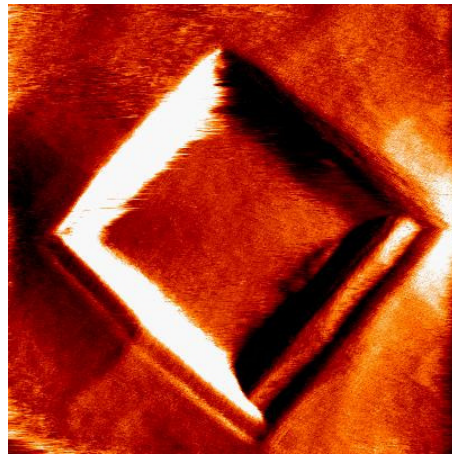


(c)

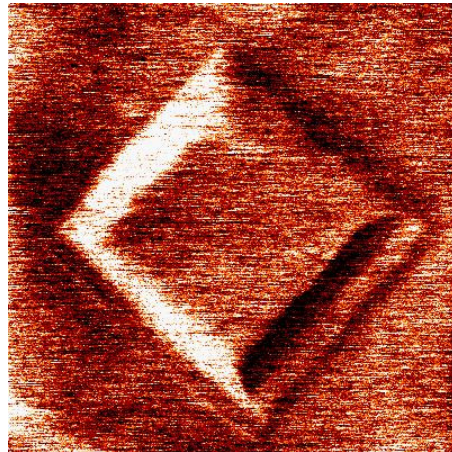
**Fig.4.5.** Quasi-periodical features seen in (a) topography, (b) normal force error signal and (c) friction force maps of a  $10 \times 10 \text{ nm}^2$  region. A different SiN tip from the situation shown in Fig.4.4. was used. Applied load: 3 nN. Velocity: 6.5 nm/s. Scan direction from left to right at 0 degrees scan angle.



(a)



(b)



(c)

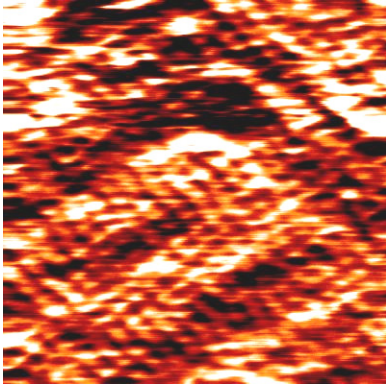
**Fig.4.6.** Friction force microscopy images of the (100) diamond surface, revealing a crystallite. Height, normal force error signal, and friction force windows. Diamond-coated tip (normal spring constant  $C = 0.4 \text{ N/m}$ ). Velocity:  $368 \text{ nm/s}$ . Applied load:  $2.59 \text{ nN}$ . Scan size is  $500 \times 500 \text{ nm}^2$ .

Most of the time scans revealed blurry morphology and no regular structure, probably due to a blunt or disordered tip. Quite often the resolution deteriorated after longer scans over the same spot; although in principle such tips have a standard radius of curvature in the order of tens of nanometers, we cannot exclude the possibility of tip damage or slight wear after a jump into contact event and subsequent scanning.

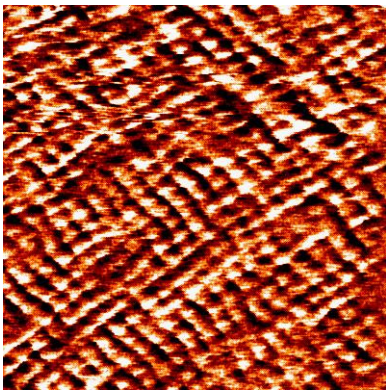
Therefore the next step in the experimental work was to use a diamond-coated tip. From the first scans it was obvious that the quality of the images very much improved and stayed unchanged after long scans, after zooming in and out on various locations, (Fig.4.6) which was a good indication of a sharp and stable tip termination. Moreover, unprecedented resolution was achieved when going down to nanometer-scale range scans. Similar perpendicular rows as seen in the STM pictures (Fig.4.2) are visible in topography, normal force error signal and friction signals, with the difference that we can really atomically resolve the outermost structure of the C-H dimers, namely the hydrogen atoms positions, separated by approximately 2.5 Angstroms distances (Fig.4.7).

The fact that features typical for the (2x1) reconstructed could be resolved, i.e. orthogonal oriented terraces separated by monoatomic steps and perpendicular atomic rows, show once again that we deal with an extremely sharp tip and excludes the possibility of having an ordered crystallite at the tip end in registry with the surface or a disordered multiple-tip contact. To ensure the reproducibility of the maps exhibiting this complex structure of the reconstructed (100) surface, several spots/regions on the sample were repeatedly imaged at different scan sizes; the typical antiphase (perpendicular) domains/atomically-resolved rows were always present in topographic, normal force and lateral force images. Furthermore, interesting atomic-scale features involving monoatomic steps can be imaged at regions where perpendicular dimers meet each other, a strong indication that we have an atomically sharp tip, or to be more precise, one single hydrogen atom-terminated tip (Fig.4.8). Remarkably, this topography scan of a *contact mode* AFM experiment shows two *individual* H-positions (indicated by arrows) in the lower domain (dotted yellow lines), which is only 5 Angstrom wide, consistent with the schematic representation of the surface C-H dimers shown in Fig.4.7(d). This further supports our belief that the end of our tip is extremely sharp. We believe that only then we would be capable of resolving the positions of individual hydrogen atoms on this complicated surface.

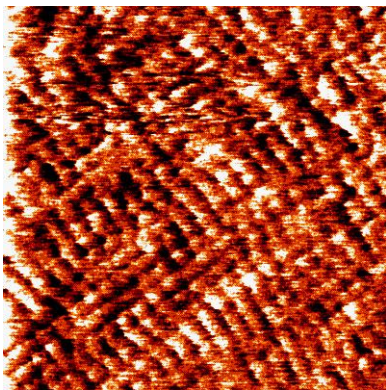
As described in chapter 1, in contact-mode AFM mostly the friction force stick-slip features reveal the periodicity of the lattice atoms for a large range of well-defined surface materials [15-17] and therefore the question whether this automatically mean that we deal with true atomic resolution or with some mechanism of periodic pattern formation. Most of the time, such images show smooth quasi-perfect surfaces and defects such as vacancies, steps or kinks usually are not atomically resolved. Germann et al. [18] carried out friction force measurements in UHV using a specially grown diamond tip on both the (100) and (111) diamond surfaces. They could resolve periodic stick-slip features only on the (100) surface, attributed to the (2x1) hydrogen-terminated reconstructed surface. Periodic rows were seen in the friction maps only, separated by a typical spacing of 2.3 Angstroms, along the [210] direction of the bulk diamond lattice; this was explained by the fact that averaging over an asymmetric tip prevented the observation of any structure perpendicular to the rows.



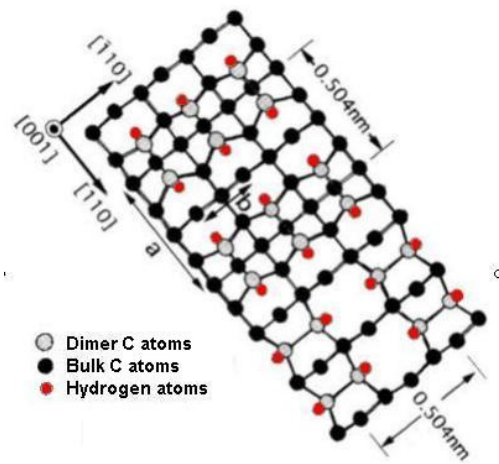
(a)



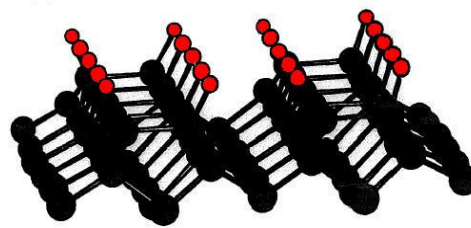
(b)



(c)



(d)



(e)

**Fig.4.7.** Real atomic resolution measured on the (2x1) reconstructed hydrogen terminated (100) diamond, simultaneously in (a) topography, (b) normal force error signal and (c) friction force. Periodicities corresponding to the individual hydrogen atoms' positions are resolved (2.5 Å spacing). Load: 3.23 nN. Scan size: 5x5 nm<sup>2</sup>. (d) Schematic top-view and (e) side-view illustration of a diamond (100) 2x1:H reconstructed surface with each dangling bond per dimer carbon atom terminated by hydrogen (red circle); "a x b" is the unit area (from Ref. [25]).

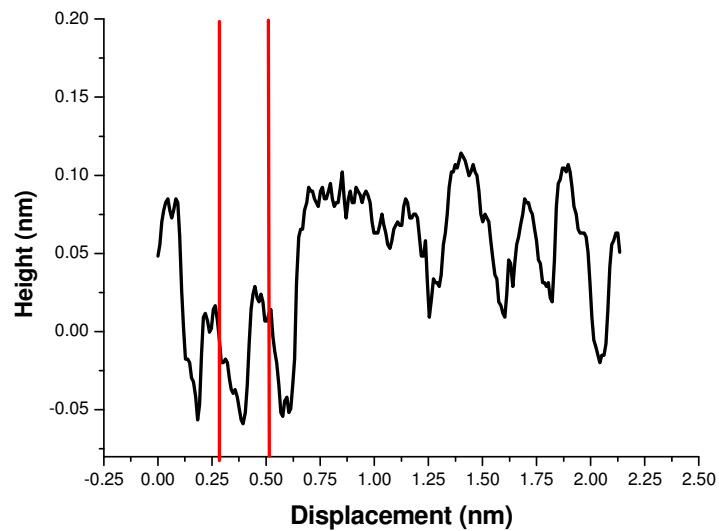
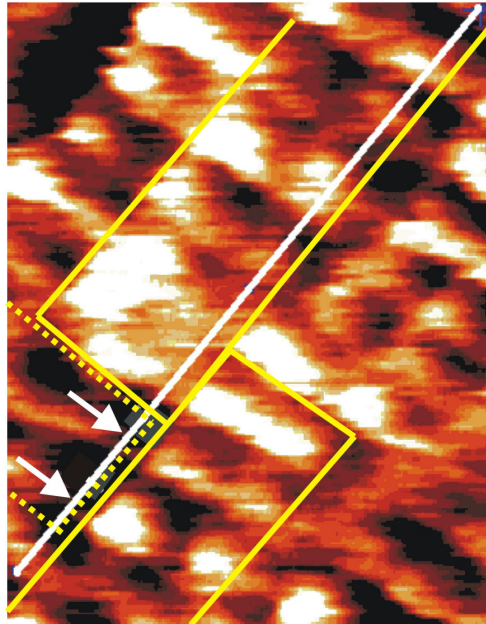


**Fig.4.8.** Remarkable resolution in the topography image (size  $1.42 \times 1.81 \text{ nm}^2$ ) of the (100) diamond surface showing atomic steps between neighboring dimer rows. Diamond-coated tip. Load 1.5 nN. The spacing between the red lines corresponds to the distance indicated with white arrows in the height map.

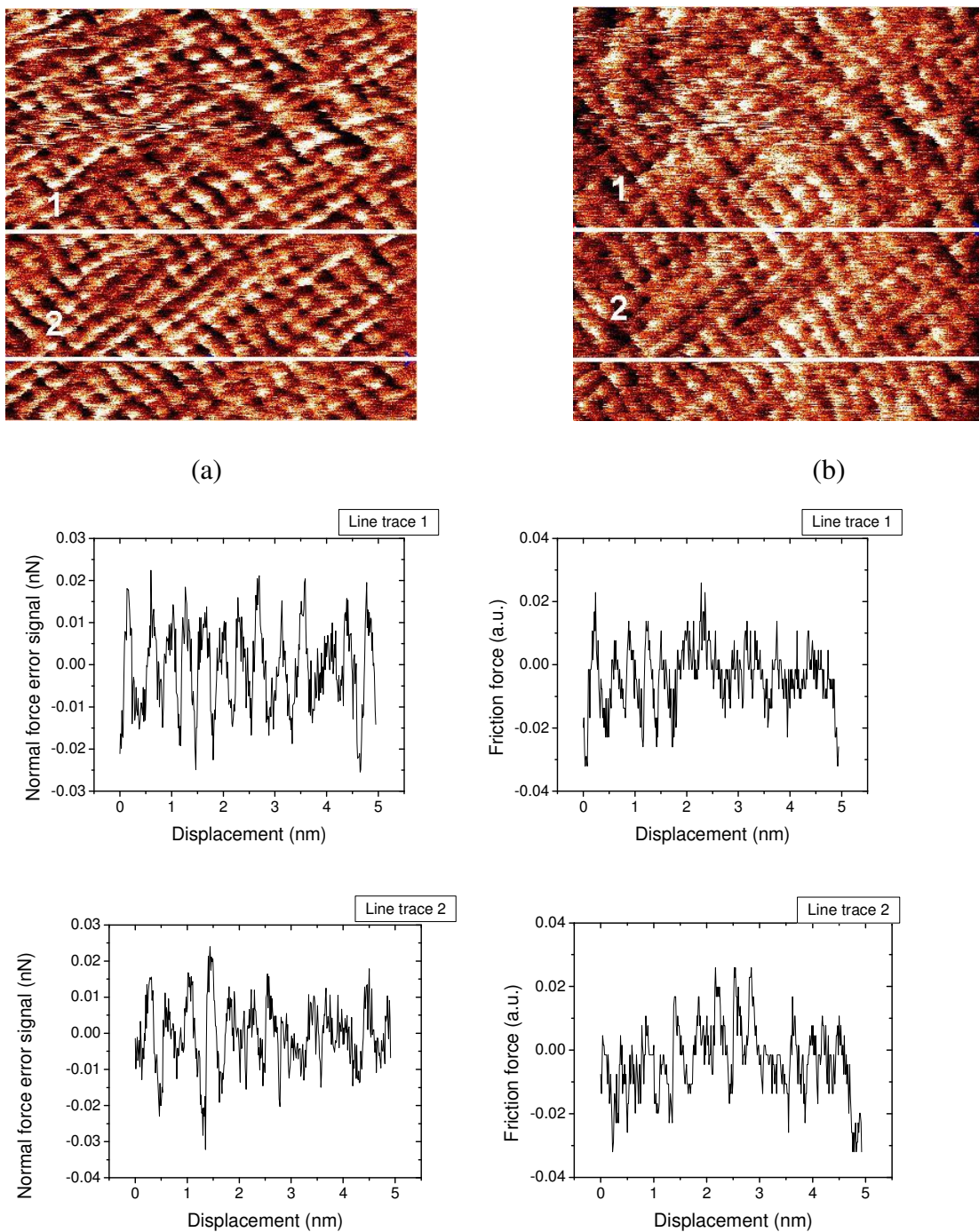


**Fig.4.9.** Line profiles along the same scan line for normal force error (a) and lateral force (b) maps, respectively for two different positions. Sharper signal is seen in the normal force. Signals are related and distortions in periodicities are visible, due to scan direction in between several dimer rows.

In Fig. 4.9, the analysis of normal and lateral force line profiles along the same scan direction is shown. It is important to mention that the measurements were performed at zero degrees scan angle, i.e. the direction of scan perpendicular to the cantilever axis, in order to avoid additional buckling effects. The contrast in the normal force is slightly better than in the lateral force and the typical saw-tooth aspect of this signal is a clear indication of a significant friction force component perpendicular to the scan direction.

This type of behavior, observed for the first time by Fujisawa et al. [19], is consistent with a complicated two-dimensional stick-slip tip trajectory in between the atomic positions of the surface. The tip attached to the cantilever in translation will tend to remain in registry with the surface lattice; this will lead to a zigzag tip motion and buckling/twisting of the compliant cantilever. From the topography, normal force error signal and friction maps it is obvious that our scan direction is off the main crystallographic directions of the (2x1)-hydrogen terminated diamond surface. Therefore scanning in between the hydrogen atoms belonging to different perpendicular dimers will induce sometimes distortions in the stick-slip periodicities for both normal and lateral force, as visible in the profile lines from Fig.4.9.

A good qualitative theoretical confirmation of the complex frictional behavior observed experimentally is provided by the *ab-initio* electronic structure calculation (Appendix 1) for movements of the diamond tip (with apex terminated by only one hydrogen atom) in a diagonal direction across the (2x1):H (100) diamond surface. The hydrogen termination on the diamond surface plays a crucial role in the observed stick-slip behavior since the main interaction is determined by the repulsion between the hydrogen atom of the tip and hydrogen atoms saturating the diamond surface.

As a result of the calculation we have found that the stick-slip character in the normal- and lateral force measurements are caused by a 2-dimensional “zig-zag” movement of the H-apex atom when it slides in the diagonal direction, with displacements of 0.25 nm, in agreement with the experimental values. (See the snap shots in Fig.4.10 and reconstructed tip path in Fig.4.11). At each slip point, the forces acting on the H-apex atom of the tip are suddenly released in the sliding (lateral force) and perpendicular to sliding direction of the tip (normal force), resulting in an abrupt displacement and relaxation of the H-apex atom as well as the surface hydrogen atoms interacting with the tip and explaining the pronounced stick-slip effect in the lateral- and normal force measurements. The repulsive interaction between the hydrogen atom-termination of the sharp tip and the hydrogen-terminated (2x1)-(100) diamond surface is the dominating factor governing the stick-slip frictional behavior.

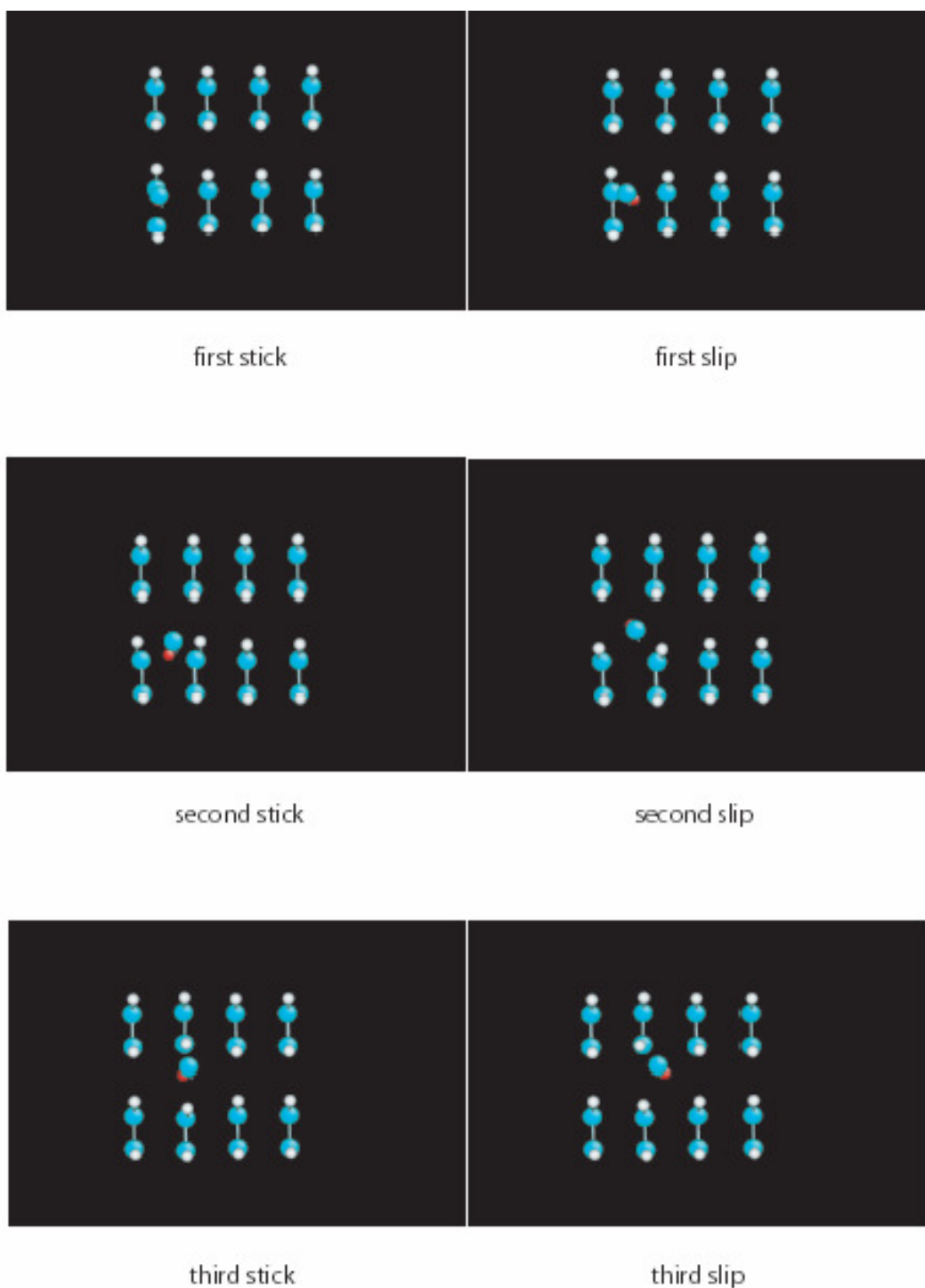


**Fig. 4.10.** The complicated trajectory of the hydrogen atom of the tip (red sphere) across the surface due to H-H interactions leads to a strong sudden response in the vertical direction followed by a suppressed movement of the tip around the surface hydrogen atoms (smaller white spheres). The carbon atoms of the diamond tip/sample are represented by light blue spheres.



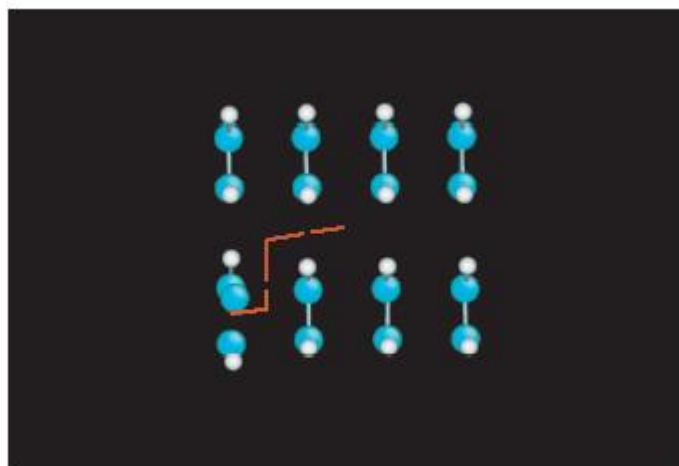


**Fig.4.11.** Reconstructed H-atom tip trajectory (red line) from Fig.4.10. revealing a zig-zag motion between the hydrogen atoms terminating the surface.

#### **4.4. Conclusion**

The friction between a diamond coated tip and a specially prepared hydrogen-terminated (100) diamond sample was studied in UHV using a friction force microscope. Tunneling experiments revealed a very flat surface and the typical atomic features (dimers) of a (2x1) surface reconstruction of the (100) diamond sample.

The friction measurements with a diamond-coated tip on the same surface led to atomic resolution: perpendicular domains, hydrogen atomic positions and atomic steps between domains could be resolved. We attribute this to an atomically sharp tip and, similar to the results on the (111) diamond surface, we believe that the repulsion between the last H-atom of the tip and the H-atoms of the surface termination is the most important ingredient controlling the complicated two-dimensional atomic scale stick-slip behavior observed.

## References

1. R.E. Clausing, L.L. Horton, J.C. Angus, P. Koidl, *Diamond and Diamond-like Films and Coatings* (NATO ASI Series, Series B: Physics Vol.266, 1991).
2. K.E. Spear, and J.P. Dismukes, *Synthetic Diamond: Emerging CVD Science and Technology*, (A Wiley- Interscience Publication, 1994).
3. H. Watanabe, S.G. Ri, and S. Yamanaka, *New Diamond and Frontier Carbon Technology* 12 (6), 369 (2002).
4. D. Takeuchi, S. Yamanaka, H. Watanabe, H. Okushi, K. Kajimura, *Appl. Surf. Sci.* 159, 572 (2000).
5. H. Okushi, *Diamond. Relat. Mater.* 10, 281 Sp. Iss. (2001).
6. T. Tsuno, T. Imai, Y. Nishibayashi, K. Hamada, and N. Fujimori, *Jpn. J. Appl. Phys.*, Part1 30, 1063 (1991)
7. H. Kawarada, H. Sasaki, and A. Sato, *Phys. Rev. B* 52, 11351 (1995).
8. K. Schiffmann and X. Jiang, *Appl. Phys. A: Solids Surf.* 59, 17 (1994).
9. R.E. Stallcup II, L.M. Villareal, S.C. Lim, I. Akwani, A.F. Aviles, and J.M. Perez, *J. Vac. Sci. Technol. B* 14, 929 (1996).
10. C. Bariain, I. R. Matias, C. Fdez –Valdivieslo, C. Elosua, A. Luquin, J. Garrido, and M. Laguna, *Sensors and Actuators, B: Chemical* 108, 535 (2005).
11. D.D. Zhou, J.J. Greenberg, *Frontiers in Bioscience* 10, 166 (2005).
12. C. Nützenadel, O.M. Küttel, L. Diederich, E. Maillard-Schaller, O. Gröning, and L. Schlapbach, *Surf. Sci.* 369, L111 (1996).
13. R.J. Hammers, U.K. Kohler, and J.E. Demuth, *J. Vac. Sci. Technol. A* 8, 195 (1990).
14. T. Tsuno, T. Tomikawa, S. Shikata, T. Imai, and N. Fujimori, *Appl. Phys. Lett.* 64, 572 (1994).
15. J. Krim, *Am. J. Phys.* 70, 890 (2002); and references therein.
16. E. Gnecco, R. Bennewitz, T. Gyalog and E. Meyer, *J. Phys.: Condens. Matter* 13, R619 (2001), and references therein.
17. M. Enachescu, R.W. Carpick, D.F. Ogletree, and M.Salmeron, *J. Appl. Phys.* 95, 7694, (2004).
18. G.J. Germann, S.R Cohen, G. Neubauer, G.M. McClelland, H. Seki, and D. Coulman, *J. Appl. Phys.* 73 (1), 163 (1993).
19. S. Morita, S. Fujisawa, and Y. Sugawara, *Surf. Sci. Rep.* 23, 3, 1996.



# Chapter 5. Friction force measurements on diamond (111) surfaces

## 5.1. Introduction

Nowadays, diamond both as bulk material and as thin film attracts a lot of attention from the fundamental research as well as from the applied physics point of view. It is well known that diamond has great hardness, wear resistance, good lubricating properties, chemical inertness, high strength and rigidity, high thermal conductivity, good radiation resistance, high sound propagation speed, good dielectric properties, and it is transparent for visible and infrared radiation. Moreover there is the possibility to modify some of the properties by doping. The investigation of these properties at scales ranging from microns down to angstroms on diamond crystal bulk or thin films could provide an excellent input for achievements in the field of material science, for optics and microelectronics.

In single crystalline shape diamond is atomically flat and the H-termination of the surface results in a small adhesive interaction. Due to its unique hardness it can be an ideal material for investigating wearless friction. Moreover extensive molecular dynamics simulations of friction between diamond (111) surfaces as a function of load, sliding direction, and chemical species on the surface have been performed [1,2], making this surface an excellent model system.

It is known that the silicon or silicon nitride tips of the standard cantilevers used in contact-mode atomic force microscopy experiments often get damaged when snapping into contact with the sample surface or scanning with increasing load and therefore the use of hard materials, such as diamond, as contacting surfaces for friction experiments on the nanometer scale could provide a robust, stable contact area between the tip and the surface during sliding. The tribological properties of diamond surfaces and diamond-coated substrates have been intensively investigated on the macroscopic level, [3,4] but the experimental knowledge on the nanoscale frictional behaviour of this material is rather limited [5,6,7].

In this chapter atomic resolution is demonstrated for topography, normal force and friction force maps of an atomically-flat hydrogen-terminated diamond (111) surface using a diamond-coated tip in UHV, *the same tip* utilized in chapter 4. The results are compared to an ab-initio electronic structure calculation (See Appendix 1), describing the forces experienced by a diamond tip with a single hydrogen atom at the tip end when slid over a hydrogen-terminated (111) surface. The very good agreement leads to the conclusion that the Coulomb repulsion between the hydrogen atoms of tip/sample termination, causing a complicated tip trajectory during scans, governs the atomic stick-slip behavior observed both experimentally and theoretically.

## **5.2. Experimental**

### **5.2.1. AFM setup details**

All the measurements were carried out in an UHV Variable Temperature AFM/STM (base pressure  $4 \times 10^{-11}$  mbar) (Omicron) as described in chapter 2.

In the first set of measurements standard silicon nitride tips with normal spring constant values of 0.12 and 0.58 N/m were used. In the next set of measurements, diamond coated ultralevers (Veeco, ULCT-DCBO series) with force constant values of 0.26 N/m and 0.40 N/m have been utilized in the friction measurements. These tips are actually silicon conical tips having a Raman verified true diamond coating (Fig.5.1); since the height ratio of the diamond peak to the non-diamond band is 2.5 and considering the large Raman scattering cross-section for  $sp^2$  carbon bonds as compared to diamond (see chapter 3) the spectrum indicates very good quality diamond. The cantilever backside is gold coated for good reflectivity. Although the diamond layer has an estimated thickness of 100 nm, its polycrystalline structure with randomly distributed crystallites corners provides an extremely hard and sharp tip termination (microtips with radii of curvature  $\leq 10$  nm) as revealed by the experiments. A small gain value for the feedback loop was used in the experiments to diminish the influence of the feedback on the measured lateral forces.

Before the friction measurements, the sample topography was checked using non-contact AFM; a silicon rectangular cantilever (series NSC12, MikroMasch) with force constants of 0.65 N/m and a resonant frequency of 41 KHz was used.

### **5.2.2. Sample/tip preparation**

The sample used in the experiments was a specially polished natural (111) diamond window, type 2b ( $3.0 \times 3.0 \times 0.5$  mm<sup>3</sup>) (Element Six B.V.) Prior to measurements, the diamond crystal was mounted on a tantalum sample holder and heated up in UHV at 410 °C in order to remove possible water and other contaminants. Although the setup could provide sputtering facilities, this is not suitable for diamond samples as surface graphitization may occur. In all the experiments, the standard silicon, silicon nitride and the diamond-coated tips were also annealed at 150 °C for the same above-mentioned reasons.

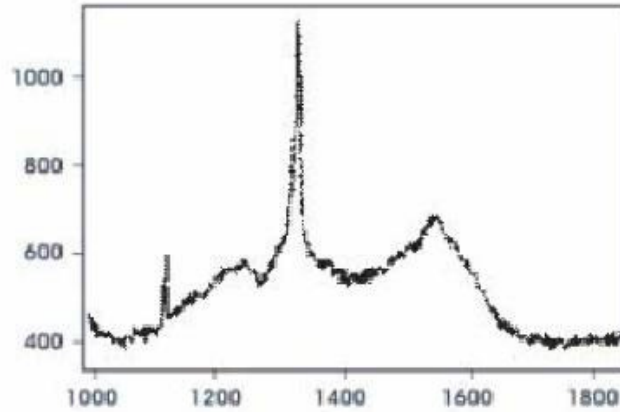


**Fig.5.1.** The Raman spectrum of the deposited diamond coating, exhibiting very good quality diamond. Vertical axis represents the Raman intensity, expressed in arbitrary units, while the horizontal one shows the Raman shift ( $\text{cm}^{-1}$ ).

### **5.3. Results and discussion**

#### **5.3.1. Sample topography on a micrometer scale**

The quality of the (111) diamond sample was first checked by means of non-contact mode atomic force microscopy (NC-AFM) in UHV on various regions and all the scans reveal an extremely flat surface over relatively large areas (RMS roughness: 0.218 nm over surfaces as big as  $1 \times 1 \mu\text{m}^2$ ). Parallel polishing lines are still visible (Fig.5.2) separating smooth regions of 50-100 nm width.

#### **5.3.2. Friction force measurements using standard silicon nitride tip**

In contact mode, the polishing traces are also visible; in both topography and friction pictures smooth terraces of 50-100 nm widths can be observed. (Fig.5.3). Achieving high resolution (features related to the expected lattice periodicities) on smaller scales (nanometer-sized) in topography and lateral force signals proved to be very difficult.

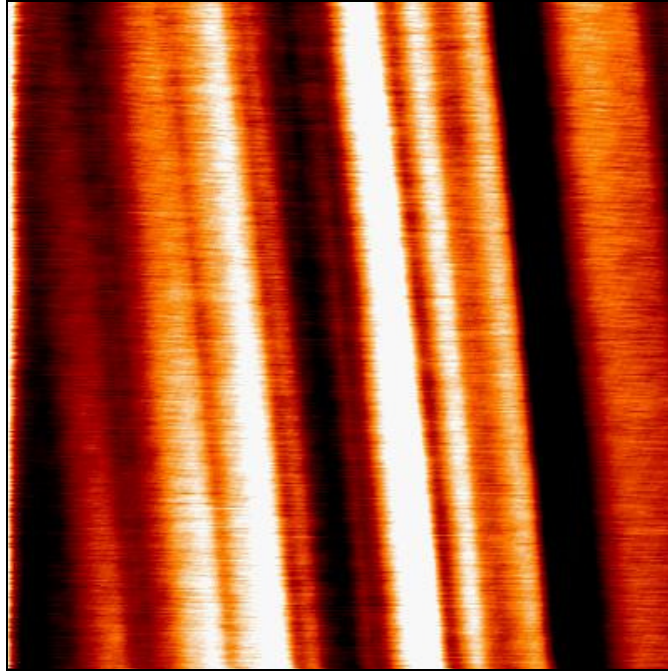
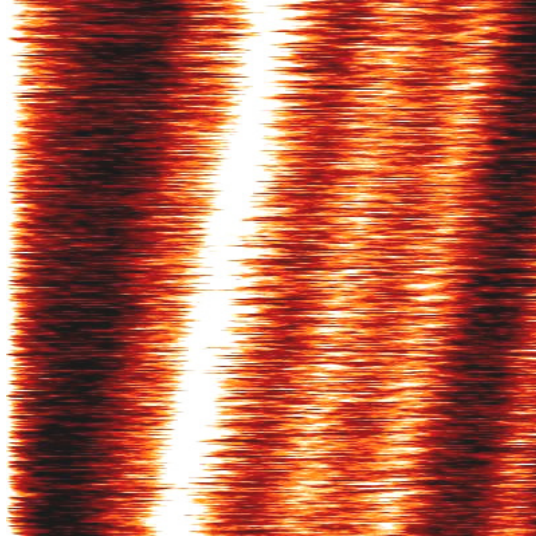


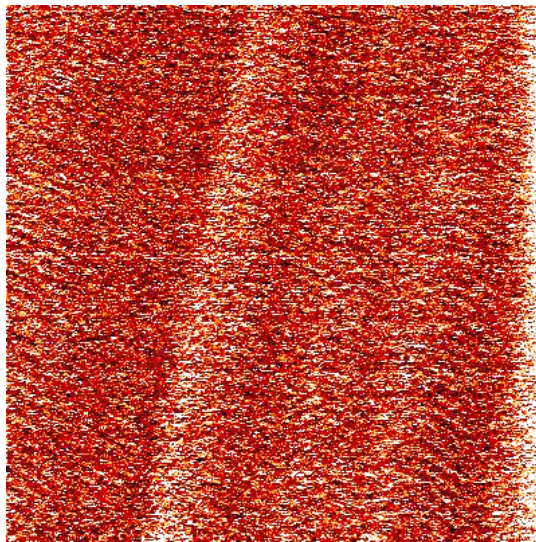
**Fig.5.2.** Non-contact mode AFM topographic image of the (111) diamond sample showing the morphology of the surface after polishing. Scan size:  $1 \times 1 \mu\text{m}^2$ . Velocity: 850 nm/s. The scale ranges from 0 to 0.864 nm (bright areas)

Several tips and a large range of loads (0-30 nN), scan velocities and loop gains have been tried and used during the measurements. Very rarely and only in the lateral force maps quasi-periodical features could be achieved. Fig.5.4 shows the best stick-slip signal obtained at an applied load of 1.88 nN.

Well-defined parallel features can be observed but the rows bear no clear relation to the expected diamond (111) lattice spacings, since the widths of the lines vary from 1 to several Angstroms. We attribute this to the convolution between the periodical atomically flat (111) diamond surface and a disordered tip termination; the resulting lateral force map will exhibit spatially-repeatable features parallel to one of the main crystallographic directions.



(a)



(b)

**Fig.5.3.** (a) Contact-mode AFM topographic image of the hydrogen-terminated diamond (111) surface. (b) Simultaneously measured friction map. The image size is 500x500 nm<sup>2</sup>. Silicon nitride tip. Load 1.5 nN. Scan velocity: 400 nm/s.



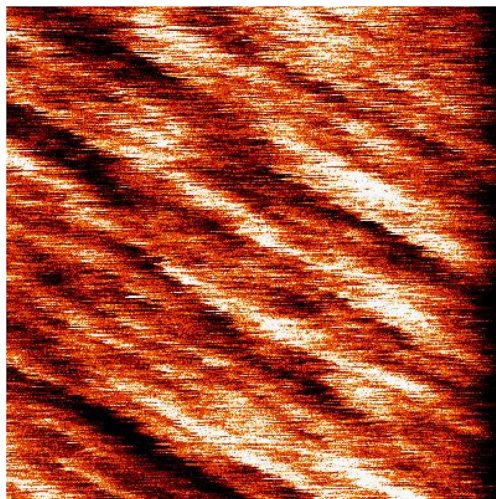


**Fig.5.4.** AFM friction image of a  $2.5 \times 2.5 \text{ nm}^2$  area. Quasi-periodical stick-slip features are visible. A silicon nitride tip was used. Applied load: 1.88 nN. Scan velocity: 3 nm/s.

### 5.3.3. Atomic scale friction between diamond coated tips and (111) diamond surface

In order to provide a hard and stable tip termination the next step was to use diamond-coated cantilevers. In fact the same diamond tip described in chapter 4 was utilized. Topographic images reveal the same polishing lines and small (10-20 nm diameter) atomically flat grains as shown in Fig.5.5. When going down to smaller scale scan areas, like  $10 \times 10 \text{ nm}^2$  and less, unprecedented resolution is achieved simultaneously in topography, normal force error signal and lateral force (Fig. 5.6), showing periodicities that we attribute to the hydrogen atoms that terminate the hydrogen (111) surface. A slight distortion from the hexagonal symmetry can be observed, probably due to the different response of the piezo-scanner with respect to the fast/slow scan directions. After the distortion correction, two representative interatomic distances in orthogonal directions exactly corresponding to the expected hexagonal unit cell,  $0.25 \pm 0.03 \text{ nm}$  and  $0.42 \pm 0.03 \text{ nm}$ , are obtained in all signals along the  $[1\bar{1}0]$  and  $[11\bar{2}]$  direction respectively. (Fig.5.7).

So far the periodicity of the lattice atoms the friction force measurements was reported on layered materials, ionic surfaces [8-14], metals (copper [15] and platinum [16]) and self-assembled monolayers [17]. No real fundamental explanation exists for the fact that friction force maps show such a good resolution while topography ones mostly do not; no observation of atomic lattice contrast in the absence of atomic scale stick-slip behavior has been reported yet. Normally the lateral force atomic lattice contrast, when it is resolved, is often clearer than normal force contrast. In this field there was always some confusion when discussing images showing lattice periodicity and naturally the tendency

is to believe that true atomic resolution is achieved in contact-mode AFM, similar to the one routinely obtained in scanning tunneling microscopy (STM).

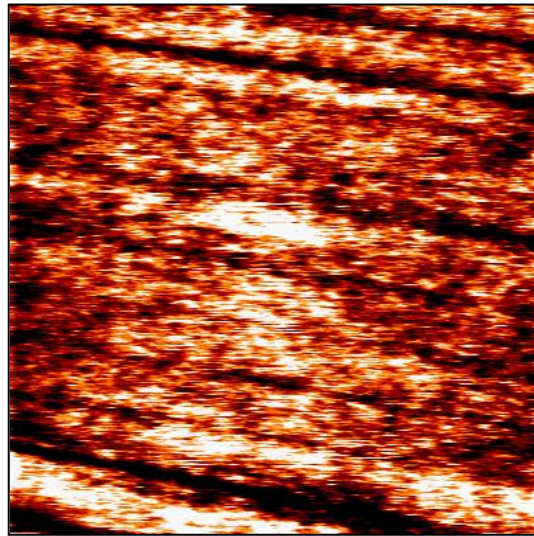
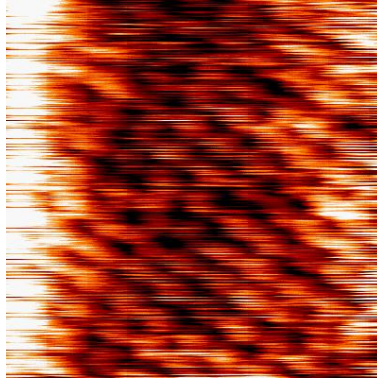


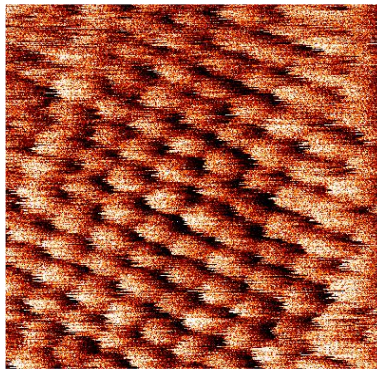
**Fig.5.5.** Contact-mode AFM topographic map of a  $500 \times 500 \text{ nm}^2$  area. A diamond-coated tip (normal spring constant  $C = 0.4 \text{ N/m}$ ) was used. The applied load is  $2.1 \text{ nN}$ . Polishing traces are visible.

Therefore it is of the essence to mention that when an AFM tip is in contact with a certain surface, for typical tip radii, loads and elastic constants of the materials involved, simple elastic contact mechanics estimations show that the contact normally involves not only a single atom. In contact-mode point defects are not resolved and the lateral resolution of the imaged features is limited by the contact area. Another important issue is the structure of the tip end; there is no good reason to expect that the tip atoms will be ordered since, for example, atomic-scale stick-slip has been repeatedly demonstrated with tips made out of amorphous silicon nitride. In the situation of an ordered tip structure, the commensurability with the sample lattice having a different spatial symmetry still remains a problem. The occurrence of the stick-slip movement for an incommensurate tip-sample interface with no preferred relative positions for the tip to reside in, is therefore remarkable if not surprising, since in principle smooth (continuous) sliding should be expected.

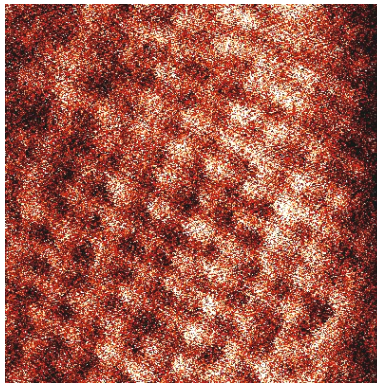
The stick-slip behavior of the frictional forces seems to be a general phenomenon for a nanometer-sized contact for a large range of materials; this is a fact, but several issues still cannot get a fundamental explanation. The question of how a (very possibly) incommensurate interface so commonly exhibits the sample lattice periodicity in the stick-slip still has to be answered. For a nanometer-size contact, can interfacial stresses really sufficiently distort the tip atoms to put them at least in a partial registry with the sample's periodicity?



(a)



(b)



(c)

**Fig.5.6.** Atomically resolved topography (a), normal force error signal (b) and friction force (c) maps of a  $2.5 \times 2.5 \text{ nm}^2$  region on the (111) diamond surface (Raw data). The applied load is 2.5 nN. Scan direction: from right to left. Scan angle: 0 degrees.

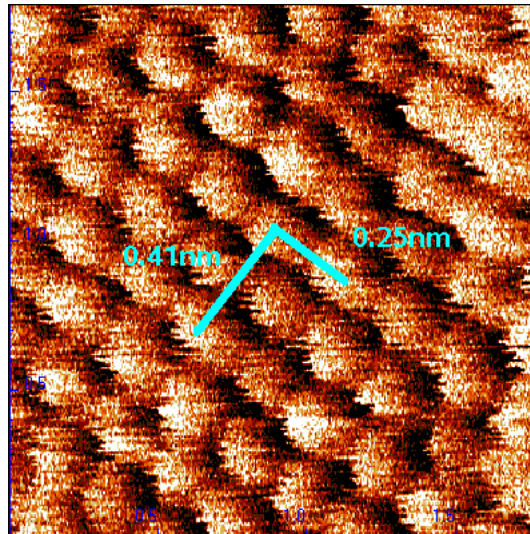


**Fig.5.7.** Typical periodicities of 2.5 and 4.1 Angstrom were observed along the  $[1\bar{1}0]$  and  $[11\bar{2}]$  directions in topography, normal force and friction force windows. The image shows a  $1.8 \times 1.8 \text{ nm}^2$  area (best resolution in normal force error signal; after distortion correction).

Whether all the atoms of the interface are involved in the periodical discontinuous motion or only a part of them is also an open issue. As mentioned before, the first observations of the periodical-atomic-scale stick-slip were made on highly anisotropic materials, like layered materials (graphite and mica). Since these materials show an easy cleavage of layers, the periodicities seen in the frictional force signal were attributed to small flakes getting attached at the tip end being in registry with the surface periodicity. However, periodical lateral forces have been also observed in the case of ionic materials, such as NaCl, which do not have such bonding anisotropy. Theoretical models tried to explain this behavior [18] showing that the contamination of the tip end with sample ions is followed by a rearrangement of ions; eventually one of them takes over the role of tip termination, mechanism leading to a further regular periodical stick-slip-like displacement of the tip.

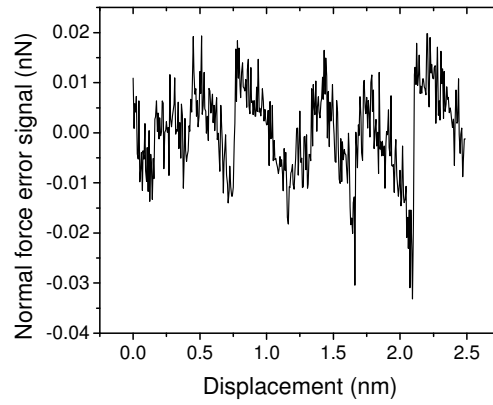
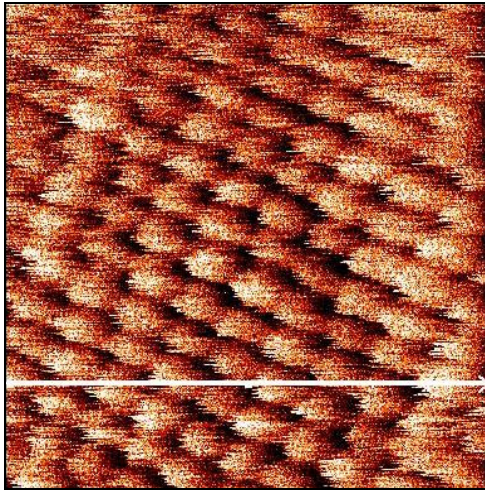
Germann et al. [7] carried out friction force measurements in UHV using a specially grown diamond tip on both the (100) and (111) diamond surface. They could resolve periodic stick-slip features only on the (100) surface, attributed to the (2x1) hydrogen-terminated reconstructed surface. On the hydrogen-terminated (111) diamond sample no features directly related to the surface structure could be achieved, possibly due to the fact that the distance between the atomic rows of the first layer of diamond (111)-(1x1) is smaller than the one corresponding to the surface of (100)-(2x1) diamond. The first observation of atomic-scale periodic friction features (stick-slip) on a (111) diamond sample (hydrogen terminated) was reported by van Oetelaar et al. [5]. Using an ultra-high vacuum atomic force microscope (and Si tips) periodic stick-slip rows were resolved, with a distance of  $1.9 \pm 0.3$  Angstroms between the features, in good agreement with the expected value of 2.5 Angstroms.

In our case we have demonstrated atomic resolution simultaneously in topography, normal force error signal and friction, resolving distances corresponding to the hydrogen atoms at the surface. There are two possible explanations for this fact: one is that we might have an ordered crystallite at the end of the tip moving in registry with the sample periodicity; however this is highly unlikely to happen for both directions [110] and [112]. The other possibility is that we have an extremely sharp tip, namely one hydrogen atom-terminated tip. In chapter 4, this possibility of having a very sharp tip end was further supported and strengthened by the results of a FFM measurement on a specially prepared atomically flat (100) diamond surface. Using *the same* diamond-terminated tip, the complicated perpendicular-rows structure of the (100) surface having very small spacings between C-H dimers was resolved, along with lattice periodicities in topography, normal force and lateral force signals.

A simple check to *estimate* the contact area (and to prove that indeed we are not dealing with a big number of atoms at the sliding interface) can be performed by applying the Derjaguin-Müller-Toporov (DMT) continuum mechanics model, described in chapter 1. We consider this particular case of stiff materials with small but long-range adhesive forces, which represents the case of H-terminated diamond interface. Previously Enachescu et al. investigated the relation between the contact area and load for an extremely hard heterocontact (tungsten carbide tip/ hydrogen-terminated (111) diamond sample) [5] and found it to be in excellent agreement with the DMT continuum mechanics model. In the DMT model for this regime, the pull-off force or critical load  $L_c$  is given by  $L_c = -2\pi\gamma R$ . We have determined the pull-off force experimentally (Fig. 5.9) by measuring the force in approach-retract displacements of the tip and sample. Our experimental value for  $L_c = -10$  nN, which is comparable with other experimental results for H-terminated diamond surfaces [19].

According to the data sheet / SEM micrographs from the diamond-coated cantilever producer, the thickness of the layer is approximately 100 nm, the macroscopic tip radius is in the range of 100-200 nm, but the tips often exhibit a nanoroughness in the 5-10 nm regime, which will definitely improve the resolution on very flat surfaces. Therefore in our DMT estimation for the contact area, we used a typical radius value of 10 nm, but we are aware of the fact that it can be even smaller. Considering the pull-off force value and our tip radius,  $R = 10$  nm, we obtain  $\gamma = 0.1$  J/m<sup>2</sup>, which is reasonable for a diamond-diamond contact [20]. These data, together with  $E_{\text{sample}} = 1164$  GPa,  $E_{\text{tip}} = 1143$  GPa and  $\nu_{\text{tip}} = 0.0691$ ,  $\nu_{\text{sample}} = 0.0791$ , values tabulated in Ref. [20] for (111)/polycrystalline diamond, will lead to a estimate contact area  $A$  of 1.00 nm<sup>2</sup> at an applied load of 2.5 nN. This value indicates that the contact only involves a few atoms. The empirical non-dimensional parameter  $\mu = 0.04 < 0.1$  [21,22], using as equilibrium spacing for the interaction potential of the surfaces  $z_0 = 2.5$  Angstrom, shows that the DMT model is appropriate to use in our case.

A closer look was taken at the contrasts for the signals depicted in Fig.5.6. Normal force signal, usually associated with a height variation of the sample, and lateral force signal, associated with the friction, reveal a different behavior from what should be expected considering the scan direction.



(b)

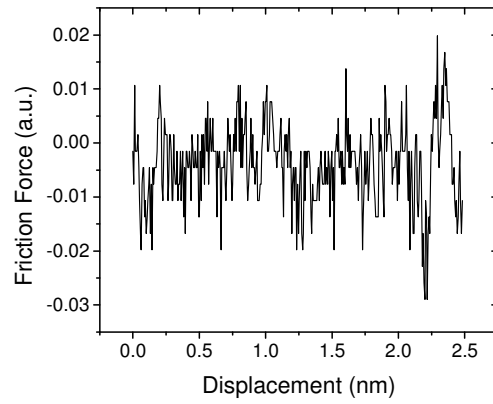
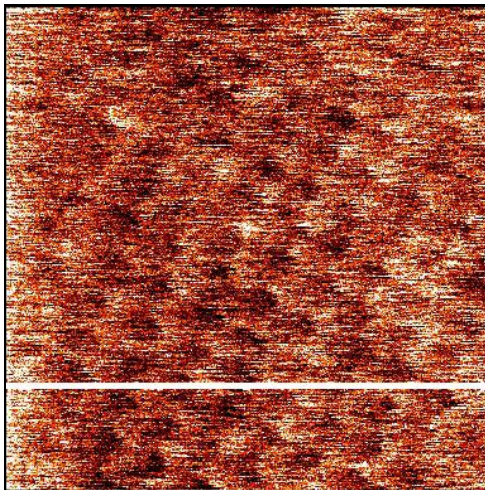


**Fig.5.8.** Raw data maps of the normal force error signal (a) and friction force signal (b). The cross-sections for the same scan line are shown on the right hand side of each image. The pattern for normal force is more pronounced. Signals seem partly synchronized with each other. Scan direction: from right to left. Scan angle: 0 degrees.

For scans in a direction along the cantilever beam, the friction signal should be mixed with the normal force signal, due to a buckling effect. However, in our case the scanning has been performed in the direction perpendicular to the cantilever axis, with a rather slow feedback, and normally on an atomically flat surface we should expect a good decoupling between the normal and friction force signals. Usually, in this way of scanning, the friction force mainly affects the torsion of the cantilever, while the bending associated with the normal forces and a finite time response of the feedback system, remains approximately constant. That is why in many cases the atomic structure in the contact AFM-mode can only be revealed from the lateral force signal, while topography, deduced from the feedback signal which cannot follow the sudden changes due to stick-slip effects, is normally weak.

In the experiment, surprisingly, a good contrast is simultaneously obtained in topography, normal force error signal and friction; profile lines for normal and lateral forces reveal both a typical saw-tooth shape, characteristic to the stick-slip behavior. A comparison of the entire maps built-up by the scan lines also shows that the normal force variation is more pronounced than the lateral force. In the normal force channel the stick-slip signal is remarkably sharp while in the lateral force channel the stick-slip signal is less developed (Fig. 5.8). Moreover, it can be seen that the signals of the normal force and the lateral force are practically not completely synchronized. The appearance of the stick-slip-like signal in the normal force channel cannot be explained by a simple cross-talking between the channels. These effects seen in both signals could appear if the interaction forces experienced by the tip lead to a complicated trajectory, not following a simple straight line.

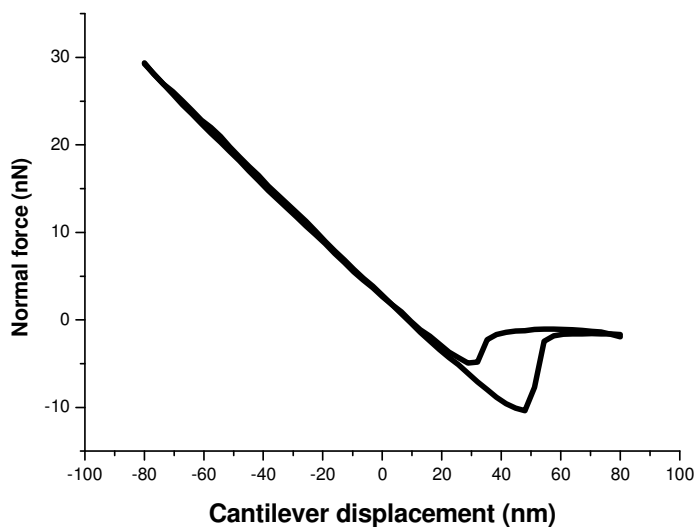


**Fig.5.9.** Force-distance curve for a diamond-coated tip on the (111) diamond surface.

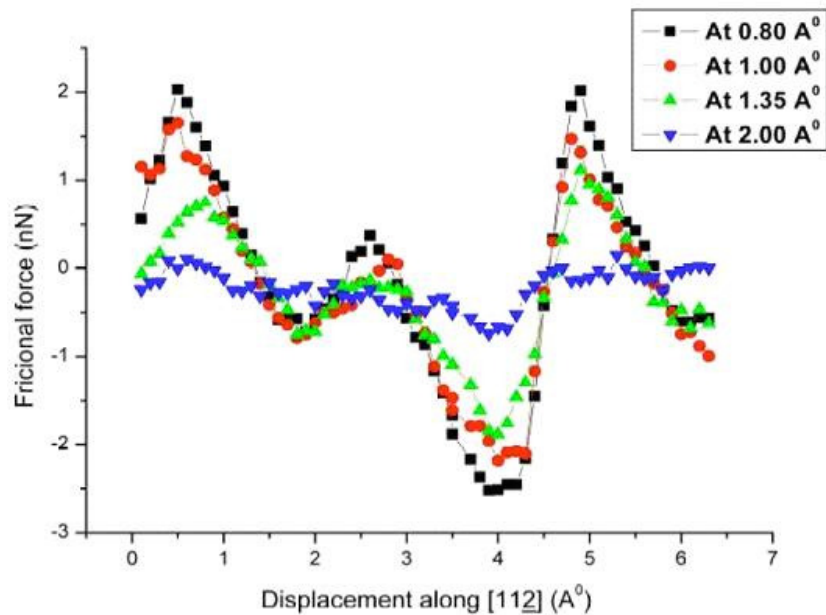
It is important to mention that with the optical beam-deflection AFM technique, longitudinal deformation (buckling) of the cantilever cannot be distinguished *a priori* from vertical deflection induced by normal forces, since both deflection events will change the angle of the cantilever in the same direction. However, for atomically flat surfaces, Fujisawa et al. [23] pointed out that the variations of normal force is so small that the measured normal force signal of an beam-deflection AFM is mostly determined by lateral (frictional) forces acting both along and perpendicular to the cantilever axis. Such a two dimensional “zigzag” stick-slip motion was experimentally observed and reported by the same group of Fujisawa et al. using a 2D FFM, and explained within a 2-dimensional Tomlinson model [24,25].

They analyzed a new stick-slip phenomenon which exerts a frictional force across the scan direction and induces the cantilever to show a square-wave behavior. In their case they found that the observed square-wave behavior was synchronized with the well-known saw-tooth behavior of the cantilever along the scan direction. To explain this, a new model was proposed, that is, the two-dimensional stick-slip model, where the stick-points have the periodicity of the lattice structure while the AFM tip shows two-dimensional stick-slip motion like a zigzag walk along the scan. The stick-point is therefore generally not on the scan line, so that the frictional force acts also across the direction of scan and not only along the scan direction. So, on the atomic scale, friction behaves differently compared to the classical (macroscopic) assumption that friction acts only against the scan direction, with sticking points continuously distributed on the scan line.

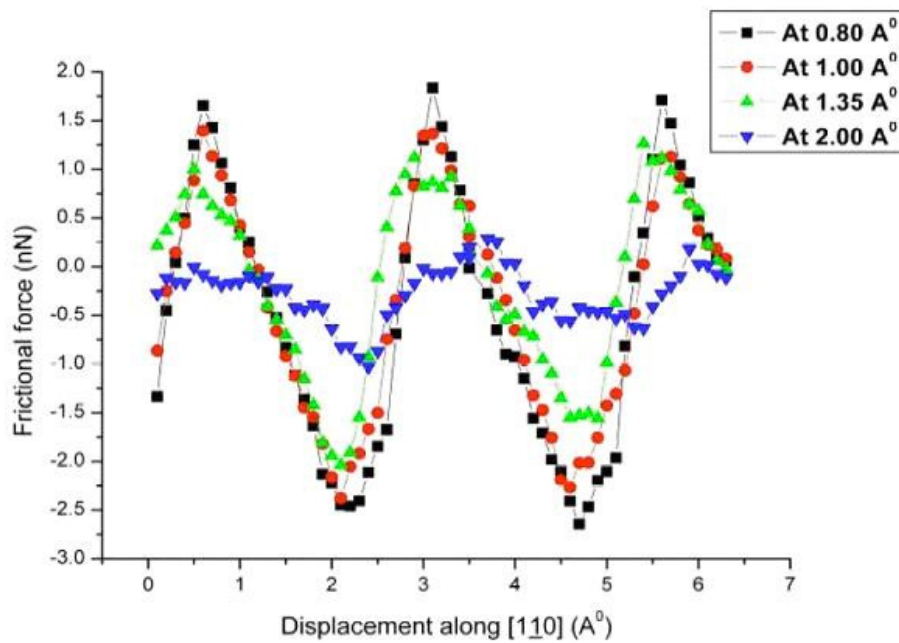
For our experiments on the hydrogen terminated-surface, the stick-slip behavior in the normal force signal also suggests that, besides the common torsion due to friction perpendicular to the beam axis, the cantilever senses a strong interaction perpendicular to scan direction. It is important to mention again that the tip/sample interface consists of two hydrogen-terminated diamond surfaces, and the effect seen in the normal/lateral force signals could be induced by a dynamical rearrangement of the hydrogen atoms while the scanning tip tries to find preferable positions within the lattice to reside in. The good resolution in topography and particularly in the normal force measurements, which show stick-points with the periodicity equivalent to the H-H atomic distances, whereas the stick-slip in lateral force signal is less pronounced, provide evidence that the tip describes a complicated trajectory along the surface.

Previously, using MD simulations Harrison et al. [1] have investigated friction occurring when two diamond (111) hydrogen-terminated surfaces are placed in sliding contact and they did observed each hydrogen atom of the upper surface following a half-circle path about the hydrogen atom on the lower surface closest to it. Once the hydrogen atoms of the upper surface have revolved around the hydrogen atoms of the second surface, the hydrogen-hydrogen repulsive interaction *pushes* the upper-surface hydrogen atoms in the sliding direction.





(a)



(b)

**Fig.5.10.** Calculated total frictional force acting on the tip along the  $[11\bar{2}]$  direction for 4 different scan heights (a). Calculated total frictional force acting on the tip along the  $[11\bar{0}]$  direction for 4 different scan heights (b). Scan: from left to right.

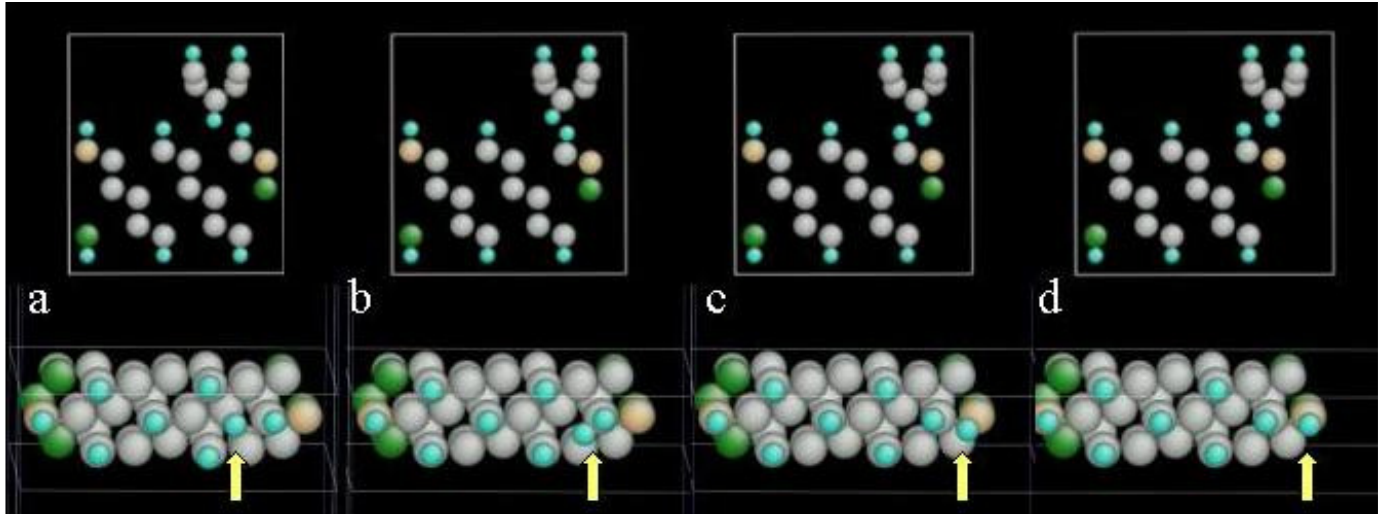


**Fig.5.11.** The calculated dynamics of surface atoms' rearrangement under the moving AFM tip. Upper part corresponds to side view, bottom-top view. Blue atoms are hydrogen, the others are carbon atoms in the crystalline diamond lattice. The snapshots are taken at four different moments. The time interval between a and b is 10 time units, b and c - 2 time units, c and d – 10 time units. Significant atomic rearrangements occur within the short time between the situations corresponding to b and c. The arrow indicates the position of the hydrogen atom attached to the tip (which can be seen in the upper part of the figure).

The experimental results are compared with an *ab-initio* electronic structure calculation (See Appendix 1), in which we slide a 17 atom diamond tip with a *single H-atom* at the apex over the diamond (111) surface at different heights above the surface. The stick-slip behavior becomes pronounced if the distance between the cantilever and the surface becomes less than 2 Angstroms (Fig.5.10). From the calculation for the movement across  $[1\bar{1}0]$  direction, the lateral force stick-slip periodicity corresponds very closely to the experimental value of 0.25 nm. The behavior of the H-apex atom of the tip, as well as the behavior of the H-atoms at the surface when the tip moves along reveal a strong interaction between them, resulting in a complex trajectory of the H-apex atom of the tip (See snapshots in Fig.5.11).

In the image the side view (up) and the top view (bottom) depict the sequence of several steps during the scanning. The time interval between (a) and (b) is five times bigger than the time interval between (b) and (c). One can see that the most remarkable changes in the rearrangement of the hydrogen atoms at the surface and at the tip apex develop within the short term represented in (b) and (c). The top view of the same process shows that a

displacement of the interacting H-atoms occurs not only in the direction of the scanning, that for this cartoons is from left to right, but also perpendicular to the tip movement direction !

It is important to mention that, in reality, when the actual scan direction is not precisely along one line of the lattice structure (even slightly off the main crystallographic direction), the interval and the amplitude of the stick-slip signal in the normal force and the lateral force become irregular, as shown in Fig.4.9. Although the calculations simulated scans just along crystalline directions and did not take into consideration a cantilever attached to the tip, they could nevertheless provide a consistent, qualitative explanation of our experimental results.

Semiclassical models [26-29], based on the Tomlinson model (1929) [30] basically try and succeed only to explain the mechanics of stick-slip behavior. However the interaction potential between the tip (containing one or multiple atoms) and sample is always assumed to be periodic, purely because this proves to be consistent with the experimental results; the crucial issue of how this potential arises remains open in these models. The complex interactions between the tip atoms and a particular H-terminated (111) diamond surface when they pass each other, cannot be explained by phenomenological models and show that detailed electronic structure calculations are necessary to explain friction features on the atomic scale.

#### **5.4. Conclusion**

We have investigated the atomic-scale friction behavior between a diamond-coated tip and a diamond (111) single-crystal surface by means of ultra-high vacuum atomic force microscopy. For the first time atomically resolved topography, normal force error signal and lateral force maps are simultaneously obtained, showing periodicities corresponding to the individual hydrogen atoms that terminate the surface. We attribute this to a very sharp tip, namely one hydrogen atom-terminated tip, describing a stick-slip movement in two orthogonal directions and causing a dynamic rearrangement of the surface atoms; these results are consistent with an *ab-initio* electronic structure calculation which reveals the fact that the repelling Coulomb interaction between the apex H-atom at the tip and H-atoms at the surface is the essential factor that governs the atomic stick-slip behavior.

## References

1. J.A. Harrison, C.T. White, R.J. Colton, and D.W. Brenner, *Phys. Rev. B* 46, 9700 (1992).
2. M.D. Perry and J.A. Harrison, *J. Phys. Chem. B* 101, 1364 (1997).
3. R.E. Clausing, L.L. Horton, J.C. Angus, and P. Koidl, *Diamond and Diamond-like Films and Coatings*, NATO ASI Series, Series B: Physics Vol.266, 1991.
4. K.E. Spear, J.P. Dismukes, *Synthetic Diamond: Emerging CVD Science and Technology*, (Wiley- Interscience Publication, 1994).
5. M. Enachescu, R.J.A. van den Oetelaar, R.W. Carpick , D.F. Ogletree , C.F.J. Flipse, and M. Salmeron, *Phys. Rev. Lett.* 81, 1877 (1998).
6. M. Enachescu, R.J.A. van den Oetelaar, R.W. Carpick , D.F. Ogletree , C.F.J. Flipse, and M. Salmeron, *Trib. Lett.* 7, 73 (1999).
7. G.J. Germann, S.R Cohen, G. Neubauer, G.M. McClelland, H. Seki and D. Coulman, *J. Appl. Phys.* 73, 163 (1993).
8. C.M. Mate, G.M. McClelland, R. Erlandsson, and S. Chiang, *Phys. Rev. Lett.* 59, 1942 (1987).
9. R. Erlandsson, G. Hadziioannou, C.M. Mate, G.M. McClelland, and S. Chiang, *J. Chem. Phys.* 89, 5190 (1988).
10. S. Morita, S. Fujisawa, and Y. Sugawara, *Surf. Sci. Rep.* 23, 1 (1996).
11. G. Meyer and N.M. Amer, *Appl. Phys. Lett.* 56, 2100 (1990).
12. R. Lüthi, E. Meyer, L. Howald, M. Bammerlin, H.-J. Güntherodt, T. Gyalog, H. Thomas, *Trib. Lett.* 1, 129 (1995).
13. L. Howald, R. Lüthi, E. Meyer, G. Gerth, H. Haefke, R. Overney, H.-J. Güntherodt, *J. Vac. Sci. Technol. B* 12, 2227 (1994).
14. S. Fujisawa, Y. Sugawara, and S. Morita, *Philos. Mag.* A7 4, 1329 (1996).
15. R. Bennewitz, E. Gnecco, T. Gyalog, and E. Meyer, *Trib. Lett.* 10, 51 (2001).
16. M. Enachescu, R.W. Carpick, D.F. Ogletree, and M. Salmeron, *J. Appl. Phys.* 95, 7694 (2004).
17. L. Howald, R. Lüthi, E. Meyer, and H.-J. Güntherodt, *Phys. Rev. B* 51, 5484 (1995).
18. A.I. Livshits and A.L. Shluger, *Phys. Rev. B* 56, 12482 (1997).
19. N.A. Burnham, R.J. Colton, and H.M. Pollock, *Nanotechnology* 4, 64 (1993).
20. C.A. Klein and G.F. Cardinale, *Mater. Res. Bull.* 27, 1407 (1992).
21. D. Tabor, *J. Colloid Interface Sci.* 58, 2 (1977).
22. K.L Johnson , *Langmuir* 12, 4510 (1996).
23. S. Fugisawa, Y. Sugawara, and S. Morita, *Microbeam Analysis* 2, 311 (1993)
24. S. Fugisawa, Y. Sugawara, S. Ito, S. Mishima, T. Okada, and S. Morita, *Nanotechnology* 4, 138 (1993).
25. S. Morita, S. Fujisawa, and Y. Sugawara, *Surf. Sci. Rep.* 23, 3 (1996).
26. D. Tomanek, W. Zhong, and H. Thomas, *Europhys. Lett.* 15, 887 (1991).
27. J.B. Sokoloff, *Thin Solid Films* 206, 208 (1991).
28. M. Weiss and F.-J. Elmer, *Phys. Rev. B* 53, 7539 (1996).
29. T. Gyalog and D.W. Brenner, in *Physics of Sliding Friction*, edited by B.N.J. Persson and E. Tosatti (Kluwer, Dordrecht, 1996), p. 403.
30. G.A. Tomlinson, *Phil. Mag.* 7, 905 (1929).



# **Chapter 6. Effect of temperature on friction between a silicon tip and the (001) surface of NaCl observed in ultra-high vacuum**

## **6.1. Introduction**

In the last decade the atomic-scale stick-slip phenomenon has been studied on various well-defined surfaces using dedicated ultra-high vacuum friction force microscopes. This captivating phenomenon revealing the lattice periodicity was observed on a broad range of materials.

One of the most investigated objects was the simple surface of cleaved ionic materials; atomically flat terraces can be easily obtained and measured in UHV [1]. Among all the alkali halides, the (001) surface of NaCl became a representative sample for analyzing atomic-scale frictional behavior. The load and velocity dependence of friction have been measured and modeled [2,3]. The nanometer-scale abrasive wear on NaCl and the dependence of wear rate on velocity and normal force was investigated [4] and the transition from stick-slip to continuous sliding in the atomic friction was also revealed for the first time by recent measurements [5]. Very little is known about the temperature dependence of atomic-scale friction on well-defined surfaces. In this chapter the effect of temperature on friction between a silicon tip and the (001) surface of NaCl, measured using a Variable-Temperature Beam-Deflection AFM operated under UHV conditions, is presented and discussed in relation to existing theoretical models.

## **6.2. Experimental**

### **6.2.1. Instrumental details**

An Omicron Variable-Temperature Beam Deflection AFM, largely described in Chapter 2, integrated in an UHV setup (base pressure  $4 \times 10^{-11}$  mbar) was used for all the measurements. The flexible combination of direct and/or resistive heating with cooling (using a liquid helium continuous flow cryostat) provides a large range of operation temperatures from typically less than 25 up to 1500 K. In the present investigation, FFM measurements were done in the interval of 25 K- room temperature; a special

proportional-integral-differential (PID) controller monitored and adjusted the temperature of the sample. Rectangular cantilevers with integrated Si tips having a normal spring constant  $C = 0.4 \text{ N/m}$  (MikroMasch, NCS12 series) were used in the friction experiments.

### **6.2.2. Sample/tip preparation**

The sample utilized was a NaCl crystal which was cleaved in air with a sharp metallic blade. This method is known to provide a clean and extremely flat (001) surface. Within 15 minutes, the crystal was further mounted on a special metallic holder with a dedicated foil screening against thermal radiation (for cooling applications), introduced in UHV and subsequently annealed at  $150 \text{ }^\circ\text{C}$  for 2 hours to remove any charges due to cleavage and the possible water or contamination due to the short air exposure. No special treatment was applied to the silicon tip; it was simply heated up in vacuum for 1 hour and it was likely covered by a silicon-oxide layer. To avoid uncertainties in the tip curvature radii, dimensions and spring constants for different cantilevers, the relative changes in friction during the whole set of experiments at various temperatures were investigated using always the *same* cantilever/tip.

## **6.3. Results and discussion**

### **6.3.1. Surface topography: micrometer scale investigation**

The quality of the cleaved NaCl surface was investigated in vacuum by means of contact-mode AFM over various regions and scan sizes. All the images show atomically flat terraces of typically several 100 nm lateral extension, which are separated by cleavage steps, consistent with previous reported UHV measurements on a broad range of different crystalline ionic materials [6]. Surface structures (i.e. steps) were reproducible on different regions of the sample and remained stable even after long scans. (Fig. 6.1).

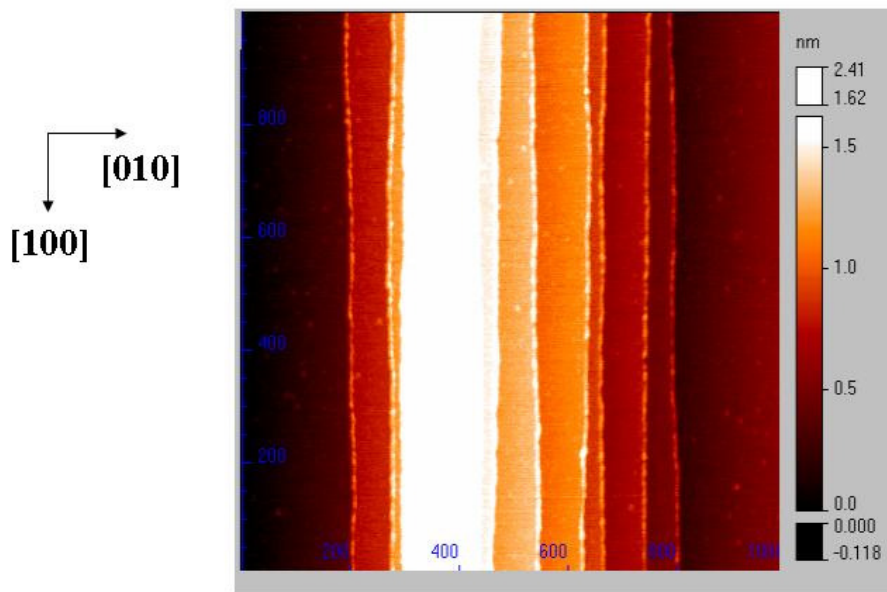


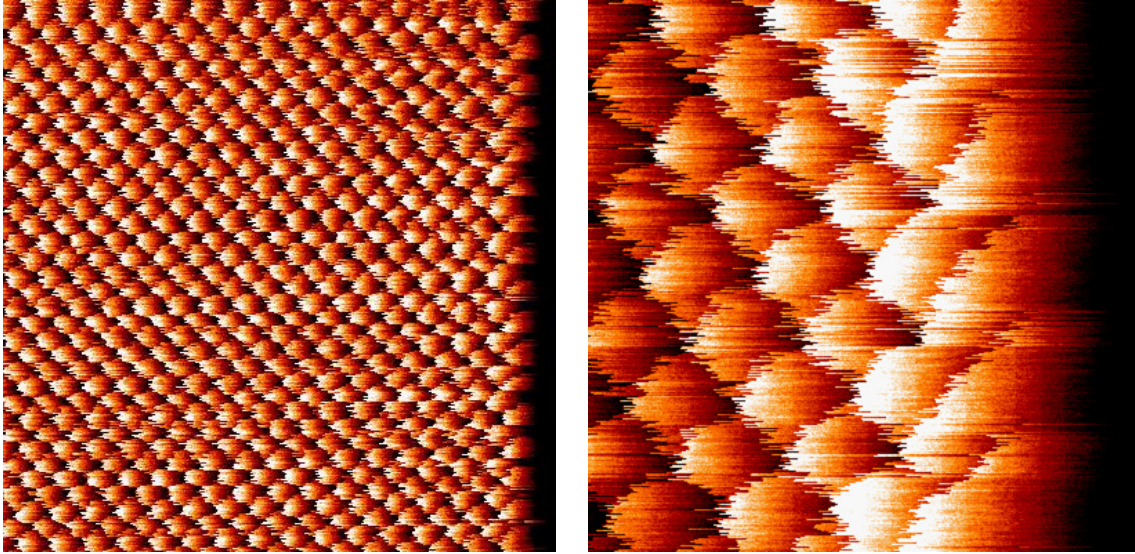
**Fig.6.1.** Topographic  $1 \times 1 \mu\text{m}^2$  image revealing the stepped NaCl (001) surface after cleavage. Large flat terraces and steps aligned mostly along the [100] direction are visible.

### 6.3.2. Atomic-scale friction: the NaCl surface at room temperature

The frictional forces were investigated down to nanometer-sized regions using the same Si tip. In order to avoid topographic influences upon the lateral force signal, all measurements were recorded far from surface steps, approximately in the middle of the broadest flat terraces. In a standard AFM experiment, even for a sharp tip termination, the contact area tip/sample is in the range of several square nanometers. In this experiment, positioning the tip on a smooth region in between distant surface steps is of the essence if one wants to get accurate information about the atomic-scale friction force.

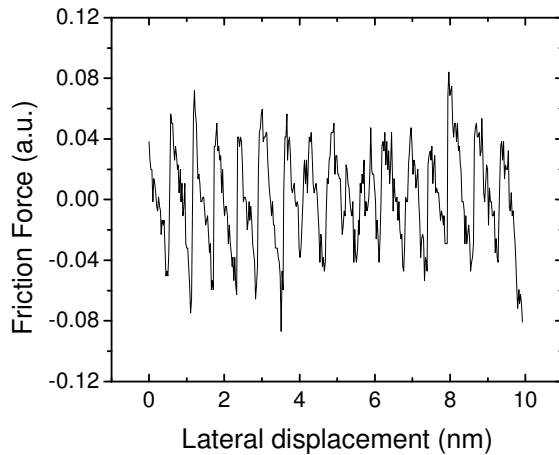
Topography, normal force error signal and friction forces were simultaneously recorded, while maintaining a constant applied load. The 0.48 nm lattice periodicity of the NaCl (001) was clearly observed in both normal and lateral force signals, effect consistent with the two-dimensional stick-slip model proposed by Morita, Fujisawa et al. [7]. Fig. 6.2 (a) and (b) show the lateral force maps of two regions different in size. The typical saw-tooth shape of the measured stick-slip signal is depicted in Fig. 6.2.(c).





(a)

(b)



(c)

**Fig.6.2.** Lateral force maps acquired on a  $10 \times 10 \text{ nm}^2$  (a) and  $2.5 \times 2.5 \text{ nm}^2$  (b) area showing lattice periodicity. (c) Friction force line profile corresponding to (a): stick-slip signal at 300 K. The scan direction is from right to left. The externally applied load: 1.5 nN. Scan velocity: 50 nm/s.

### 6.3.3. Temperature effect on friction measured within the 25 K – room temperature interval

After achieving lattice periodicity in the stick-slip signal at room temperature, the next step in the experiment was to try to analyze what the effect of the temperature would be upon the periodical lateral force signal. Therefore the sample was first cooled down to 25

K and lateral force measurements were successively performed at several (increasing) temperatures up to room temperature. Before each measurement, the tip was withdrawn a few coarse steps while the new temperature of the sample was stabilized at a set value using a PID controller. Then the standard tip auto-approach procedure was applied until the snap-into-contact takes place due to adhesive forces. The tip was then kept into contact with the cold sample surface for a couple of minutes to allow thermal equilibrium for the tip end and sample surface.

In any AFM experiment, the normal force acting on the tip is always the sum between the adhesion force exerted between tip end/surface atoms and the so-called applied load, which is to be chosen and set before the scan starts. To be able to compare frictional forces at different temperatures, the other scanning parameters such as applied load and scan velocity should be kept similar for all measurements. The moment when the tip jumped into contact with the sample surface was taken as reference zero normal deflection for the cantilever. For all the cases, an extra external load of 1.5 nm was applied on the Si cantilever. Although friction is known to show very little dependence on velocity at normal scan rates, the speed was also maintained constant for all the situations, i.e. 50 nm/s.

In Fig.6.3 the lateral force map (a) measured at 25 K is shown, together with a typical friction line trace (b). It is obvious that the lateral contrast became much less sharp compared to the one seen in the room-temperature signal. The lattice periodicity is still recognizable in the line profile, but when comparing with Fig. 6.2.(c) significant differences are visible, namely the long initial sticking part and the amplitude of the periodical part.

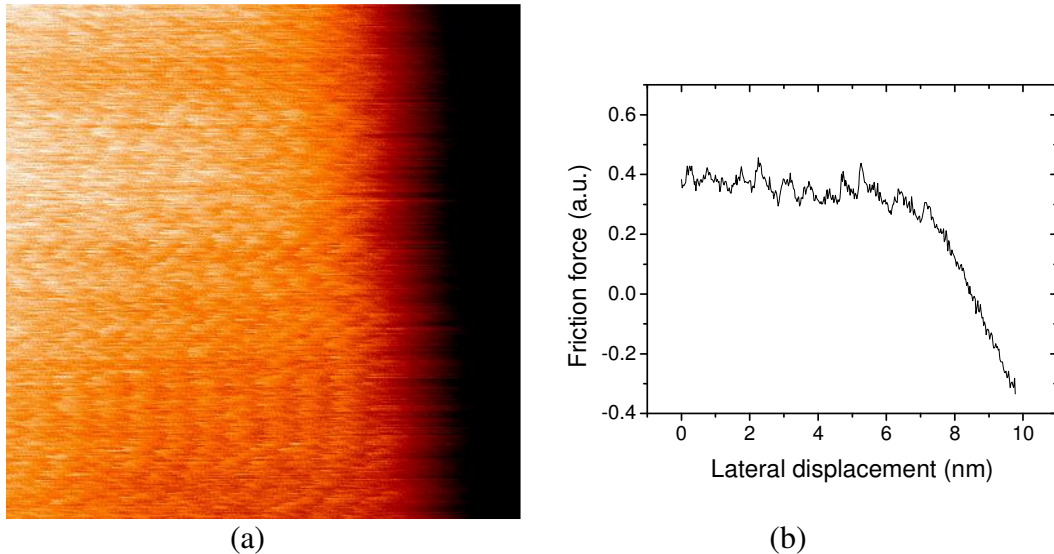


**Fig.6.3.** (a)  $10 \times 10 \text{ nm}^2$  lateral force image of NaCl (001) in UHV at 25K. (b) Corresponding friction force line trace at 25 K. The signal becomes less sharp and differences in force amplitude can be observed. Note the difference in the vertical scale for the stick-slip line compared to Fig.6.2.(c). Same applied load: 1.5 nN.

Similar measurements were carried out at several temperatures between 25 K and room temperature. For all the measurements, the lateral force was recorded while scanning the tip forward and backward in the (100) direction over the NaCl(001) surface. The hysteresis area enclosed in the loop formed by the two lines of the same scan is a measure of the energy dissipated via friction during one cycle. In literature, the average friction force is normally calculated by dividing the area of hysteresis by two times the scanned distance. Fig.6.4 shows such friction loops while recording forward/backward lateral forces at room temperature and 25 K respectively. Energy dissipation and mean friction forces obviously vary with temperature.

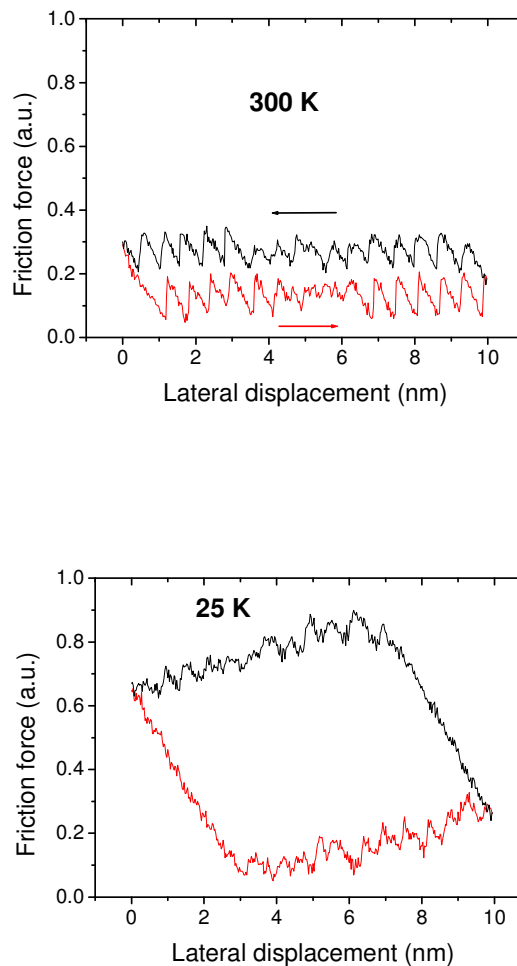


**Fig.6.4.** Friction loops for two temperatures showing differences in energy dissipation and average friction. The same previous scan parameters were used (load and velocity).

The dissipated energy per cycle/average friction was plotted as a function of temperature for all the values used in the experiments and the result can be seen in Fig.6.5.

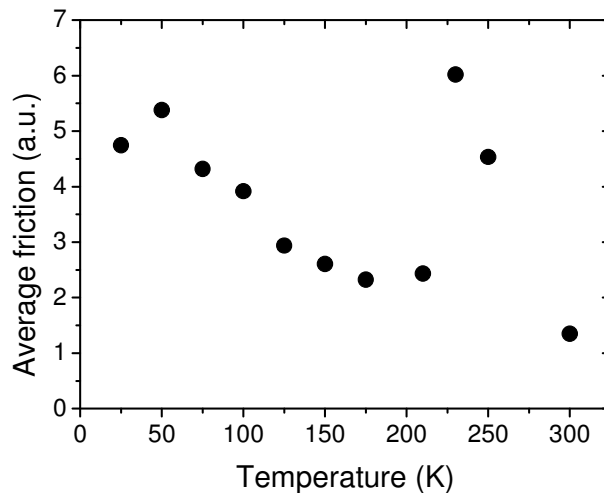


**Fig.6.5.** Temperature dependence of the mean lateral force (or energy dissipation).

The first conclusion is that there are obvious differences in the average friction when varying the temperature. The sharpness of the lateral force maps is much more reduced below 25 K and, in general, measured friction at lower temperatures (interval 25- 210 K) seems to be higher compared to the room temperature one. For two temperature points (230 and 250 K) the friction value appears to be comparable or higher than the value measured at 25 K.

When looking at the typical force signals at temperatures below 300 K one could see that they consist of a (variably) long sticking part, followed by a regular or (sometimes) less regular, periodic part.

The amplitudes of this periodical lateral force signals for all the temperatures were also analyzed. In Fig.6.6 the standard deviation (which is the square root of the average squared deviation from the mean) of the force amplitudes as a function of temperature is depicted. The values corresponding to the interval 25-210 K are smaller than the 230-300 K range; it is interesting to notice that differences occur again around the temperature value of 230 K.

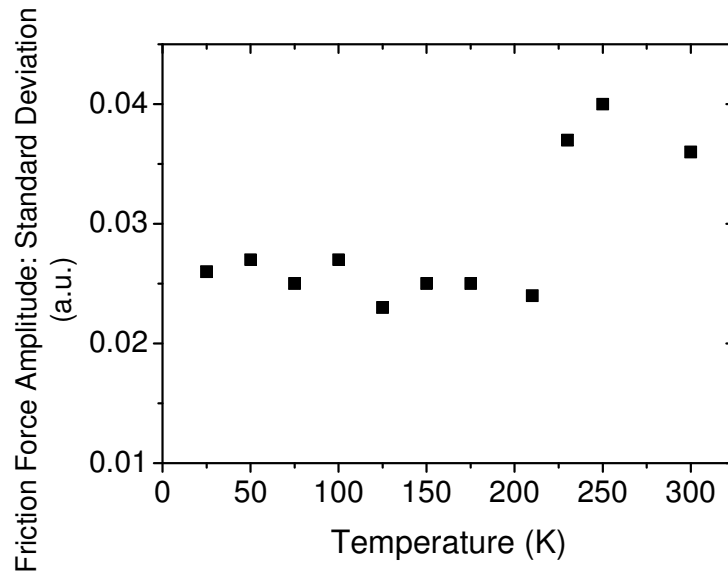


**Fig.6.6.** Analysis of the lateral force amplitude as a function of sample temperature.

### 6.3.4. Theoretical models

The fact that from our experiments the measured average values of friction forces at low temperatures are higher compared to the one corresponding to room temperature (with the exception of two temperature points) is not surprising. Gnecco et al. [2,3] have demonstrated the velocity dependence of atomic-scale frictional processes on well-defined surfaces. Using a one-dimensional Tomlinson model and including the effects of thermal activation, they obtained a formula for the dependence of the lateral force on velocity and temperature right before a slip process. The physics behind this formula can be briefly described in the following way: the AFM tip has to overcome a certain energy barrier to be able to slip. This jump can be activated by thermal fluctuations and the tip can further move to the next relaxed position. According to the model, the lower the scan velocity is, the higher is the probability for an early thermally activated jump. Consequently, the friction force will decrease with increasing temperature and increase with increasing velocity. At a finite temperature, the lateral force necessary to induce a jump will be less than the value determined at zero temperature, which is clearly qualitatively consistent with the experimental results shown in Fig.6.4 and 6.5. However, in their mathematical formula, the temperature dependence of the friction force is weak compared to the velocity dependence, and the energy barrier simulated in the model predicts a variation in the mean force of only 25% over the temperature range from 0 to 300 K. This is much smaller than the factor of approximately 3.53 between the friction at 25 K and room temperature, according to our measurements.

Using molecular dynamics (MD) calculations Harrison et al. [8] investigated the friction between two atomically flat (111) diamond surfaces in sliding contact in the case of relative movements in different crystallographic directions, as a function of applied load, sliding velocity and temperature. The normal force and the frictional force acting on each lattice were calculated by summing the forces on each rigid-layer atom and averaging this sum over 20 time steps. The sliding plane between surfaces was XY, while the friction coefficient  $\mu$  was defined as the average frictional force, divided by the average normal force, e.g.  $\langle F_y \rangle / \langle F_z \rangle$ . The average normal pressure  $\langle P_z \rangle$  is defined as  $\langle F_z \rangle$  divided by the area of the rigid layer in the XY plane. The influence of temperature upon friction coefficient is shown in Fig.6.7.

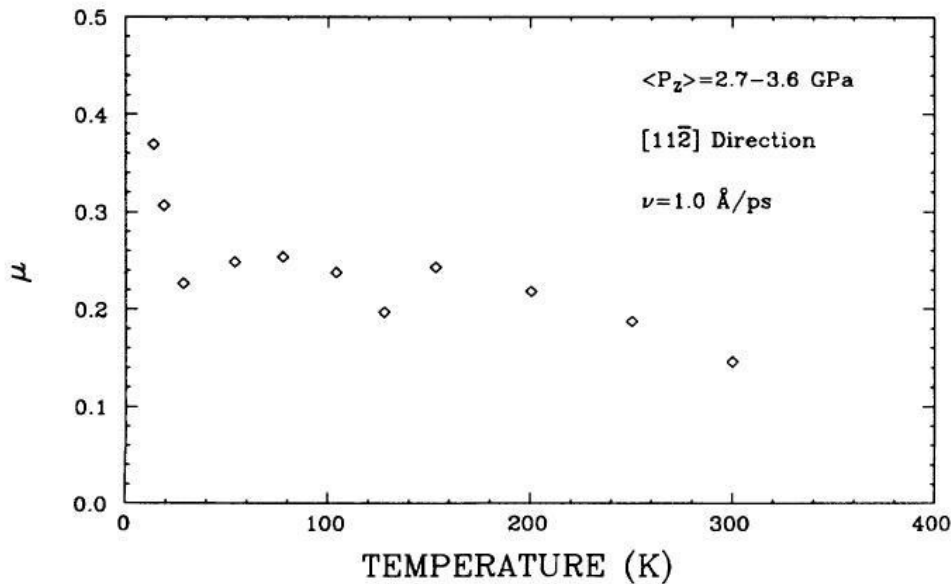


**Fig.6.7.** Coefficient of friction as function of temperature. Sliding direction is [112] at a velocity of  $1 \text{ \AA/ps}$  on a diamond (111) surface. From Ref. [8].

The value of the friction coefficient was found to be greatest at 10 K, followed by a sharp drop in the temperature interval from 10 to 50 K. An approximately constant value for  $\mu$  is obtained from 50 to 150 K; then from 150 to room temperature (300) K, the friction coefficient decreases as the temperature increases. This behavior was explained following the atomic motion of the hydrogen termination of both contacting diamond surfaces. For the hydrogen atoms of the upper surface to slide past the hydrogen atoms on the lower surface they should first get pushed away from each other in the sliding plane (XY) so they can further revolve about one another. For temperatures higher than 150 K, the increased level of thermal motion can facilitate this type of process; therefore friction coefficient between surfaces will be smaller. The thermal motion at very low temperature (i.e. 10 K) is negligible and relative movements of hydrogen atoms when they pass each other will become extremely difficult, leading to high value for  $\mu$ . Although the above-

mentioned work refers to the sliding friction between the surfaces of a different material (diamond), and on a different velocity regime, it still gives a general, intuitive image on what should be expected in terms of temperature effects upon friction forces, i.e higher friction in the absence of thermal motion (at low temperature).

An extensive work in the field of scanning force microscopy on insulators has been carried out by Shluger et al.; their results and related reports on theoretical models can be found in an excellent review article [9] where the possibility of obtaining atomic and chemical resolution in contact and non-contact mode SPM are discussed in great details. For contact-mode AFM on NaCl or other ionic crystals, it is demonstrated that even in the “softest” scan conditions and in the absence of tip contamination, scanning is always likely to induce strong tip and surface deformations. After jumping into contact, the tip (simulated by a sharp corner of a  $(\text{MgO})_{32}$  cube) will get contaminated with ions from the sample surface. At room temperature, a scan along the [110] surface axis of a LiF surface was simulated at constant height for a speed of 1m/s. In the beginning the scanning is unstable; the cluster of surface material adjusts itself and redistributions of ions along the tip and between sample and tip end occur until a stable configuration is formed. At that moment only one ion takes over the role of tip end, and regular, reproducible stick-slip behavior, having the sample lattice periodicity, can be seen in the plot of tip-sample system total energy.

This proves that tip contamination due to adhesion to the surface atoms may promote periodic AFM imaging, if the material collected from the sample surface can create a stable structure on the tip. Moreover, the tip reaches optimal scanning conditions by exchanging atoms (ions) with the surface and changing its structure. This effect called “self-lubrication”, “self-healing” or dynamic “self-organization” could be a more general effect and might explain why, on ionic surfaces, the surface lattice periodicity can be obtained in AFM for a variety of tips and large applied loads. However their simulation used a very sharp tip which is normally not always the case in real experiments. For large contact area between tip and sample more complicated behavior can be expected and temperature can be a very important factor affecting the atomic (ionic) rearrangements at the sliding interface. Therefore a possible explanation for some irregularities in the friction force signals at lower temperatures and especially for the high friction loops obtained for two temperature values, can be found in the complicated rearrangements of atoms at the interface. It is easy to understand that at low temperature the atoms or ions will have less mobility to rearrange themselves in an optimal (energetically favorable) configuration. This is a possible reason for the long sticking part of the friction lines; this could be consistent with a higher static friction due to accumulation of sample atoms (or ions) on the tip and at the interface after the jump into contact. At low temperature quick atomic readjustment is not possible due to little thermal fluctuations and the scan starts with a complicated, possibly larger-size tip apex configuration.

Such a “contamination” effect can in principle occur at any temperature, but it is most likely to happen when thermal motion is substantially reduced, namely at lower temperature. Since the structure of the tip can in principle change after every jump-to-contact event, (and we do a tip/sample approach before each measurement at a certain

temperature), it is not surprising that some of the friction loops, i.e. at 230 and 250 K, show larger energy dissipation or mean friction value.

Another important issue for our experiments is the total normal force applied on the tip during the measurements at different temperatures, force which in the end can determine or influence the friction force. As briefly mentioned before, in all the experiments, the normal force acting on the tip will be the sum between adhesion and applied load. We have indeed maintained the applied load at a constant value of 1.5 nN for all the scans, but the question is, of course, whether the adhesion properties of the sample stay unchanged as well for the entire temperature interval 25-300 K. It is well known that in vacuum cold surfaces act as cryo-pumps, adsorbing residual gases. A freshly cleaved ionic surface of (001) NaCl should be no exception.

Although adsorption of water on ionic surfaces like alkali halide surfaces has been studied theoretically [10-12] and experimentally [13-18], essential issues such as how much water adsorbs and how quickly the water reacts with the surface are still under debate. Water physisorbs on perfect surfaces with quite low adsorption energies: 0.4-0.5 eV for NaCl and KCl and 0.25 eV for LiF [11-13], and therefore the amount of adsorbed water will strongly depend on temperature. For example, surface second harmonic generation investigations [14] show that on NaCl surface an ordered monolayer coverage of water is achieved only after two days' exposure in air at a relative humidity of 50%. However Estel et al. [13] show that even at a vacuum of  $2 \times 10^{-10}$  Torr adsorption happens very quickly if the surface is cooled down to 170 K. In the present work, the UHV system provided a base pressure of  $4 \times 10^{-11}$  mbar. While cooling down the sample (25 K) a pumping effect was always observed, i.e. the pressure gauge in the AFM chamber indicated that pressure was beyond its detection limit, demonstrating a lower pressure in the system than the initial ( $4 \times 10^{-11}$  mbar) value. Nevertheless we do not expect to have significant amount of adsorbed water/ice on the cleaved sample surface at low temperatures since in the present design of the Variable-Temperature Beam Deflection AFM, the backside of the sample holder is cooled via a highly flexible copper braid that ensures the thermal connection with the liquid helium cryostat. A typical cooling procedure might take up to 1-1.5 hour and far before the sample reaches say 25 K, the copper braid, having a much larger surface area than the sample and a lower temperature than the backside of the sample will have already been exposed to residual gases and water and collected most of them.

#### **6.4. Conclusion**

Atomic-scale friction between a silicon tip and the atomically flat (001) NaCl surface was investigated in ultra-high vacuum at various sample temperatures in the interval from 25 to 300 K. The temperature dependence of measured average friction forces is found to be in good qualitative agreement with theoretical models that consider a thermally-activated discontinuous tip movement during scanning. Higher mean friction values observed for two temperature values were attributed to possible changes in the tip apex configuration.



## References

1. L. Howald, H. Haefke, R. Lüthi, E. Meyer, G. Gerth, H. Rudin, and H.-J. Güntherodt, *Phys. Rev. B* 49, 5651 (1994)
2. E. Gnecco, R. Bennewitz, T. Gyalog, Ch. Loppacher, M. Bammerlin, E. Meyer, and H.-J. Güntherodt, *Phys. Rev. Lett.* 84 (6), 1172 (2000).
3. E. Gnecco, R. Bennewitz, T. Gyalog, and E. Meyer, *J. Phys.: Condens. Matter* 13, R619 (2001).
4. E. Gnecco, R. Bennewitz, A. Socoliuc, and E. Meyer, *Wear* 254, 859 (2003).
5. A. Socoliuc, R. Bennewitz, E. Gnecco, and E. Meyer, *Phys. Rev. Lett.* 92, 134301 (2004).
6. R.W. Carpick, *The Study of Contact, Adhesion and Friction at the Atomic Scale by Atomic Force Microscopy*, Ph.D. Thesis (University of California, Berkeley, December 1997), chapt. 7.
7. S. Morita, S. Fujisawa, Y. Sugawara, *Surf. Sci. Rep.* 23, 3 (1996).
8. J.A. Harrison, C.T. White, R.J. Colton, and D.W. Brenner, *Phys. Rev. B* 46 (15), 9701 (1992).
9. A.L. Shluger, A.I. Livshits, A.S. Foster, and C.R.A. Catlow, *J. Phys.: Condens. Matter* 11, R295 (1999); and references therein.
10. B. Wasserman, S. Mirbt, J. Reif, J.C. Zink, and E. Matthias, *J. Chem. Phys.* 98, 10049 (1993).
11. L.N. Kantorovich and A.L. Shluger, *J. Chem. Phys.* 1, 1341 (1982) (in Russian).
12. L.N. Kantorovich, A.L. Shluger, and Yu.E. Tiliks, *J. Chem. Phys.* 3, 894 (1984) (in Russian).
13. J. Estel, H. Hoinkes, H. Kaarmann, H. Nahr, and H. Wilsch, *Surf. Sci.* 54, 393 (1976).
14. P. Tepper, J.C. Zink, J. Reif, and E. Matthias, *Phys. Rev. B* 42, 9685 (1990).
15. P. Tepper, J.C. Zink, J. Reif, H. Schmelz, B. Wasserman, and E. Matthias, *J. Vac. Sci. Technol. B* 7, 1212 (1989).
16. R.A. Lad, *Surf. Sci.* 12, 37 (1968).
17. P.B. Barraclough and P.G. Hall, *Surf. Sci.* 46, 393 (1974).
18. S. Folsch, A. Stock, and M. Henzler, *Surf. Sci.* 264, 65 (1992).

## **Appendix 1. Computational method**

The actual calculations were performed by **Juan Amir** in our group (Department of Applied Physics, Molecular Materials and Nanosystems (M2N) Group, Eindhoven University of Technology, The Netherlands).

In this work we have studied the effect of sliding a diamond tip over the (111) unreconstructed hydrogen terminated and the (100)-(2x1):H diamond surfaces by means of a fast local-orbital minimal basis DFT pseudopotential method (Fireball96) [1]. This technique offers a very favorable accuracy/efficiency balance if the atomic-like basis set is chosen carefully, opening the way to large scale simulations including hundreds of atoms with a modest computational cost. This approach is complemented with more accurate (but time consuming) standard plane wave DFT calculations using CASTEP [2] that confirm the basic findings of the FIREBALL simulations. In particular, both methods show the same periodic features in the frictional force along the [11 $\bar{2}$ ] direction.

The tip/sample contact has been described with a hydrogen terminated slab with 8 (111) planes and 5x5 lateral periodicity (with a total of 200 atoms) and a (111)-oriented diamond tip with 17 C atoms (stacked on 5 layers), where all the dangling bonds (in particular the tip apex) are saturated by hydrogen atoms. For the case of (100) surface the same tip was used, while the sample was represented by a hydrogen-terminated slab with 14 (100)-(2x1) planes and 4x4 lateral periodicity (in total 273 atoms). In FIREBALL, the valence wave functions are expanded in a set of strictly localized pseudo-atomic orbitals [3] (they are exactly zero for distances larger than the cut-off radius  $R_c$ ). The FIREBALL code is used with a non-local norm conserving Hammann-Bachelet pseudopotentials [4,5] and the local density approximation (LDA) [6] as exchange-correlation functional. We have used a minimal basis that includes s and p orbitals with a cutoff radii of  $R_c = 3.5$  a.u for C and a single s orbital with a cut-off radius of  $R_c = 3.0$  a.u. for H. This basis provides a good description of bulk diamond structural properties with a lattice parameter  $a = 3.6247$  Angstrom, bulk modulus  $B = 3.89176$  Mbar and a pressure derivative ( $dB/dp$ ) = 2.58217 (experiment:  $a = 3.557$  Angstrom,  $B = 4.43$  Mbar and ( $dB/dp$ ) = 4.07). For the CASTEP plane wave calculations we used the generalized gradient approximation (GGA-PBE) [7] as the exchange-correlation energy and the Vanderbilt ultra-soft pseudo-potentials (USP) [8]. The kinetic energy cut-off for the plane waves is 310 eV. The plane wave basis with the use of (USP) provides a better description of bulk diamond structural properties with a lattice parameter  $a = 3.5322$  Angstrom,  $B = 3.79967$  Mbar and ( $dB/dp$ ) = 3.484.

The sliding has been simulated as a stepwise process. The tip is displaced in steps of 0.1 Angstroms along the slide direction. At each tip position the structure of the interacting tip-surface system is relaxed, allowing the atoms to displace to their ground state configuration using a conjugate gradient minimization technique. This quasi-static approach is justified since the experimental scans are performed with velocities of the order of 10 nm/s, which are slow enough to allow the tip and surface atoms to relax. Notice that the top (bottom) noninteracting surfaces of the tip (sample) top/bottom are passivated by hydrogen atoms and the last two layers are kept fixed in their ideal bulk

positions during the structural relaxation to represent the bulk diamond termination. The normal and lateral total tip-surface forces are calculated as the sum of forces on the atoms that are kept fixed on the tip. We have generated theoretically four different constant-height scans in each direction. The heights quoted in Fig.4.11 correspond to the initial normal distance between the hydrogen atom at the tip apex and the nearest surface hydrogen atom that is initially right below it. Animations showing the stick-slip behavior have been created from the results of these simulations.

#### References:

1. A.A. Demkov, J. Ortega, O.F. Sankey, and M.P. Grumbach, *Phys. Rev. B* 52, 1618 (1995).
2. M.C. Payne, M.P. Teter, D.C. Allan, T.A. Arias, and J.D. Joannopoulos, *Rev. Mod. Phys.* 64, 1045 (1992), (CASTEP is available from Accelrys Inc.).
3. O.F. Sankey and D.J. Niklewski, *Phys. Rev. B* 40, 3979 (1989).
4. D.R. Hammann, M. Schluter, and C. Chiang, *Phys. Rev. Lett.* 43, 1494 (1979).
5. G.B. Bachelet, D.R. Hamman, and M. Schluter, *Phys. Rev. B* 26, 4199 (1982).
6. P. Hohenberg and W. Kohn, *Phys. Rev.* 136, B864 (1964).
7. J.P. Perdew, K. Burke, and M. Ernzerhof, *Phys. Rev. Lett.* 77, 3865 (1996).
8. D. Vanderbilt, *Phys. Rev. B* 41 (Rapid Communications), 7892 (1990).

## ***Appendix 2. Growth of (100) single crystalline diamond samples***

### **Preparation of single-crystal diamond layers (Institute for Material Research (IMO), Diepenbeek, Belgium)**

Single-crystal diamond layers were grown using microwave plasma enhanced chemical vapour deposition. As substrate for the grown layers (100) oriented high-pressure-high-temperature (HPHT) diamond substrates (from Sumitomo Electric Industries Ltd., Itami Research Laboratories, Japan) were used. After oxidising the substrate in a mixture of sulphuric acid and potassium chlorate at 300 °C for 30 minutes, the sample is placed in the vacuum chamber and pumped down to a vacuum of  $3 \times 10^{-9}$  Torr. First a hydrogen plasma is created at 800 °C, 68 Torr, at a power of 500 Watt and a hydrogen flow of 500 sccm. After 5 minutes an amount of 1.5 sccm methane is added to the plasma. This plasma is maintained for 300 minutes after which the methane is removed again from the plasma and only the hydrogen plasma is used for removing the graphite on the grown diamond layer and this for another 5 minutes. The layer is approximately grown at a rate of 1 µm per hour and has a roughness of a few nanometers as measured by AFM.

### **The hydrogenation of the diamond layer**

After the growth of the single-crystal layer a chemical oxidization was performed, using the same mixture as described above, to remove all graphite and dirt on the surface of the sample. Then the sample was put back into the deposition chamber and the hydrogen plasma was started. For further investigations of the electrical properties related to hydrogen termination of the surface, samples undergo different treatments during hydrogenation. The layer that is named #1 is the layer that is hydrogenated without adding oxygen during the hydrogenation process. The grown layer named #2 is the hydrogenated layer where oxygen is added during the hydrogen surface passivation process. For the first sample, #1, we ignite a plasma at a temperature of 700 °C, 75 Torr, 3000 Watt and a hydrogen flow of 1000 sccm. This plasma is maintained for about 30 seconds. With this method the surface of the diamond is hydrogenated, showing a resistance of 100 kΩ. For the second sample, #2, the same plasma is created as for the first sample only now we add an amount of 10 sccm oxygen. So the plasma consists of 1% of oxygen. A lower surface resistance of 50 kΩ is then reached. Since we were interested in investigating the surface morphology of the sample by STM for subsequent FFM measurements, sample #2 was used for all measurements as it showed higher surface conductivity.



## Summary

Friction is one of the most fascinating and yet elusive phenomena in physics. Everyday life cannot be imagined in the absence of friction. It allows us to walk, to climb stairs, to sit in a chair, to stop a car, to handle tools. In technological applications friction is the evil of all motion and huge amounts of money are spent annually on energetic and mechanical losses due to friction and wear. Friction is also responsible for natural disasters like earthquakes, landslides and avalanches. Along the centuries mankind has tried to understand and control friction but in spite of the huge volume of experimental knowledge with remarkable technical applications, very little is known about the fundamental, elementary processes taking place on the atomic level at the interface between sliding surfaces.

The contact between two apparently flat solids consists in reality of a very large number of micro-protrusions or asperities belonging to both contacting surfaces. Studying and understanding the processes responsible for the occurrence of friction at the buried interface of a single-asperity became the tasks of a new but rapidly expanding science called *nanotribology*.

In the present work we have used a variable-temperature ultra-high vacuum atomic force microscope (VT-UHV-AFM) to investigate the frictional properties, namely the stick-slip behavior, of (100) and (111) crystalline diamond and (001) sodium chloride surfaces. While diamond is a technologically important material and a perfect candidate for an ideal friction experiment, NaCl is well established as a representative model, standard surface for nanotribological investigations. In order to properly simulate the interface with a single asperity at the nanoscale, sharp AFM-tips are used on atomically flat surfaces. The ultra-high vacuum conditions are an essential ingredient for well-defined and reproducible experiments.

A hard, stable and sharp AFM-tip termination is of the essence for friction measurements. Therefore, using a hot-filament assisted chemical vapor deposition (HF-CVD) of diamond, a method of growing individual good quality diamond crystallites at the apexes of standard Si AFM tips was demonstrated; the resulting tips showed sharpness, hardness, stability and reliable behavior during friction measurements.

We have investigated the atomic-scale friction behaviour between standard silicon nitride tips and diamond-coated tips and a specially prepared hydrogen-terminated (100) diamond sample by means of ultra-high vacuum atomic force microscopy. Tunneling experiments revealed a very flat surface and the typical atomic features (dimers) of a (2x1) surface reconstruction of the hydrogen-terminated (100) diamond sample. When using a diamond-terminated tip, for the first time atomically resolved topography, normal force error signal and lateral force maps are simultaneously obtained and perpendicular domains, hydrogen atomic positions and atomic steps between domains could be observed. This was attributed to a very sharp tip, namely one hydrogen atom-terminated tip, describing a stick-slip movement in two orthogonal directions and causing a dynamic rearrangement of the surface atoms; these results were consistent with an *ab-initio* electronic structure calculation which reveals the fact that the repulsive interaction between the apex H-atom at the tip and H-atoms at the surface is the essential factor that governs the atomic stick-slip behaviour.

Similar experiments were carried out in UHV on a (111) crystalline diamond surface with standard silicon nitride and diamond-coated tips. The friction measurements with the same diamond-coated tip on this surface led to atomic resolution: the measured periodicity is consistent with the one of the individual hydrogen atoms of the diamond surface. This reconfirmed the use of an atomically sharp tip and, similar to the results on the (100) diamond surface, we believe that the repulsion between the last H-atom of the tip and the H-atoms of the surface termination is the most important ingredient controlling the complicated two-dimensional atomic scale stick-slip behavior observed experimentally.

Finally, atomic-scale friction between a silicon tip and the atomically flat (001) NaCl surface was investigated in ultra-high vacuum at various sample temperatures in the interval from 25 to 300 K. The temperature dependence of measured average friction forces is found to be in good qualitative agreement with theoretical models that consider a thermally-activated discontinuous tip movement during scanning and predict higher friction forces at low temperature. Higher mean friction values observed for two temperature values were attributed to possible changes in the tip apex configuration.

## Samenvatting

Wrijving is een van de meest fascinerende, echter onbegrepen fenomenen in de fysica. Het leven van elke dag is niet voor te stellen zonder wrijving. Wrijving stelt ons in staat te lopen, de trap op te gaan, in een stoel te zitten, te remmen in een auto en om gereedschap te hanteren. In technologische toepassingen is wrijving vaker een nadeel en grote hoeveelheden geld worden jaarlijks uitgegeven aan de energetische en mechanische verliezen ten gevolge van wrijving en slijtage. Wrijving is ook verantwoordelijk voor natuurrampen zoals aardbevingen, aardverschuivingen en lawines. Eeuwenlang heeft men geprobeerd om wrijving te begrijpen en te beheersen, maar ondanks de grote hoeveelheid empirische kennis en opzienbarende technologische toepassingen, is er weinig bekend over de fundamentele elementaire processen die plaatsvinden op atomaire schaal op het grensvlak van twee ten opzichte van elkaar bewegende oppervlakken.

Het grensvlak tussen twee schijnbaar vlakke vaste stoffen bestaat in werkelijkheid uit een groot aantal microscopische uitsteeksels en onregelmatigheden van elk van de oppervlakken. Het bestuderen en begrijpen van de processen die verantwoordelijk zijn voor het optreden van wrijving op een grensvlak met slechts één microcontact zijn de taken geworden van een nieuw maar snel groeiend onderzoeksgebied genaamd *nanotribologie*.

Voor het onderzoek dat beschreven is in dit proefschrift is een variabele-temperatuur ultrahog vacuüm atomaire kracht microscoop (VT-UHV-AFM) gebruikt om de wrijvingseigenschappen, in het bijzonder het stick-slip gedrag, te onderzoeken van (100) en (111) diamant en (001) natriumchloride kristaloppervlakken. Diamant is technologisch gezien een belangrijk materiaal en een perfecte kandidaat voor het uitvoeren van een ideaal wrijvingsexperiment, terwijl NaCl een standaard modeloppervlak is voor nanotribologieonderzoek. Om een grensvlak met slechts één microcontact op nanometerschaal correct te simuleren is gebruik gemaakt van het grensvlak tussen een scherpe AFM tip en atomair vlakke oppervlakken. De ultrahog-vacuüm condities zijn essentieel voor het verrichten van goedgedefinieerde en reproduceerbare experimenten. Een hard, stabiel en scherp uiteinde van de AFM-tip is essentieel voor het verrichten van wrijvingsexperimenten. Daarom is in dit werk de groei van individueel hoge kwaliteit diamantkristallen aangetoond op het uiteinde van standaard silicium AFM tips door gebruik te maken van chemische damp depositie met een heet filament (HF-CVD). De resulterende tips toonden het gewenste harde, stabiele, scherpe en betrouwbare gedrag tijdens wrijvingsmetingen.

We hebben het wrijvingsgedrag tussen een speciaal geprepareerd H-getermineerd (100) diamantoppervlak met behulp van ultrahog vacuüm AFM. Tunneling experimenten lieten een erg vlak oppervlak zien en de karakteristieke atomaire ordening (dimeren) van een (2x1) gereconstrueerd oppervlak van een H-getermineerd (100) diamantoppervlak. Bij het gebruik van de diamant-getermineerde tip zijn voor het eerst met atomaire resolutie de oppervlaktetopografie, het normaalkracht foutsignaal en de laterale kracht tegelijkertijd gemeten en loodrecht georiënteerde domeinen, atomaire posities van waterstof en atomaire stappen tussen de domeinen konden worden opgelost. Dit schrijven we toe aan de zeer scherpe tip, namelijk een tip getermineerd met één waterstofatoom die een stick-slip beweging beschrijft in twee orthogonale richtingen en daarbij een



dynamische herordening van de oppervlakteatomen bewerkstelligd. Deze resultaten zijn consistent met *ab-initio* elektronische structuur berekeningen die aantonen dat de afstotende wisselwerking tussen het H-atoom op het tipuiteinde en de H-atomen op het diamantoppervlak de essentiële factor is die het atomaire stick-slip gedrag bepaalt. Vergelijkbare experimenten zijn uitgevoerd in ultrahoog vacuüm op een diamant (111) kristaloppervlak met standaard siliciumnitride en diamant-getermineerde tips. De wrijvingsmetingen op atomaire schaal met dezelfde diamant-getermineerde tip leidden tot atomaire resolutie; de gemeten periodiciteit overeen komt met die van de waterstofatomen aan het diamant oppervlak. Dit bevestigt het gebruik van een atomair scherpe tip en analoog aan de resultaten van het (100) diamantoppervlak, stellen we dat de afstotende wisselwerking tussen het H-atoom op het uiteinde van de tip en de waterstofatomen aan het (100) diamantoppervlak de belangrijkste factor is die het gecompliceerde gemeten tweedimensionale stick-slip gedrag op atomaire schaal bepaald. Tenslotte is onder ultrahoog-vacuüm condities op atomaire schaal de wrijving tussen een silicium tip en het atomair vlakke (001) NaCl oppervlak onderzocht bij verschillende preparaattemperaturen tussen 25 en 300 K. De gemeten temperatuurafhankelijkheid van de gemiddelde wrijvingskracht komt kwalitatief goed overeen met theoretische modellen die een thermisch geactiveerde, discontinue tip beweging beschrijven tijdens het scannen en een grotere wrijvingskracht voorspellen bij lagere temperaturen. Gemiddeld hogere wrijvingskrachten, gemeten bij twee temperaturen, worden toegeschreven aan mogelijke veranderingen op atomaire schaal van het tipuiteinde.

## Publications

- G. Tanasa, O. Kurnosikov, C.F.J. Flipse, J.G. Buijnsters and W.J.P. van Enkevort:  
*Diamond deposition on modified silicon substrates: Making diamond atomic force microscopy tips for nanofriction experiments, Journal of Applied Physics, 1 Aug. 2003; 94(3): 1699-704.*
  
- G. Tanasa, J. Amir, O. Kurnosikov, P. Jelinek, R. Perez, M.C. Payne and C.F.J. Flipse:  
*Stick-slip mechanism of friction observed on hydrogen-terminated diamond surfaces,*  
submitted
  
- G. Tanasa, O. Kurnosikov and C.F.J. Flipse:  
*Ultra-high vacuum friction force microscopy on (001) NaCl surface: Temperature effect on friction,*  
in preparation
  
- C.F.J. Flipse, G. Tanasa, W. Deferme, O. Kurnosikov, M. Nesladek, J. Amir :  
*Role of oxygen doping on the surface electronic structure of hydrogen terminated diamond(100),*  
in preparation



## Acknowledgements

It is time for me to try (within a few lines) to express all my gratitude to those who have contributed to this work and encouraged me throughout the last years.

First of all, I would like to thank my supervisor Kees Flipse for his permanent support en enthusiasm, for his ideas, for the deep analytical discussions and his tireless will to understand the fundamentals. From you I have learnt that knowledge is nothing without imagination...

Special thanks to my first promotor René Janssen for the freedom I had in my project, for his constant openness and constructive suggestions. I am really grateful for your infinite patience and accuracy in reviewing the chapters of this thesis.

Further I would like to thank Hidde Brongersma for his support during the initial stage of my project within the FOG group.

Many special thanks to Oleg Kurnosikov for his great help throughout all this period. I will never forget the long hours you have spent with me in the lab, the skills and knowledge I have learnt, your permanent encouragement and wise advices. It is you who taught me that hard work always pays off...

A special thought for Arnoud Denier van der Gon and his family... we received his early death with great sadness. He will always be in our memories...

Thanks to Ivan Buijnsters and Willem van Enkevort (Radboud University Nijmegen) for their help on the HF-CVD and Raman experiments. Thank you Wim Deferme and Milos Nesladek (IMO Diepenbeek, Belgium) for the good quality diamond samples and fruitful collaboration.

Special thanks to FOM for the financial support of this project.

Many thanks to all former and actual members of FOG, M2N, SMO and Calipso groups, for a good work environment and the special atmosphere.

Thank you Marzenna Schoutese-Brzezinska and Gadisa Oueddan, Gerard Wijers, Wijnand Dijkstra, Erwin Timmerman and Rein Rumphorst for your professional help and efficiency. Beste Rein, hartstikke bedankt voor de Nederlandse les, je mooie verhalen en de fantastische sfeer!

Special thanks to my office/lab colleagues for the good collaboration and great moments we had together: Juan Amir, Jean-Michel Wulveryck, Joris Hagelaar, Gunnar Timmermans and Marc Ponjée. Juan, thanks a lot for the theoretical support to my experimental results, for your humor and your DJ abilities. It is useless to mention here that your impressive, subtle and (sometimes) bone-breaking football skills and ball possession are legendary... Jean-Mi, thank you and Alexandra for the first trip to Paris and the wonderful time we always had. Joris, I always enjoyed our sharp and deep discussions about various matters of life. Singing with you in the lab while cooling down your LT-STM with liquid helium was every time a privilege... Thank you and Dorine for

the enjoyable evenings spent together and all your help. And Marc, sharing the same lab with you kept me alert and focused on my experiments. Thanks for your support, for the great fun we always had, for example during your pooling lessons... Looking forward to the tennis, which should be a sport for stronger arms... And don't forget that sometimes a bad haircut can be a sign for good changes in life...

For the beautiful atmosphere in the group I would also like to thank Martijn Kemerink, Frank Janssen, Jiri Cervenka, Rik van Laarhoven, Nick Podaru, Ron Willems, Jason Jenette, Hans Gommans, Klara Maturova, Cristina Popa and Jan-Maarten Kramer. To Marco de Ridder, Veronica Tiba and Hans Dalderop many thanks for their support, especially in the early stage of my arrival here. Special thanks to Dilna Sreenivasan and K.B. Jinesh for the interesting conversations over different cultures and the Dutch language.

Thank you Tienke, Hannah, Talitha, Noemi and Jannes de Vries for your friendship and hospitality! Thanks to Gabi and Emiel, Marianna and Frans, Sorinela and Mugurel for the rare, but nevertheless enjoyable times spent together. Thanks to Willem Doorewaard for the stay in his hospitable house.

Special thanks to everybody from "Al. I. Cuza" University of Iasi, Romania, who contributed to my education and particularly prof. Dumitru Luca for his constant support and for bringing me in contact with the Netherlands.

And Irina, I want to thank you for all those beautiful years... All my respect and best wishes to you, your parents, Oana and Laur!

These acknowledgements wouldn't have been possible without the permanent support and affection from home. All my gratitude and love to my parents, to Ștefania, Ana-Alexia, Radu-Mihai and Ștefan. Thank you!

## Curriculum Vitae

- **1973, March 18<sup>th</sup>**: Born in Piatra Neamț, Romania
- **1992**: Graduated from “C. Negruzzi” Theoretical High School Iași, Romania. Specialty: Mathematics & Physics.
- **1992-1997**: Bachelor Degree in Physics, Faculty of Physics, “Al. I. Cuza” University of Iași, Romania.
- **1997-1999**: Master of Science Degree in the field of Thin Film Physics, Faculty of Physics, “Al. I. Cuza” University of Iași, Romania. High school physics teacher (2 years).
- **1999-2000**: Assistant at Solid State Physics Department, “Al. I. Cuza” University, Iași, Romania. Seminars and laboratories: Solid State Physics, Heat and Thermodynamics.
- **February 2000 - 2004**: Ph.D. candidate at the Department of Applied Physics, Surfaces and Interfaces Science / Molecular Materials and Nanosystems Group, Eindhoven University of Technology, The Netherlands.
- **November 2004 - present**: Flow & Temperature Control Systems Analysis, Development and Engineering Department, ASML Netherlands B.V., Veldhoven, The Netherlands.

